# Preparation of Functional Polymer Nanoparticles Using Semibatch Microemulsion Polymerization

by

Hui Wang

A thesis
presented to the University of Waterloo
in fulfillment of the
thesis requirement for the degree of
Doctor of Philosophy
in
Chemical Engineering

Waterloo, Ontario, Canada, 2012

# AUTHOR'S DECLARATION

I hereby declare that I am the sole author of this thesis. This is a true copy of the thesis, including any required final revisions, as accepted by my examiners.

I understand that my thesis may be made electronically available to the public.

## Abstract

The present project is related to two aspects of research (i) to develop a new technique to synthesize fine nano-size polymer particles with unique and controllable properties; (ii) to synthesize novel functional polymer nanoparticles aiming to overcome the central challenge that has limited the commercialization of green latex hydrogenation, i.e. the *optimal interplay of accelerating the hydrogenation rate, decreasing the required quantity of catalyst, and eliminating the need for an organic solvent*. Focusing on these two objectives stated above, the following studies were carried out.

(1) Development of Micellar Nucleation Mechanism for Preparation of Fine Polymer Nanoparticles. Polymer nanoparticles below 20 nm with a solid content of more than 13 wt% and a narrow molecular weight polydispersity ($\overline{M}_w/\overline{M}_n \sim 1.1$) were prepared using a micellar nucleation semibatch microemulsion polymerization system emulsified by sodium dodecyl sulfate (SDS), with SDS/monomer (methyl methacrylate) and SDS/$H_2O$ weight ratios of up to 1:16 and 1:100, respectively. It was found that for benzoyl peroxide (BPO), micellar nucleation is more favorable for the synthesis of smaller polymer nanoparticles than ammonium persulfate (APS), which gives rise to homogeneous nucleation and 2,2'-azobisisobutyronitrile (AIBN), which involves partially heterogeneous nucleation. In the polymerization process, there exists a critical stability concentration (CSC) for SDS, above which the size of the nanoparticles is to be minimized and stabilized. With an increase in the monomer addition rate, the polymerization system changes from a microemulsion system to an emulsion system. A mechanism was proposed to describe the micellar nucleation process of semibatch microemulsion polymerization. This technique will pioneer a significant new way to use a simple but practical method to synthesize narrow PDI polymers, which is a very meaningful new development.

(2) Diene-Based Polymer Nanoparticles: Preparation and Direct Catalytic Latex Hydrogenation. At the first stage of this study, poly(butadiene-*co*-acrylonitrile) nanoparticles were synthesized in a semibatch microemulsion polymerization system using Gemini surfactant trimethylene-1,3-bis (dodecyldimethylammonium bromide), referred to as GS 12-

3-12, as the emulsifier. The main characteristic of this GS emulsified system lies in that the decomposition rate of initiator was increased considerably at a low reaction temperature of 50 °C because of the acidic initiation environment induced by GS 12-3-12. The particle size can be controlled by the surfactant concentration and monomer/water ratio and a particle size below 20 nm can be realized. The obtained latex particles exhibit a spherical morphology. The microstructure and copolymer composition of the polymer nanoparticles was characterized by FT-IR and $^1$H NMR spectroscopy. The effects of the surfactant concentration on the particle size, Zeta-potential, polymerization conversion, copolymer composition, molecular weight, and glass transition temperature ($T_g$) were investigated. The kinetic study of the copolymerization reaction was carried out, which indicated that an azeotropic composition was produced. The relationship between $T_g$ and number-average molecular weight can be well represented by the Fox-Flory equation. Finally, the semibatch process using conventional single-tail surfactant SDS was compared.

In the second stage of this study, the prepared unsaturated nanoparticles were employed as the substrates for latex hydrogenation in the presence of Wilkinson's catalyst, i.e., $RhCl(P(C_6H_5)_3)_3$. The direct catalytic hydrogenation of poly(butadiene-*co*-acrylonitrile) nanoparticles in latex form was carried out under various experimental conditions in the presence of Wilkinson's catalyst without the addition of any organic solvents. In order to appreciate the important factors which influence the nature and extent of this type of hydrogenation, the effects of particle size within the range from 17.5 to 42.2 nm, temperature from 90 to 130 °C, and catalyst concentration from 0.1 to 1.0 wt% (based on the weight of polymer) on the hydrogenation rate were fully investigated. The kinetics study shows that the reaction is chemically controlled with a fairly high apparent activation energy, which is calculated to be between 100 and 110 kJ/mol under the experimental conditions employed. Mass transfer of both hydrogen and catalyst involved in the reaction system was discussed. The analysis of mass transfer of reactants coupled with the reaction kinetics indicated that the catalysis of hydrogenation proceeds at the molecular level. The competitive coordination of the active catalyst species $RhH_2Cl(PPh_3)_2$ between the carbon-carbon unsaturation and the

acrylonitrile moiety within the copolymer was elucidated based on the reaction kinetics of the hydrogenation.

(3) Poly(methyl methacrylate)-poly(acrylonitrile-*co*-butadiene) (PMMA-NBR) Core-Shell Polymer Nanoparticles: Preparation and Direct Catalytic Latex Hydrogenation. PMMA-NBR core-shell structured nanoparticles were prepared using a two stage semibatch microemulsion polymerization system with PMMA and NBR as the core and shell respectively. The GS 12-3-12 was employed as the emulsifier and found to impose a pronounced influence on the formation of the core-shell nanoparticles. A spherical morphology of the core-shell nanoparticles was observed. It was found that there exists an optimal MMA addition amount which can result in the minimized size of PMMA-NBR core-shell nanoparticles. The formation mechanism of the core-shell structure and the interaction between the core and shell domains was illustrated. The PMMA-NBR nano-size latex can be used as the substrate for the following direct latex hydrogenation catalyzed by Wilkinson's catalyst to prepare the PMMA-HNBR core-shell nanoparticles. The hydrogenation rate is rapid. In the absence of any organic solvent, the PMMA-HNBR nanoparticles with a size of 30.6 nm were obtained within 3 h using 0.9 wt% Wilkinson's catalyst at 130 °C under 1000 psi of $H_2$. This study provides a new perspective in the chemical modification of NBR and shows promise in the realization of a "green" process for the commercial hydrogenation of unsaturated elastomers.

## Acknowledgements

At the time I am completing my Ph. D. thesis, I would like to gratefully acknowledge the following people:

First of all, I would like to express my sincere gratitude to my two supervisors, Professor Garry L. Rempel and Professor Qinmin Pan. They promoted me here from nowhere. Without their help, there is no chance I could gain the opportunity to pursue the polymer research in the University of Waterloo. With their great kindness, patience, insight, understanding and support, I made a great progress in my research area and start to become a qualified researcher. I truly appreciate that they found and made me.

Co-op undergraduate students: Michael Hammond, Stephen Scott, Richard Kwon, Youssef Helwa for their outstanding work and valuable time shared with me.

Dr. Jialong Wu for generously providing his time, knowledge, and experience with me whenever I need his help. Mrs. Yan Liu for her kind help as a friend and lab mate. Dr. Lijuan Yang, Dr. Yin Liu (Allen), Dr. Minghui Liu (Karl), and Dr. Akpan Enefiok (Robert) for their cooperation in research as professional colleagues.

Mr. Robert Harris (University of Guelph, Canada) for his assistance with the TEM operation.

Financial support of the Natural Sciences and Engineering Research Council of Canada (NSERC) and Canada Foundation for Innovation (CFI).

My beloved family!

# Table of Contents

# List of Figures

# List of Tables

# Chapter 1
# Introduction

## 1.1 Research Scope

The field of polymer nanoparticles is one of the most attractive areas in the modern nanoscience and nanotechnology, which meets a wide range of applications and market needs based on their unique properties.

The technique for the preparation of particles plays a vital role in determining the required properties for particular applications. It is very desirable to develop economically viable techniques capable of producing acceptable particles with the desired properties. Currently, polymer nanoparticles can be synthesized via physical and chemical processes. The physical route is used to prepare nanoparticles through dispersion of the aimed polymers, which includes solvent evaporation, salting-out, nanoprecipitation, dialysis and supercritical fluid technology that involves the rapid expansion of supercritical solution (RESS) and rapid expansion of supercritical solution into liquid solvent (RESOLV). On the other hand, the polymer nanoparticles can be directly synthesized by the polymerization of monomers using various polymerization techniques including conventional emulsion, microemulsion, miniemulsion, semibatch microemulsion, surfactant-free emulsion, interfacial, and controlled/living radical polymerizations (C/LRP). The choice of preparation method is made on the basis of a number of factors such as the type of polymeric system, area of application, size requirement, and so forth. Generally, the conventional, micro, mini, and semibatch microemulsion polymerizations are the four principal techniques currently in use to synthesize polymer nanoparticles. In the present research, a new technique so called *micellar nucleation semibatch microemulsion polymerization* was developed, trying to produce the very small nanoparticles such as below 20 nm with a narrow distribution of PDI close to 1 for free radical polymerization. In addition, a high solid content was reached when using a low level of surfactant. This technique will pioneer a significant new way to use a simple but practical method to synthesize narrow PDI polymers, which is a very meaningful new development.

The properties of nanomaterials can differ significantly from those at larger scales because of nano-structure induced effects. These differences pertain to the evolution of structural, thermodynamic, electronic, spectroscopic, electromagnetic and chemical features, among others. The novel properties of nanomaterials thus provide a unique opportunity to employ such nano-structure materials to work out the challenges encountered in the current scientific research and commercial production. Catalytic hydrogenation constitutes an important process of chemical modification of polymers. The current commercial process for the hydrogenation of unsaturated polymers such as NBR, styrene butadiene rubber (SBR) and natural rubber (NR) usually involves a number of cumbersome steps, including purifying polymer from the latex, dissolving the polymer in large amounts of organic solvent, and recovering the organic solvent after the hydrogenation operation. This process not only raises environmental concerns but increases the cost of production. Therefore it is of great interest to develop a green and economical process for catalytic hydrogenation of diene-based polymers. Because most of polymers are commercially produced in the latex form, the direct hydrogenation of unsaturated polymers in the emulsion form thus stands for a substantial promising route. However, although a considerable amount of effort has been made to optimize the latex hydrogenation process, one significant challenge that is inherent to almost all hydrogenation systems has been preventing the further development of latex hydrogenation, that is, *the optimal interplay of accelerating the hydrogenation rate, decreasing the required quantity of catalyst, and eliminating the need for an organic solvent*.

With this thought in mind, a series of diene-based polymer nanoparticles with or without a complex architecture were designed and synthesized for the first time aiming to overcome the above mentioned challenge. The progress is very encouraging. For example, when 17 nm nanoparticles of a diene polymer were used as the substrates, a high conversion of 95 mol% was obtained within 18 h using only 0.1 wt% $RhCl(P(C_6H_5)_3)_3$. The latex hydrogenation process was completely free of organic solvent and no crosslinking was found. This study confirms the advantages in designing nanoscale materials and shows great promise in realization of a green process for the commercial hydrogenation of unsaturated elastomers in latex form.

## 1.2 Objectives

This project is related to (i) developing new techniques to synthesize nano-size polymer particles with desired unique properties; (ii) preparing novel functional polymer nanoparticles aiming to solve the dilemma encountered between the current lab technology and industrial production. More specifically the following issues will be considered in this project relating to the above two objectives:

1) Development of synthesis approach and concepts for polymer nanoparticles in particular their elaboration.
2) Better understanding of the influence of the size and nano-structure of polymer nanoparticles on their physicochemical properties.
3) Better understanding of the influence of interfaces on the properties of colloidal polymer nanoparticles.
4) Investigation of catalytic applications of polymer nanoparticles.
5) Better understanding of the mechanism and kinetics of the catalytic hydrogenation with nanoparticles as the substrate.
6) Transfer of developed technologies into industrial applications including the development of the industrial scale of both synthesis methods of polymer nanoparticles and green latex hydrogenation process.

## 1.3 Outline

Chapter 1 provides an introduction about this project and the structure of this thesis.

Chapter 2 contains a literature review pertinent to the research undertaken. First, the fundamental knowledge related to the polymer nanoparticles was covered. Next, the applications of polymer nanoparticles for green catalysis, biomedical field, and conducting materials were addressed. Finally, the techniques that can be employed to prepare the polymer nanoparticles were reviewed. Conventional emulsion, microemulsion, miniemulsion, and semibatch microemulsion polymerizations are the four principal techniques currently in use to synthesize the polymer nanoparticles. Surfactant is a key component in controlling the polymerization process, and Gemini surfactant represents a promising direction to develop the new surfactant systems in the future. It was summarized

that more efforts are required to develop robust synthesis technique, prepare new functional nanoparticles and explore the potential applications of polymer nanoparticles.

Chapter 3 describes the experimental techniques used and analytical methods for characterization. The experimental techniques used in this project include the synthesis technique, i.e. *semibatch microemulsion polymerization*, and hydrogenation technique, i.e. *direct catalytic latex hydrogenation*. The characterization methods used for the polymer and emulsion involve pH of Latex, Isolation of Polymer, Particle Size and Its Distribution, Molecular Weight and its Distribution, Normal TEM, Cross Section TEM, SEM, FTIR, Polymer Composition and Hydrogenation Degree, $^1$H NMR, Zeta-potential, Cross-linking Examination, and Glass Transition Temperature.

Chapter 4 focuses on development of micellar nucleation mechanism for preparation of fine polymer nanoparticles. PMMA nanoparticles below 20 nm with a solid content of more than 13 wt% and a narrow molecular weight polydispersity ($\overline{M}_w / \overline{M}_n \sim 1.1$) were prepared using a micellar nucleation semibatch microemulsion polymerization system emulsified by sodium dodecyl sulfate (SDS), with SDS/monomer (MMA) and SDS/$H_2O$ weight ratios of up to 1:16 and 1:100, respectively.

Chapter 5 and Chapter 6 report the preparation and direct catalytic latex hydrogenation of diene-based polymer nanoparticles. At the first stage of this study, the poly(butadiene-*co*-acrylonitrile) nanoparticles were synthesized in a semibatch microemulsion polymerization system using the Gemini surfactant trimethylene-1,3-bis (dodecyldimethylammonium bromide), referred to as GS 12-3-12, as the emulsifier (Chapter 5). The particle size can be controlled by the surfactant concentration and monomer/water ratio and a particle size below 20 nm can be reached. The effects of the surfactant concentration on the particle size, Zeta-potential, polymerization conversion, copolymer composition, molecular weight, and glass transition temperature ($T_g$) were investigated. The kinetic study of the copolymerization reaction was carried out, which indicated that the azeotropic composition was produced. The relationship between $T_g$ and number-average molecular weight can be well represented by the Fox-Flory equation. Finally, the semibatch process using monomeric and conventional

surfactant sodium dodecyl sulfate (SDS) was compared. In the second stage of this study (Chapter 6), the prepared unsaturated nanoparticles were employed as the substrates for latex hydrogenation in the presence of Wilkinson's catalyst, i.e. $RhCl(P(C_6H_5)_3)_3$. The direct catalytic hydrogenation of NBR nanoparticles in the latex form was carried out under various experimental conditions in the presence of Wilkinson's catalyst without the addition of any organic solvent. The effects of particle size within the range of 17.5 to 42.2 nm, temperature from 90 to 130 °C, and a catalyst concentration of 0.1 to 1.0 wt% (based on the weight of polymer) on the hydrogenation rate were fully investigated. Mass transfer of both the hydrogen and catalyst involved in the reaction system was considered and discussed. The analysis of the mass transfer of reactants coupled with the reaction kinetics indicated that the catalysis of hydrogenation proceeds at a molecular level. The competitive coordination of the active catalyst species $RhH_2Cl(PPh_3)_2$ between the carbon-carbon unsaturation and acrylonitrile units within the copolymer was elucidated based on the reaction kinetics of hydrogenation.

Chapter 7 presents another perspective to realize the "green" process for the commercial hydrogenation of unsaturated elastomers in latex form. The NBR substrate was stretched as a thin layer for the subsequent latex hydrogenation through preparing poly(methyl methacrylate)-poly(acrylonitrile-*co*-butadiene) (PMMA-NBR) core-shell structured nanoparticles with NBR as the shell. The GS 12-3-12 was employed as the emulsifier and found to impose a pronounced influence on the formation of core-shell nanoparticles. It was found that there exists an optimal MMA addition amount which can result in the minimized size of PMMA-NBR core-shell nanoparticles. The formation mechanism of the core-shell structure and the interaction between the core and shell domains was illustrated. The PMMA-NBR nano-size latex can be used as the substrate for the following direct latex hydrogenation catalyzed by Wilkinson's catalyst to prepare the PMMA-HNBR core-shell nanoparticles. The hydrogenation rate is rapid. In the absence of any organic solvent, the PMMA-HNBR nanoparticles with a size of 30.6 nm were obtained within 3 h using 0.9 wt% Wilkinson's catalyst at 130 °C under 1000 psi of $H_2$.

Chapter 8 summarizes the milestones and contributions achieved in completing this project, as well as the detailed conclusions derived from Chapter 4 to Chapter 7.

Chapter 9 suggests the focuses of future research.

# Chapter 2
# Literature Review

The essence of "nano-" science and technology is based on the understanding and control of matter at dimensions of roughly 1 to 100 nm size domain, where unique phenomena enable novel applications different from those of bulk material.[1,2] The unique properties of these various types of intentionally produced nanomaterials give them novel electrical, catalytic, optical, magnetic, mechanical, thermal, and imaging features that are highly desirable for applications in commercial, medical, military, and environmental sectors.[3,4]

Polymer nanoparticles are a subset among the large fields of nanotechnology, which has generated a significant amount of attention in academia and industry and has become a prominent area of current research and development. The past decade has witnessed the fast expansion of the field of polymer nanoparticles and the application of polymer nanoparticles in a wide spectrum of areas ranging from electronics to photonics, conducting materials to sensors, medicine to biotechnology, pollution control to environmental technology, and so forth.[3] In addition, the polymer nanoparticles can also extend their applications through incorporating more complex nano-structures, such as core-shell architecture.

## 2.1 Definition of Polymer Nanoparticles

Polymer nanoparticles are frequently defined as solid, colloidal particles in the range 1-1000 nm. The term polymer nanoparticle is a collective term covering any type of polymer nanoparticle, but specifically for nanospheres, nanocapsules, and nanogels. Nanospheres are matrix particles whose entire mass is solid and molecules may be adsorbed at the sphere surface or encapsulated within the particle.[3] Nanocapsules are vesicular systems, acting as a kind of reservoir where the entrapped substances consisting of a liquid core (either oil or aqueous solution) are confined to an interior cavity surrounded by a solid material shell.[5] Nanogels are nanoscale hydrophilic, three-dimensional cross-linked polymer networks that swell in the presence of water.[6]

## 2.2 Nano-Structure Induced Effects

Nano-structure induced effects constitute a fascinating aspect of nanomaterials, which pertain to the evolution of structural, thermodynamic, electronic, spectroscopic, electromagnetic and chemical features of these finite systems with different nano-structure. Roughly two kinds of "nano-structure induced effects" can be distinguished:[7]

First the *size effect*, in particular the *quantum size effects* where the normal bulk electronic structure is replaced by a series of discrete electronic levels, and second the *surface or interface induced effect*, which is important because of the enormously increased specific surface in particle systems.

While the *size effect* is mainly considered to describe physical properties, the *surface or interface induced effect*, plays an important role for chemical processing, in particular in connection with heterogeneous catalysis. Experimental evidence of the *quantum size effect* in small particles has been provided by different methods, while the *surface induced effect* could be evidenced by measurement of thermodynamic properties such as vapour pressure, specific heat, thermal conductivity, and melting point of nanomaterials.

## 2.3 Application of Polymer Nanoparticles

Green energy and healthcare are two important aspects related to human beings and have a direct influence on the quality of our well-being life. New methods and materials for green chemistry and sustainable energy development and early diagnosis and treatment of diseases are indispensable. Among them, polymer nanoparticles are emerging as multifunctional nanoscale materials that have great potential to offer promising opportunities in various areas related to green energy and healthcare. Herein some application examples of polymer nanoparticles were described with emphasis on the green catalysis, biomedical applications, and conducting materials.

### 2.3.1 Green Catalysis

The term green chemistry is defined as the "utilisation of a set of principles that reduces or eliminates the use or generation of hazardous substances in the design, manufacture and

application of chemical products" by the US Environmental Protection Agency around ten years ago, and is becoming the common used term used to describe the development of more eco-friendly, sustainable chemical products and processes. Green chemistry requires that the dispersion of harmful chemicals in the environment must be minimized or, preferably, completely eliminated. Green chemistry covers a broad range of topics and in this section; an overview is provided which focuses on the recent success towards developing green and economical technologies for catalytic hydrogenation of diene-based polymers.

Catalytic hydrogenation constitutes an important process of chemical modification of polymers as it not only provides a pertinent way to improve the mechanical, chemical, physical and thermal properties of unsaturated polymers, but also offers an efficient synthetic route to synthesize the novel polymers with controlled molecular weight, required microstructures, and unique stereochemistries that are difficult or too expensive to achieve by conventional polymerization.[8-10] The selective hydrogenation of the carbon-carbon double bonds in nitrile butadiene rubber (NBR) is such a typical commercial process. The produced hydrogenated NBR (HNBR) shows more resistance than NBR towards oxidative and thermal degradation while maintaining its elastomeric properties in chemically aggressive environments, as well as notable improvements in mechanical properties characterized by tensile strength, elongation, abrasion resistance, and hardness. Thus, HNBR has been extensively used for hoses, seals, belts and gaskets for oil exploration and processing and under-the-hood rubber components of automobiles, and so forth.

The current commercial process for the hydrogenation of unsaturated polymers such as NBR, SBR and NR usually involves a number of cumbersome steps, including purifying polymer from the latex, dissolving the polymer in large amounts of organic solvent i.e. solution hydrogenation, and recovering the organic solvent after the hydrogenation operation. This process not only raises environmental concerns but increases the cost of production. It is therefore very desirable to directly hydrogenate the unsaturated polymers in latex or bulk form as such a process would avoid the tedious hydrogenation steps and thereby eliminate the need of large amounts of organic toxic solvent.

The pioneer work on bulk hydrogenation of olefinic polymers can be traced to Gilliom and co-worker's reports.[11,12] However, the relevant studies with the bulk hydrogenation appear rare after Gilliom and co-worker's work, probably due to the difficulties resulting from the mass transfer and heat transfer involved in the reactions. Latex hydrogenation is thus becoming important, especially when the hydrogenated product in latex form is the desired end-use product or only surface/gradient hydrogenation of a product is required.

The latex hydrogenation can be achieved via two major technical routes: diimide route and catalysis route. The diimide hydrogenation has been drawing much attention since Wideman reported the first diimide hydrogenation of diene-based polymers in 1984.[13] In the diimide hydrogenation, the hydrogenated polymers are formed through the reduction reaction between the diimide and carbon-carbon double bonds (C=C), and therefore the requirements for specialized hydrogenation apparatus were circumvented. However, the gel problem occurring during hydrogenation has been the major obstacle for the diimide hydrogenation to become a practical process.[14] In contrast, catalytic latex hydrogenation was performed under a gaseous hydrogen environment using a Group VIIIB metal complex as the catalyst, and in most cases, a rhodium-based complex was employed. Singha et al. studied the latex hydrogenation of NBR using a water soluble analog of Wilkinson's catalyst $RhCl(DPM)_3$ (DPM is diphenyl phosphino benzene *m*-sulphonate).[15] A conversion of 60 mol% was achieved with 0.5 mol% catalyst to NBR solid in 12 h under 1 atm $H_2$ pressure at 75 °C. However, crosslinking occurred during the hydrogenation and the gel content of the latex was found to increase with the procession of the hydrogenation. Mahittikul et al. hydrogenated natural rubber latex (NRL) using $OsHCl(CO)(O_2)(PCy_3)_2$[16] or $[Ir(cod)(PCy_3)(py)]PF_6$[17] as catalysts. A higher conversion of greater than 95 mol% was achieved in both catalyst systems under proper experimental conditions. However, the organic solvent monochlorobenzene (MCB) that may cause lung, kidney and/or liver damage was still required in these two studies in order to reach a desired degree of hydrogenation. Chemtob et al. studied the direct hydrogenation of purely linear polybuta-1,4-diene (1,4-PB) latex in the presence of $RuCl_2(PPh_3)_3$ and complete hydrogenation was observed in 8 h using a catalyst loading around 10 wt% over PB under 20 MPa hydrogen at 130 °C.[18] However,

dichloromethane that is toxic to lungs, the nervous system, liver, etc, was still required. Kotzabasakis et al. studied the hydrogenation of polybutadiene (PB) latex using a water-soluble Rh/TPPTS complex [TPPTS=$P(C_6H_4$-*m*-$SO_3Na)_3$] and reported that this catalyst is very active for the hydrogenation process.[19] The turn over frequency (TOF) can reach 1245 $h^{-1}$ through adjusting the experimental conditions and a conversion of 80 mol% was obtained at this TOF. However, this study still could not circumvent the need of organic sovent and *n*-hexane was used to dissolve the PB in order to form an emulsion system. In another report of Kotzabasakis et al., the need of organic solvent can be obviated in the case of using a water soluble polymer polybutadiene-1,4-*block*poly(ethylene oxide) (PB-*b*-PEO) as the substrate.[20] However, most of diene-based polymers are highly water-insoluble. Wei et al. reported a latex hydrogenation of water-insoluble polymer NBR catalyzed by oil-soluble Wilkinson's catalyst, which is usually written as $RhCl(PPh_3)_3$, $RhCl(P(C_6H_5)_3)_3$, or $RhCl(TPP)_3$ and a conversion higher than 95 mol% was reached in the absence of organic solvents.[21] In this study, the added excess triphenylphosphine (TPP) plays a crucial role to transport the catalyst into the latex particles thereby no alien solvent was used. However, the hydrogenation rate is quite slow, which became the main obstacle limiting the further development of this technique.

All these observations point to the notion that the central challenge inherent in almost all hydrogenation systems which is preventing the commercialization of latex hydrogenation involves *the optimal interplay of accelerating the hydrogenation rate, decreasing the required quantity of catalyst, and eliminating the need for an organic solvent*.

We have met this challenge completely through integrating the advantages of polymer nanomaterials, as will be shown in Chapter 6 and Chapter 7. In brief, we first synthesized a type of NBR nanoparticles of less than 20 nm with narrow molecular weight and particle size distributions. The prepared unsaturated nanoparticles were employed as the substrates for the latex hydrogenation in the presence of Wilkinson's catalyst, i.e., $RhCl(P(C_6H_5)_3)_3$. When 17 nm nanoparticles were used as the substrate, a high conversion of 95 mol% was obtained within 18 h using only 0.1 wt% $RhCl(P(C_6H_5)_3)_3$. The latex hydrogenation process was completely free of organic solvent and no crosslinking was found. We also prepared a type of

PMMA-NBR core-shell structured nanoparticles with PMMA and NBR as the core and shell, respectively. The prepared unsaturated core-shell nanoparticles were then hydrogenated in latex form in the presence of $RhCl(P(C_6H_5)_3)_3$. In the absence of any organic solvent, the PMMA-HNBR nanoparticles with a size of 30.6 nm were obtained within 3 h using 0.9 wt% $RhCl(P(C_6H_5)_3)_3$ at 130 °C under 1000 psi of $H_2$. The present synthesis and following green hydrogenation process can be extended to latices made from semibatch microemulsion containing other diene-based polymers like SBR. These two studies confirm the significance in designing nanoscale materials and show great promise in realization of a green process for the commercial hydrogenation of unsaturated elastomers in latex form.

### 2.3.2 Development of Targeted Drug Delivery Devices for Cancer Therapy

Drug delivery is becoming an increasingly important aspect of medicine, particularly nowadays in developing more efficient and specific drugs. The rapid development of drug delivery research will increase the understanding of disease pathways and give birth to new opportunities to prevent and treat diseases.[22-27] Effective targeted cancer therapies are clearly needed to develop "smart delivery vehicles" that will enhance survival and minimize adverse effects.[26] An emerging strategy which holds great promise involves nanoparticle conjugates, also referred to as ‘nanovectors’ for targeting metastatic cancer through the delivery of drug laden nanoparticles conjugated to targeting moieties.[27] The nanoscale drug-delivery systems can be used to deliver both small-molecule drugs and various classes of biomacromolecules, such as peptides, proteins, plasmid DNA and synthetic oligodeoxynucleotides.[28-30] Four types of covalent drug-polymer conjugates have been described for potential combination therapies (two or more drugs administered simultaneously or use of a combination of two types of therapy): (i) a polymer-drug conjugate plus non-conjugated free drug; (ii) a polymer-drug conjugate plus a second polymer-drug conjugate; (iii) a single polymeric carrier of a combination of drugs; and (iv) polymer-directed enzyme prodrug therapy.[31]

Natural polymers such as chitosan, albumin, heparin, dextran, gelatin, alginate, and collagen as well as synthetic polymers, such as polyethylene glycol (PEG), polyglutamic acid

(PGA), polylactic acid (PLA), polycarprolactone (PCL), poly-d,l-lactide-co-glycolide (PLGA) and *N*-(2-hydroxypropyl)-methacrylamide copolymer (HPMA) have been widely used to prepare nanoparticles and encapsulate drugs for cancer therapy.[32-35] In many cases the polymeric nanoparticles are comprised of a hydrophobic core containing the anticancer agent and a hydrophilic surface layer for the stabilization of nanoparticles in an aqueous environment.

Based on their structural features, polymeric nanoparticles can be further classified into nanocapsules, nanospheres, and nanogels.[36] In nanocapsules the shells are usually filled with an aqueous or oil solution, which can contain a solubilized drug. In nanocapsules, the drug can be physically loaded in the interior if soluble in the liquid phase contained in the nanocapsule, or via conjugation to the polymer chains. Nanospheres consist of a solid mass, which may be impregnated with an anticancer agent.[37,38] In nanospheres, the drug can also be dispersed or covalently bound to the polymer matrix, while in micelles, hydrophobic drugs are generally encapsulated in their hydrophobic interior. Hydrogels are hydrophilic, three-dimensional cross-linked polymer networks that swell in the presence of water. Nanoscale hydrogels, or "nanogels", offer straightforward synthesis and relatively high drug-loading capacity.[39] Hydrogel matrices are advantageous for use in drug delivery because of their ability to prevent payload aggregation, as well as the high biocompatibility and tunable properties.[40,41] They can be designed to respond to many physiological stimuli, including ionic strength, pH and temperature.[41] Generally, the drug is loaded *via* self-assembly processes based on non-covalent interactions into the hydrogel after the hydrogel was synthesized. Both charged and hydrophobic biomolecules can be incorporated into hydrogel networks. Other classes of polymeric nanoparticles include polymeric micelles, which consist of amphiphilic block copolymers that self-assemble into micelles in aqueous solutions, nanotubes, and dendrimers.[42-45]

### 2.3.3 Polymeric Nanoparticles for Imaging

Polymeric nanoparticles have been loaded with gadolinium complexes or magnetic nanoparticles in order to image cancer by magnetic resonance imaging (MRI). Traditionally

magnetic nanoparticles (magnetite) have been encapsulated in the core of polymeric micelles.[43] Recently, the amphiphilic block copolymers of maleimide-terminated poly(ethyleneglycol)-block-poly(D, L-lactide) and methoxyterminated poly-(ethylene glycol)-block-poly(D, L-lactide) copolymer were used to encapsulate the magnetic nanoparticles together with doxorubicin into their micelles for imaging.[44]

### 2.3.4 Tissue Engineering

Great progress has been achieved over the past few decades in the field of tissue engineering.[45,46] The underlying principle is that the dissociated cells have the ability to reassemble into structures that resemble the original tissue.[40] In order to control and direct cell behavior, a defined biomimetic environment which surrounds the cells and promotes specific cell interactions is necessary. Critical environmental parameters include a scaffolding material, soluble factors and external physical stimulations.[47]

Both natural and synthetic materials have been evaluated as scaffolds for tissue engineering. Natural materials include collagen,[48] silk protein,[49] Matrigel,[50] small intestinal submucosa,[51] agarose,[52] alginate,[53] and chitosan.[54] Although these materials show promise in tissue repair, critical issues regarding biocompatibility, mechanical properties and degradation cannot be neglected. On the other hand, synthetic materials can be created with improved biocompatibility, controlled degradation and tunable mechanical properties.[55] Furthermore, bioactive moieties and functional groups can be readily incorporated into the polymeric system, giving rise to smart and responsive materials.[56] Synthetic polymers such as poly(lactic acid), poly(glycolic acid) and their co-polymers, poly(lactic acid-co-glycolic acid), poly(anhydride), poly(4-hydroxybutyrate), poly(urethane), polyphosphoesters and polyphosphazenes have been employed as degradable scaffolds for a variety of tissues and organs.[40]

### 2.3.5 Preparation of Nano-Structured Conducting Polymer

Since the discovery of the first conducting polymer, polyacetylene (PA) doped with iodine in 1977,[57,58] there has been an increasing amount of interest and enhanced research into the nano-structured conducting polymers because their highly π-conjugated polymeric chains

and metal-like conductivity. In addition, the remarkable characteristics of conducting polymer nano-structures are a result of their size (1-100 nm) and large surface area, referred to as the size effect, hence the electrical properties of the conducting polymer nano-structures are expected to be different from those of their bulk materials. These unique properties indicate that they can be regarded not only as excellent molecular wires, but also as basic units for the formation of nanodevices.[59] Polypyrrole (PPy), polyaniline (PANI), polythiophene (PT), poly(3,4-ethyelenedioxythiophene) (PEDOT) and poly(para-phenylene vinylene) (PPV) are the typical conducting polymers, which received the most widespread research attention.[60]

The conducting polymer nanomaterials show great promise in various applications, including chemical sensor and biosensor, transistor and switch, data storage, supercapacitor, photovoltaic cell, electrochromic device, field emission display, actuator, optically transparent conducting material, surface protection, and substituent for carbon nanomaterials.[60] For example, in order to demonstrate the use of nanoparticles in the solar cell devices, Kietzke et al.[61,62] prepared a type of nanoparticles with mean diameters of approximately 50 nm, containing either the pure polymer components hole accepting polymer, PFB [poly(9,9-dioctylfluorene-2,7-diyl-co-bis-N,N'-(4-butylphenyl)-bis-N,N'-phenyl-1,4-phenylenediamine)], and electron accepting polymer, PFBT [poly(9,9-dioctylfluorene-2,7-diyl-co-benzothiadiazole)], or a mixture of PFB and PFBT in each particle. They studied the photovoltaic devices based on these particles with respect to the correlation between external quantum efficiency and layer composition. The properties of devices containing a blend of single-component PFB and PFBT particles were shown to differ significantly from those of solar cells based on blend particles, even for the same layer composition. An external quantum efficiency of approximately 4% is measured for a device made from polymer blend nanoparticles containing PFB:F8BT at a weight ratio of 1:2 in each individual nanosphere. Fabrication methods and more detailed applications of conducting polymer can be obtained from the review articles of Jang[60] and Pron and Rannou.[63]

## 2.4 Preparation Techniques for Polymer Nanoparticles

Two pathways can be employed to conveniently prepare polymer nanoparticles: dispersion of preformed polymers and direct polymerization of monomers using classical polymerizations.[3] Several techniques have been developed and successfully utilized to prepare polymer nanoparticles by dispersing preformed polymers, including solvent evaporation,[64] salting-out,[65] nanoprecipitation,[66] dialysis[67] and supercritical fluid technology[68] which involves RESS[69] and RESOLV.[70] On the other hand, polymer nanoparticles can be directly synthesized through the polymerization of monomers using various polymerization techniques characterized by conventional emulsion, microemulsion, miniemulsion, semibatch microemulsion, surfactant-free emulsion[71] and interfacial,[72] and controlled/living radical polymerizations (C/LRP).[73,74] The choice of preparation method is made on the basis of a number of factors such as the type of polymeric system, area of application, size requirement, and so forth.

The processing of performed polymer requires specialized equipments. For example, RESS and RESOLV need high pressure equipment. However, most polymers have poor solubility or even non-solubility of the polymers in supercritical fluids. In addition, when the polymer particles are formed, they must be protected to prevent the coalescence. Otherwise, the polymer chains of particles will penetrate into each other, which will become worse when the temperature is higher than their $T_g$. Under this condition, the polymer particles will form block due to the coalescence process.

Conventional, micro, mini, and semibatch microemulsion polymerization are the four principal techniques currently in use to synthesize polymer nanoparticles through the polymerization of monomers. In these four emulsion polymerization systems, surfactant is a key component in controlling the polymerization process, which plays an important role in formulating polymers that preserve microstructures of tunable topology and the length scale of the parent microemulsion template.[75]

### 2.4.1 Surfactant

Surfactant is one type of molecule that comprises both hydrophilic and hydrophobic groups simultaneously. The major function of surfactants is to stabilize the suspended particles in the emulsion systems. The surface activity of the surfactant can be evaluated using the hydrophile-lipophile balance (HLB) values, which can be calculated based on the structure of surfactant molecules. The HLB values (0-20) reflect the hydrophilicity of surfactant, and it increases with increasing hydrophilicity. Generally, the critical micelle concentration (CMC) increases with HLB values. Table 2-1 provides a general guide for the choice of surfactants that are most suited to meet the requirements of the specific application.

**Table 2-1 Ranges of HLB values and corresponding areas of applications**

| HLB Range | Application |
|---|---|
| 3-6 | Water-in-oil emulsions |
| 7-9 | Wetting |
| 8-18+ | Oil-in-water emulsions |
| 3-15 | Detergency |
| 15-18 | Solubilization |

#### 2.4.1.1 Single-tail Surfactants

Single-tail surfactants can be classified into three types: anionic, nonionic and cationic surfactants. Anionic surfactants are the most commonly used type in emulsion polymerization. These include sulfates (sodium lauryl sulfate), sulfonates (sodium dodecylbenzene sulfonate), fatty acid soaps (sodium or potassium stearate, laurate, palmitate), and the Aerosol series (sodium dialkyl sulphosuccinates) such as Aerosol OT (AOT, sodium bis(2-ethylhexyl) sulfosuccinate) and Aerosol MA (AMA, sodium dihexyl sulphosuccinates). The sulfates and sulfonates are useful for polymerization in acidic medium where fatty acid soaps are unstable or where the final product must be stable

towards either acid or heavy-metal ions. The AOT is usually dissolved in organic solvents to form the thermodynamically stable reverse micelles.[76]

Nonionic surfactants usually include the Brij type, Span-Tween 80 (a commercial mixture of sorbitol monooleate and polysorbate 80), Triton X-100 [polyoxyethylene(9)4-(1,1,3,3-tetramethylbutyl)-phenyl ether], PEO, PVA, and hydroxyethyl celluloseare surfactants. Nonionic surfactants are seldom used alone, since their efficiency in producing stable emulsions is less than that of the anionic surfactants. The nonionic surfactants such as PEO and PVA are usually used in combination with anionic surfactants to improve the freeze-thaw and shear stability of the polymer or to assist in controlling the particle size and its particle size distribution (PSD). The presence of the nonionic surfactant imparts a second mode of colloidal stabilization, cooperated by both the electrostatic stabilization endowed by the anionic surfactant and the steric interference with the van der Waals attraction between polymeric particles. Anionic surfactants are generally used at a level of 0.2-3 wt% based on the amount of water and the nonionic surfactants used at the 2-10% level.[76] Nonionic surfactants are also of use where the final polymer latex is expected to be insensitive to changs in pH over a wide range

Cationic surfactants such as dodecylammonium chloride (DAC), cetyltrimethylammonium bromide (CTAB), and dodecyltrimethylammonium bromide (DTAB) are much less frequently used than anionic surfactants due to their relatively inefficient emulsifying action or adverse effects on initiator decomposition. In addition, the cationic surfactants are much more expensive than anionic surfactants.

#### 2.4.1.2 Gemini-type Surfactants

Gemini (dimeric) surfactants are made up of two surfactants like moieties connected at the level of the head groups or on alkyl chains in close vicinity to the head groups by a spacer group of varying nature and length (Figure 2-1). The Gemini surfactant was first reported in the literature as early as 1974,[77] but has only been the object of a renewed interest in the last decade.[78,79] The Gemini surfactants such as those commercialized by Sasol GmbH (Marl, Germany) can be found in the market.

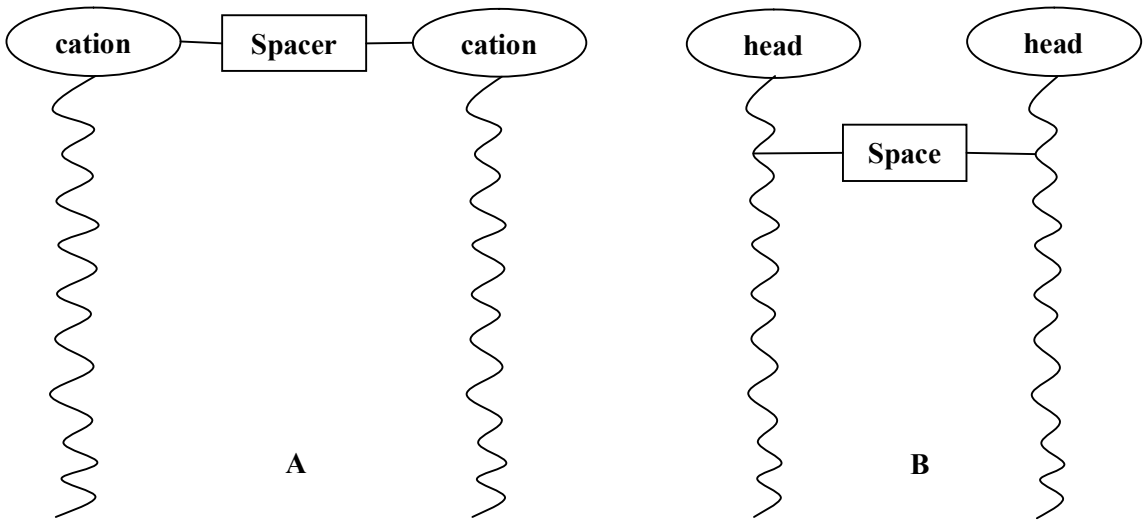


**Figure 2-1 Schematic representation of Gemini surfactant with the spacer group connecting (A) the two head groups (often the case for cationic surfactants), and (B) the alkyl chains at a location very close to the head group (case of nonionic and anionic Gemini surfactants).**

The Gemini surfactant provides a promising direction to develop new surfactant systems which not only support the interface stabilization of polymerizable (micro)emulsions but enable the synthesis of preserved particles at lower surfactant loads.[80] It is common knowledge that excess surfactant in the product will render a considerably negative impact on the properties and post-treatment of synthesized bulk polymers or polymeric latices, due to the fact that the common recipes involved in the (micro)emulsion polymerizations still require large amounts of expensive surfactant.[81,82] Nevertheless, the separation process is tedious and costly.[83,84] Recent studies showed that two approaches can be used to design and develop new surfactant systems with improved emulsifying properties.[80,85-87] The first route is to prepare the surfactants with diverse organic counterions by means of the assemblies of conventional cationic surfactants with multivalent counterions.[85] The second one is to replace the conventional single-tail surfactants using the Gemini surfactant.[80,86] It was reported very recently that the amount of Gemini surfactant used in the polymerization of aniline is much less than that of conventional surfactant as a micelle stabilizer.[87] Up to now, only a few cases have been reported on the use of the assemblies of Gemini surfactant

molecules as a platform for polymerization reactions and the studied monomers were only limited to styrene[80,86] and aniline.[87]

Compared to the conventional single-tail surfactants, the Gemini surfactants have the following advantages:[88-89]

(1) The CMC values of Gemini surfactants are at least one order of magnitude lower than that of corresponding conventional single-tail surfactants with a similar head group. The CMC values of commonly reported Gemini surfactants and some classic conventional surfactants are listed in Table 2-2.

(2) It is observed that the Gemini surfactants are 10-100 times more efficient in decreasing the surface tension of water and the interfacial tension at an oil/water interface than single-tail surfactants.

(3) The Gemini surfactants have better solubilizing, wetting, foaming, and lime-soap dispersing ability than conventional surfactants.

(4) Some types of Gemini surfactants with a short spacer have some special rheological properties such as viscoelasticity and shear-thickening at relatively low concentration when they are dissolved in water.

(5) The micelles present in the aqueous solutions of some types of Gemini surfactants can form unusual shapes for instance ring-like or elongated with numerous branches.

Gemini surfactants with an enormous variety of structures can be synthesized through connecting any two identical or different single-tail surfactants by a spacer group that can be hydrophilic or hydrophobic, flexible or rigid, heteroatomic, aromatic, and so forth. Therefore, the structures and properties of Gemini surfactants can be well controlled based on a given application. Considering the practical applications of Gemini surfactant, the phase behavior is the most important factor to govern its properties.

The concept of Gemini surfactants has currently been extended to more complex homologues including the trimeric surfactants made up of three surfactant-like moieties connected by two spacer groups and tetrameric surfactants, and so forth. The new Gemini

and oligomeric surfactants that will be synthesized in the future are anticipated to possess novel and unexpected properties.[88]

**Table 2-2 CMC values of representative single-tail and Gemini surfactants[78]**

| Surfactant | CMC/mM |
|---|---|
| 1 $C_{12}H_{25}N^+(CH_3)_3\ Br^-$ (DTAB) | 16 |
| 2 $C_{12}H_{25}N^+(CH_3)_3\ Cl^-$ (DTAC) | 22 |
| 3 $C_{16}H_{33}N^+(CH_3)_3\ Br^-$ (CTAB) | 1 |
| 4 $C_{12}H_{25}OSO_3^-Na^+$ (SDS) | 8 |
| 5 $C_{12}H_{25}N^+(CH_3)_2$-$(CH_2)_n$-$N^+(CH_3)_2C_{12}H_{25}\ 2Br^-$ ($n$ = 3–8) | 1 |
| 6 $C_{12}H_{25}N^+(CH_3)_2$-$(CH_2)_{16}$-$N^+(CH_3)_2C_{12}H_{25}\ 2Br^-$ | 0.12 |
| 7 $C_{16}H_{33}N^+(CH_3)_2$-$(CH_2)_2$-$N^+(CH_3)_2C_{16}H_{33}\ 2Br^-$ | 0.003 |
| 8 $C_8H_{17}N^+(CH_3)_2$-$(CH_2)_3$-$N^+(CH_3)_2C_8H_{17}\ 2Br^-$ | 55 |
| 9 $C_{12}H_{25}N^+(CH_3)_2$-$(CH_2)_2$-O-$(CH_2)_2$-$N^+(CH_3)_2C_{12}H_{25}\ 2Cl^-$ | 0.5 |
| 10 $C_{16}H_{33}N^+(CH_3)_2$-$(CH_2)_5$-$N^+(CH_3)_2C_{16}H_{33}\ 2Br^-$ | 0.009 |
| 11 $C_{16}H_{33}N^+(CH_3)_2$-$(CH_2)_2$-O-$(CH_2)_2$-$N^+(CH_3)_2C_{16}H_{33}\ 2Br^-$ | 0.004 |
| 12 $C_{16}H_{33}N^+(CH_3)_2$-$CH_2$-$(CH_2$-O-$CH_2)_3$-$CH_2$-$N^+(CH_3)_2C_{16}H_{33}\ 2Br^-$ | 0.02 |
| 13 $C_{12}H_{25}N^+(CH_3)_2$-$CH_2$-CH(OH)-$CH_2$-$N^+(CH_3)_2C_{12}H_{25}\ 2Br^-$ | 0.8 |
| 14 $C_{12}H_{25}N^+(CH_3)_2$-$CH_2$-$C_6H_4$-$CH_2$-$N^+(CH_3)_2C_{12}H_{25}\ 2Br^-$ | 0.03 |
| 15 $C_{12}H_{25}N^+(CH_3)_2$-$CH_2$-CH(OH)-CH(OH)-$CH_2$-$N^+(CH_3)_2C_{12}H_{25}\ 2Br^-$ | 0.7 |
| 16 $C_{12}H_{25}N^+(CH_3)_2$-$CH_2$-CH(OH)-$CH_2$-$N^+(CH_3)_2$-$CH_2$-CH(OH)-$CH_2$-$N^+(CH_3)_2C_{12}H_{25}\ 3Cl^-$ | 0.5 |
| 17 $C_{12}H_{25}OPO_2^-$-O-$(CH_2)_6$-$OPO_2^-$-$OC_{12}H_{25}\ 2Na^+$ | 0.4 |
| 18 $C_{10}H_{21}$O-$CH_2$-CH($OSO_3^-$)-$CH_2$-O-$(CH_2)_2$-O-$CH_2$-CH($OSO_3^-$)-$CH_2$-$OC_{10}H_{21}\ 2Na^+$ | 0.01 |

### 2.4.2 Emulsion Polymerization

Emulsion polymerization has traditionally been the most important process for manufacturing polymer colloids, especially for (meth)acrylate type monomers. The emulsion system usually consists of an initiator which can be water-soluble or oil-soluble, a chain transfer agent, and a surfactant. The largest portion of the monomer (>95%) is dispersed and forms large monomer droplets with sizes over the range of 1 to 10 μm depending on the stirring rate. The monomer droplets are stabilized by surfactant molecules absorbed on their surfaces. When the concentration of surfactant exceeds the CMC, the surfactant molecules will be self-assembled as the micelles, which contain 50 to 100 surfactant molecules per micelle. The size of micelles is between 4-5 nm. The size of monomer-swollen micelles, which contains around 2% monomer, is typically between 5-15 nm. The polymerization site is located inside of the micelles. The concentration of micelles ($10^{19}$-$10^{21}$/L) is much higher than the concentration of monomer droplets (about $10^{12}$-$10^{14}$/L), which results in that the initiator induced radicals are more likely to enter a micelle than a monomer droplet.[90] As the polymerization proceeds, the monomer molecules are transferred to the growing micelles

from the monomer droplets. When the conversion of monomers reach around 50 to 80%, the monomer droplets will disappear and the micelles at last become large polymer-containing droplets. This suspension system is the so-called latex. In an inverse emulsion polymerization, the hydrophilic monomer rather than hydrophobic one in a normal emulsion, is dispersed in an organic liquid.

It has been well recognized that there are three distinct intervals existing in the progression of an emulsion polymerization. Interval Ⅰ is the initial stage where the particle formation takes place, i.e. micelles. The mechanism of particle nucleation is mainly divided into the homogeneous nucleation and heterogeneous nucleation. The nucleation type is determined by the solubility of monomers and the initiators in the aqueous phase. Interval Ⅱ is characterized by a constant number of particles (polymerization location) and the presence of monomer droplets. The monomer-swollen particles grow and the monomer concentration within these particles is maintained constant by means of the monomer diffusing through the water phase from the monomer droplets. Interval Ⅲ begins with the disappearance of monomer droplets, after which the monomer concentrations in both the monomer-swollen particles and water phases decrease continuously.[90,91]

There are some requirements for monomers used for the emulsion polymerization. The primary requirement for monomers is that they must have a limited water solubility and be soluble in the polymer as well. However, the solubility should not be too high, otherwise this monomer would tend to polymerize in the water phase. In the mechanism for emulsion polymerization one of the driving forces is the absorption of monomer into the polymeric particle; if the monomer and polymer are not mutually soluble then this process will not be efficient. Many different vinyl monomers are currently used in practical emulsion polymerization, including: acrylates, methacrylates, St, AN (in copolymers), VAc, isoprene, and BD. In addition, the monomers would not react with water, surfactants and other additives.

### 2.4.3 Microemulsion

An oil-in-water (O/W) or water-in-oil (W/O) microemulsion product consists of fine oil (or water) droplets (10 to 100 nm in diameter) dispersed in the continuous aqueous (or oily) phase with the aid of relatively large amounts of surfactant and/or cosurfactant (e.g., SDS and n-pentanol for O/W microemulsion). The produced polymeric particles generally have sizes of 10-100 nm, which is much smaller than that obtained by emulsion polymerization ranging from 100 to 500 nm. Although many of the characteristics of microemulsion polymerization parallel those of emulsion polymerization such as consisting of at least ternary mixtures of oil, water, and surfactant, the details are not exactly the same. First, the emulsion system is thermodynamically unstable, and exhibits flocculation and coalescence. In contrast, the microemulsion is a thermodynamically stable system. Second, microemulsion appears as a transparent liquid system while the emulsion usually appears translucent and milky white. Third, the water-soluble initiators are commonly used in the emulsion polymerization, but there are many reports of microemulsion polymerization with oil-soluble initiators.[82,92-93] Finally, the nucleation in emulsion polymerization occurs almost exclusively in the early portion of the process (interval I). Nevertheless, the nucleation in the microemulsion occurs over a larger portion of the process due to the large amount of micelles present. In contrast to emulsion polymerization, the reaction kinetics of the microemulsion polymerization is characterized by two polymerization rate intervals and the interval of constant rate characteristic of the emulsion polymerization is missing.[94-96] The polymerization rate of microemulsion was observed to increase with time, reach a maximum, and then decrease.

Microemulsion polymerization typically can involve three nucleation mechanisms: monomer droplet nucleation, micellar nucleation, and homogeneous nucleation. At the initial stage of polymerization, the monomer droplets have a fairly large surface area, which can easily capture the free radicals generated in the aqueous phase to form the particle nuclei. This is called microemulsion droplet nucleation. After the formation of the latex particles, the monomer molecules inside the droplets will diffuse out and enter the latex particles through the continuous phase in order to maintain the monomer concentration within these growing

particles. With increasing numbers and volumes of the growing particles, more and more monomers are required inside the particles. Therefore, in the early stage of polymerization at around 4% monomer conversion, the monomer droplets disappeared, which results in the formation of a large amount of mixed micelles comprised of surfactant, cosurfactant, and a small amount of monomers. These mixed micelles have very large surface area and thereby continue to capture the radicals in the aqueous phase to form the particle nuclei until the completion of the polymerization. It has been noted that the water solubilities of monomers have a significant effect on the particle nucleation process (i.e., relatively hydrophobic styrene versus relatively hydrophilic MMA). With respect to styrene, the droplet nucleation is predominant, however the micellar nucleation can not be ruled out. Nucleation taking place in the aqueous phase plays an important role, and a mixed mode of particle nucleation (droplet nucleation and homogeneous nucleation) is operative in the MMA polymerization. Mendizabal et al.[97] concluded that the extent of homogenous nucleation increases with increasing solubility of the monomer in water in the microemulsion.

Although microemulsions can be used as an attractive pathway to prepare the fine latex particles, the formulation of microemulsions has been suffering from severe constraints due in a large part to the high surfactant level required to not only emulsify the relatively low amount of monomers but also achieve their thermodynamic stability. This fact is in contradiction to the requirement of high solid contents in engineering polymers. That is one important reason that hinders the wide application of microemulsion polymerization in industry. In order to alleviate these limitations involved in the microemulsion polymerization, a monomer-starved semibatch microemulsion polymerization was thereby put forward and studied extensively by many investigators, and will be introduced in Section 2.4.5.

### 2.4.4 Miniemulsion

A miniemulsion (also known as nanoemulsion) is a special case of an emulsion. Miniemulsions are typically formed by subjecting a mixture of water, monomer, co-stabilizer, surfactant, and initiator to a high shear process (sonication, high pressure

homogenisers, in-line mixers, etc) that break up the oil phase into sbumicro sized monomer droplets.[98] The key differences between emulsion polymerization and miniemulsion polymerization are utilization of a co-stabilizer and a high-shear device. Miniemulsion polymerizations are very useful for producing high solid content latices, which have typically a size between 50 and 500 nm. Both water-soluble and oil-soluble initiators can be employed in miniemulsion polymerization. Many different monomers such as acrylates, methacrylates, fluoroacrylates, and acrylamides have been well performed via miniemulsion polymerization. The polymerization of the monomer droplets leads to particles which ideally keep their size.

The initial miniemulsion was not stable enough to start the polymerization reaction. In the miniemulsion system, there are two degradation mechanisms tending to destabilize the monomer droplets. The first destabilization mechanism is the coalescence of the interactive monomer droplets due to attractive Van der Waals force. The second one is the Ostwald ripening process. This emulsion destabilization mechanism refers to diffusional degradation of droplets caused by transport of monomers from the small droplets with a higher chemical potential, to dissolve in water, diffuse through the aqueous phase, and then enter the larger droplets. Therefore, larger monomer droplets will continue to grow in size at the expense of smaller droplets. Ultimately, the miniemulsion will be destabilized by this diffusional degradation process.

In order to minimize the above mentioned two destabilization mechanisms, besides the normal surfactant, addition of an extremely hydrophobic species (hydrophobes) is indispensable.[99] Generally, the colloidal stability of the emulsion can be improved significantly by incorporation of 1-5 wt% costabilizer into the disperse phase. The existence of the hydrophobe can effectively retard the diffusion of monomer molecules from small monomer droplets to large ones due to an osmotic pressure effect. Diffusion of monomer species from a small monomer droplet to a large droplet results in a concentration gradient for costabilizer between these two droplets. However, unlike common monomers such as MMA, the extremely hydrophobic costabilizer molecules in the small monomer droplet are incapable of being dissolved in water, not to mention diffusing across the continuous aqueous phase and then entering the large droplet. Therefore, the hydrophobe cannot migrate from the

small droplets to the larger ones to counterbalance the resultant concentration gradient between these two droplets. This will then build up an osmotic pressure, which will force the monomer molecules in the large droplets to diffuse back to the small droplets, in order to relax the concentration gradient for the costabilizer established between these two droplets and a relatively stable miniemulsion is obtained. As a result, the total oil-water interfacial energy of this dispersed system is greatly reduced. The miniemulsions are thus thermodynamically unstable, but kinetically metastable, with lifetimes as long as several months. Typical examples of the costabilizer include long-chain alkanes such as hexadecane and alcohols such as cetyl alcohol. The preparation of a stable miniemulsion generally involves specially designed recipes and procedures. Such a homogenization process requires a relatively long pre-emulsification period with intensive mixing and a certain amount of emulsifier and coemulsifer. In the case of a long chain alcohol with gel formation, strong agitation is required. While, a mild agitation is usually sufficient to prepare a stable miniemulsion. When a long-chain alkane is used, a large shear force is required to prepare a stable miniemulsion.

Recently, quite a few studies have been reported using the miniemulsion system as the toolbox. Tsavalas et al.[100] carried out a miniemulsion polymerization with a three-component acrylic system consisting of MMA, BA, and AA in the presence of an unsaturated polyester resin. A high level of cross-linking (over 70%) was observed during polymerization in this particular hybrid system. Electron microscopy was used to examine the hybrid particle morphology and it was found that the acrylic matrix contained an internal domain of polyester resin. Gooch et al.[101] also carried out a hybrid miniemulsion polymerization with acrylic monomers (MMA, BA, and AA) in the presence of oil-modified polyurethanes (OMPU). Li et al.[102] used miniemulsion polymerization to prepare the urethane/BMA latex and a particle size with around 50 nm was reached. Blends prepared from these particles show evidence of phase separation.[103] The hybrid miniemulsion polymerization of acrylate in the presence of linoleic acid and sunflower seed oil can be used to provide better homogeneity of the hybrids, which is able to improve the elastomeric mechanical properties.[104]

### 2.4.5 Semibatch Microemulsion

The microemulsion polymerization is an effective method to prepare the fine nanoparticles with both high molecular weight and interesting morphologies, which however requires a high surfactant concentration to emulsify a relatively low monomer content, typically 1 to 3 g surfactant per gram of polymer.[105] That is one important reason that hinders the wide application of microemulsion polymerization in industry due to the fact that large amounts of retained surfactant in the latex has a considerab negative impact on the properties of synthesized polymers and the separation process is tedious and costly.[106] In order to alleviate this drawback, a monomer-starved semibatch microemulsion polymerization was put forward. Semibatch microemulsion polymerization is a new and effective approach for preparing nano-size polymer particles and has attracted significant attention. Different terms such as modified microemulsion,[107-109] multiple addition,[110] differential,[111] Winsor-I,[112-114] modified Winsor-1,[115] and semibatch or semicontinuous (micro)emulsion polymerization[116-120] have been used to describe this process.

The semibatch microemulsion polymerization is a unique process for manufacturing fine polymer nanoparticles while maintaining a high weight ratio of polymer to surfactant. By controlling the monomer feeding rate, the polymer chain growing radicals will consume the monomer molecules faster than the rate of monomer molecules added into the reaction system, by which the monomer "starved" condition is produced and maintained until the end of polymerization. Therefore, the monomer molecules are considered to be delivered to the reaction locus from an external reservoir rather than from the interior of nanodroplets (e.g. microemulsion mechanism). It has been recently shown that this process can produce a large number of small particles of high MW with narrow distribution.[111] The monomer-starved semibatch microemulsion polymerization provides a practical way to enhance particle formation and thus to produce nanolatices. A large difference in number of particles ($N_p$) of the order of $10^1$-$10^3$ can be observed between batch and semibatch microemulsion polymerization processes.[106] Note that polymerization under monomer-starved conditions can lead to a greater enhancement in particle formation if monomers are water soluble. The exit of radical to water phase significantly increases as monomers, or monomeric transferred

radicals, become more soluble in the water phase. This leads to a higher flux of radicals in the water phase and an increase in nucleation.

In a common semibatch operation mode, some fractions of reactants, i.e. the initial charge, are initially charged into the reactor, and the rest of the formulation is continuously provided as feed over some period of time (Figure 2-2).

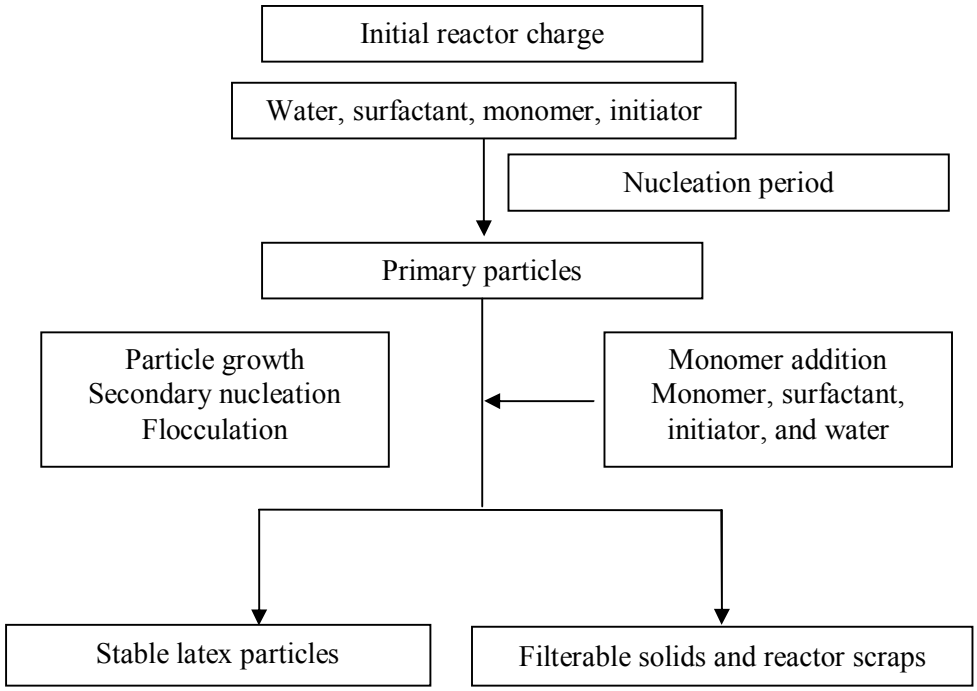


**Figure 2-2 Flow chart for a typical semibatch (micro)emulsion polymerization process.**

Specifically, there are three popular modes of semibatch operation processes. The first one is the fully semibatch microemulsion process, in which the polymerization starts with an aqueous solution only containing a surfactant and an initiator (micellar solution), and then the monomer feed is provided in very small drops at a given rate. The second one is the seeded polymerization mode, where all the recipe ingredients, and an initial charge of monomer(s), are added to the reactor initially; the remaining monomer is then fed in at some predetermined flow rate. The third one is the emulsion addition mode which consists of

charging all the recipe ingredients with some of the monomer and emulsifier, and feeding in the remainder of the monomer/emulsifier mixture. In a semibatch reactor, the rate of polymerization will depend on whether or not the system becomes flooded with monomer during the reaction.

Wessling[121] studied the reaction kinetics of semibatch (micro)emulsion polymerization based on a mass balance and developed a kinetic model for the rate of polymerization at near-steady state condition:

$$R_p = \frac{R_a}{1 + [N_A/(k_p N_p \tilde{n})](\mathrm{MW}_m/\rho_m)R_a} \quad (2\text{-}1)$$

where $R_p$ is the rate of polymerization, $S^{-1}$; $R_a$ is the monomer feed rate, L/(s•L(aq)); $N_A$ is Avogadro's constant; $k_p$ is the propagation rate constant, L/(mol•s); $N_p$ is the number of latex particles per unit volume of water, $\tilde{n}$ is the average number of free radicals per particles, and $\mathrm{MW}_m$ and $\rho_m$ are the molecular weight and the density of monomer, respectively.

As depicted in Eq. (2-1), under the monomer-starved conditions, i.e., $R_a < R_p$, the rate of polymerization $R_p$ approaches the magnitude of $R_a$ because $R_a$ is small. Likewise, when the reaction system is operated under monomer-flooded conditions, i.e., $R_a$ is sufficiently large, the rate of polymerization $R_p$ is equal to the term $[(k_p N_p \tilde{n})/N_A](\rho_m/\mathrm{MW}_m)$. In other words, under monomer-flooded conditions, the latex particles are saturated with monomer throughout the polymerization and the rate of polymerization is independent of the monomer feeding rate until the monomer addition is completed. Although the monomer-flooded condition can increase the productivity of latex manufacturing through shortening the semibatch cycle time, this condition should be avoided in commercial production because of the high exothermic heat activity. Chern et al.[122] studied the effects of various reaction parameters on the colloidal stability of acrylic latex particles emulsified by SDS during the polymerization. They reported that the higher the polarity of latex particle surfaces, the lower the amount of surfactant that can be absorbed on the oil-water phase. In addition, they found that the latex particles will lose their colloidal stability rapidly above a certain level of solid content due to the so-called crowding effect. Roy et al.[123] carried out a copolymerization

of MMA and n-butyl arylate (BA) using microemulsion polymerization through semicontinuous addition of a monomer emulsion to obtain a 40 wt% solid content of latex of about 30 nm particle size using 4 wt% Dowfax 2A-1 as surfactant and 0.4 wt% acrylamide as cosurfactant. Ming et al.[124] produced a microlatex of PMMA by adding the monomer very slowly to a prepolymerized ternary microemulsion. Number-average diameters of 33-46 nm and solid content of 6-24 wt% were achieved using DTAB of less than 1 wt% of the reaction mixture. They also reported a poly(methyl acrylate) (PMA) nano-size latex of about 15 nm containing up to 30 wt% PMA at a high polymer to SDS weight ratio of 25:1. In those reports mentioned above, an initial microemulsion consisting of the monomer was usually prepared before the semicontinuous addition of additional monomer. He et al.[125] directly added the monomer into the mixture of surfactant, initiator and water via a differential manner, by which the surfactant consumption was further reduced without detrimental effects on the size of the nanoparticles and solid content. A PMMA nano-size latex with a size of 13-16 nm and a solid content of 13.7 wt% was synthesized with monomer/surfactant and water/surfactant weight ratios up to 18:1 and 120:1 respectively. He et al.[126] also employed the differential microemulsion polymerization to synthesize the PMMA/PS core shell nanoparticles. They showed that when starting the polymerization with a small amount of MMA to form nanoseeds, the size of the PS particles was significantly decreased and particles smaller than 20 nm were achieved at an SDS/(St+MMA) weight ratio of 0.043.

#### 2.4.5.1 Consideration of Semibatch Microemulsion Polymerization in Large-Scale Production

Semibatch (or semicontinuous) reactors are industrially important for copolymer production due to their versatility and most commercial products are currently manufactured via semibatch operated reactors.

The choice of reactor configuration, polymerization process, and mode of operation is dependent upon the desired copolymer composition, molecular weight and distribution, and end-use considerations. Using a semibatch microemulsion process has several appealing properties. The cold monomer feed(s) allow for greater productivity by controlling the

exotherm should the reactor be limited in cooling capacity. The operation usually results in a lower residual monomer content in the latex. This reduces or eliminates the need for recovery and recycle of monomer which, in turn, may help to eliminate and effectively control the buildup of undesirable impurities in the feed stream.

Alternatively, seeded polymerizations can be used to eliminate the particle nucleation stage, thus controlling the particle size distribution. The growth rate of the particles and the rate of polymerization can be controlled by the rate of addition of monomer. The breadth of PSD in a monomer starved semibatch microemulsion polymerization can also be altered by variation in the rate of monomer addition. PSD of emulsion latices, in addition to the average size of particles, has significant implications on properties such as latex rheology, film formation, adhesion, etc. It has been shown experimentally,[127] and then confirmed by simulation,[128] that the PSD of particles formed in the semibatch microemulsion polymerization with a neat monomer feed depicts a shoulder at the smaller size range when nucleation starts under flooded conditions and then continues into starved conditions. This condition may occur when the rate of monomer addition is sufficiently high to allow polymerization to start under flooded conditions, but not too high to prevent extension to starved conditions. One may apply strategies to improve productivity by minimizing the semibatch feed time and increase $R_p$ should the system become flooded with monomer.

Molecular weight considerations in semibatch processes are more complex. The monomer concentration in the particle, $[M]_p$, will affect the molecular weight of the copolymer produced. As mentioned, a low feed rate results in a truly starved-fed reaction (i.e., a low $[M]_p$). This decreased concentration of monomer in the particles may decrease the rate of polymerization in the particles, thereby lowering the molecular weight of the polymer produced.

Copolymer composition is a function of the reactivity ratios and the concentration of monomers at the reaction site. Copolymer composition and composition drift may be controlled by monomer addition policies, combined with initiator addition and temperature programming policies run in parallel, especially in the diffusion-controlled regime.

#### 2.4.5.2 Particle Nucleation Stage

Particle nucleation by far is the most important phenomenon in free radical polymerization. It has generated much research interest and remains the most active and sought-after subject in the kinetics of free radical polymerization.

On the one hand, in the seeded semibatch microemulsion polymerization, the nucleation stage was completed via a microemulsion polymerization nucleation mechanism before the monomers were added subsequently. Afterward, the average particle size will increase with the continuous feeding of monomers, similar to that in conventional batch emulsion polymerization. The extent of increase in the particle size after nucleation depends on the number of particles in the latex. The rise in the size of particles can be slowed down by using a lower $R_a$. This produces a larger $N_p$ and breaks down the growth over a larger number of particles.

On the other hand, in a fully semibatch microemulsion polymerization, polymerization starts with monomer-swollen micelles with no monomer droplets present, and particle formation occurs under fully monomer-starved conditions via addition of a neat monomer feed. Micellar nucleation and homogeneous nucleation mechanisms are the predominant nucleation forms and homogenous nucleation becomes more important with the increase of hydrophilicity of the monomers. The end of nucleation is marked by depletion of emulsifier micelles. The number of particles will be stabilized after completion of nucleation. Particle growth continues under monomer starved conditions with further addition of monomer.

Sajjadi carried out a series of monomer-starved semibatch (micro)emulsion polymerizations including the MMA, VAc and BA and proposed that a common feature of nucleation process under starved conditions is a decrease in the average size of particles in the initial stage of nucleation for polymerizations using intermediate feed rates before a subsequent increase with further addition of monomer.[106] Note that in the monomer-starved semibatch microemulsion polymerization, the monomer concentration in the growing particles does not remain constant and varies during nucleation. The early particles are swollen with more monomer and can grow to a greater extent than the later particles that

retain less monomer. However, the free radicals are very difficult to be captured by the polymer particles during the early stage of nucleation because a large number of ready-to-be-used micelles are present in the system. This indicates that the entry of radicals from the aqueous phase plays an insignificant role in the growth of the early particles. Alternatively, the early particles have a greater chance to retain the primary radicals, formed by transfer to monomer, and undergo a subsequent growth. As the polymerization proceeds with time, the newly initiated polymer particles progressively become leaner in the monomer and smaller in size so that the chance of retaining the primary radical becomes slimmer. As a result, the average size of particles may decrease accordingly until the monomer concentration in the polymer particles reaches a near-steady state value. Afterward, the average particle size will increase with time, similar to that in a conventional batch emulsion polymerization. The end of nucleation can be determined from the levels off of $N_p$ or from surface tension-time curves where the surface tension starts increasing.[106]

In addition, there is a decrease in the size of particles with decreasing monomer feeding rate. This is because the lower $R_a$ can produce a larger $N_p$ and breaks down the growth over a larger number of particles, which thus leads to the smaller particle size and narrower particle size distribution.

In short, nanolatices with low consumption of emulsifier and high solids content can be produced by taking advantage of monomer starved semibatch microemulsion polymerization.

## 2.5 Summary

Polymer nanoparticles represent a promising research direction to provide new solutions to the challenges encountered in current scientific research and technological innovation. In this review, the fundamental knowledge related to the polymer nanoparticles was covered. The applications of polymer nanoparticles in green catalysis, the biomedical field, and conducting materials were addressed. There are two main strategies that can be employed to prepare the polymer nanoparticles characterized by the dispersion of preformed polymers and the direct polymerization of monomers. Conventional emulsion, microemulsion, miniemulsion, and semibatch microemulsion polymerization are the four principal techniques currently in use to

synthesize the polymer nanoparticles. Surfactant is a key component in controlling the polymerization process, and Gemini surfactant stands for a promising direction to develop the new surfactant systems in the future. More effort is required to develop robust synthesis technique, prepare new functional nanoparticles and explore the potential applications of polymer nanoparticles.

# Chapter 3
# Experimental Techniques and Characterization Methods

## 3.1 Experimental Techniques

### 3.1.1 Synthesis of Polymer Nanoparticles

The polymer nanoparticles prepared in this project include poly(methyl methacrylate) (PMMA), poly(acrylonitrile-*co*-butadiene) (NBR), hydrogenated poly(acrylonitrile-*co*-butadiene) (HNBR), PMMA-NBR core-shell, PMMA-HNBR core-shell nanoparticles. Among them, PMMA, NBR, and PMMA-NBR are synthesized using semibatch microemulsion polymerization techniques. Various polymerization systems are implemented differing in the way of different monomers, temperature, reactor (glassware or Parr stainless steel reactor), surfactant (SDS or Gemini surfactant), initiator (APS, AIBN, or BPO) as well as the stages employed in the semibatch polymerization (one stage or two stage).

### 3.1.2 Preparation of Hydrogenated Polymer Nanoparticles

The hydrogenated polymer nanoparticles including HNBR and PMMA-HNBR core-shell nanoparticles were prepared through *Direct Catalytic Latex Hydrogenation*.

A catalyst pre-dispersion approach was employed in the present latex hydrogenation. It is called the catalyst pre-dispersion method because there is an introduction period allowing for the mass transfer of catalyst into the latex particles before the initiation of hydrogenation.

The latex hydrogenation of polymer nanoparticles containing olefin functional groups was carried out in the same Parr reactor. A measured volume of the polymer latex (25 mL) with added distilled water (75 mL) was first mixed with a certain amount of $RhCl(P(C_6H_5)_3)_3$ and the required additive TPP with a weight ratio of 10:1 to the catalyst. The TPP plays a vital role in the hydrogenation as it maintains the activity of Wilkinson's catalyst. The mixture was then degassed with three quick $N_2$ cycles and subjected to bubbling $N_2$ under about 1.38 MPa for 20 min at room temperature at an agitation speed of 200 rpm. The resulting mixture was heated up to a setup temperature and stabilized for 2 h under 600 rpm. The

hydrogenation reaction commenced when the hydrogen gas with a pressure of 6.89 MPa was introduced into the reactor. The hydrogen pressure (6.89 MPa), hydrogenation temperature, and agitation speed (600 rpm) were maintained constant throughout the reaction period. Aliquots were taken at various time intervals through a dip tube and then characterized using FT-IR to obtain the degree of hydrogenation. After a given reaction time, the system was cooled down to room temperature and depressurized to obtain the final product.

## 3.2 Characterization Methods

### 3.2.1 pH of Latex

The pH measurements were performed using a Corning Scholar 425 pH meter equipped with a combined glass electrode (Corning Inc. Corning, New York, US). The pH meter was subjected to a two point calibration prior to use with standard buffer solutions of pH 4.0 and 10.0. For each latex sample, three measurements were carried out and the mean value was reported.

### 3.2.2 Isolation of Polymer

In a typical washing process, around 5 mL of latex was first added continuously into 50 mL of methanol which was being stirred (100 rpm). The methanol suspensions were then filtered through a Buchner funnel. The agglomerated small polymer crumbs were collected and put on a piece of wire gauze, and then rinsed with a large amount of water and methanol alternatively three times to make sure that all materials which are entrapped inside the polymer network were removed. Finally, the crumbs were compacted, followed by drying at room temperature under vacuum until a constant weight was reached. The polymerization conversions of monomer(s) were calculated by a gravimetric method.

The solid content ($S$ wt%) was calculated using below equation:

$$S\% = W_d/W_L \times 100\% \qquad 3\text{-}1$$

where $W_d$ and $W_L$ represent the weight of the polymer and latex, respectively.

The polymerization conversion ($C$ wt%) was calculated using below equation:

$$C\% = W_d / W_m \times 100\% \qquad 3\text{-}2$$

where $W_d$ and $W_m$ represent the weight of the polymer and added monomers, respectively.

### 3.2.3 Particle Size and Its Distribution

The size and number size distribution (non-negative least squares method) of the polymer particles of the synthesized latex were determined by dynamic light scattering (DLS) at 25 °C using a Nanotrac 150 particle size analyzer (BETATEK Inc., Canada) and reported as the number average diameter. The calculations of the particle size distributions were performed using Microtrac FLEX 10.2.14 software available from BETATEK Inc., which employed single-exponential fitting, non-negatively constrained least-squares (NNLS), cumulants analysis, and CONTIN particle size distribution analysis routines.

### 3.2.4 Molecular Weight and Its Distribution

The molecular weight and polydispersity index were determined by size exclusion chromatography (SEC, Model 305 TDA, Viscotek, Houston, US). The dried PMMA-NBR samples were first dissolved in THF and filtered through a 25 mm syringe filter with 450 nm GHP membrane (Pall Corp., New York, US) and then 100 μL of the solution was injected into the SEC analysis column using THF as eluent at a flow rate of 1.0 mL/min. The detectors are a triple detector system with a multi-angled laser light scattering setup equipped with an RI detector and Viscometer detector. Polystyrene standard (PS 99 K, $\overline{M}_w$=98251, $\overline{M}_n$=96722, IV=0.477 in THF at 30 °C) was used for calibration.

### 3.2.5 Normal TEM

A LEO 912 AB 100 kV Energy Filtered Transmission Electron Microscopy (EFTEM) (Carl Zeiss Inc., Germany) was used to confirm the size and observe both the morphology and core-shell structure of the polymer nanoparticles. When preparing samples for the normal TEM measurement, the nano-size latex was first diluted with distilled water and then 10 μL of the diluted solution was incubated on a 400-mesh copper grid at room temperature. Excess

solution was drawn off the edge of the grid with tissue paper. Next the grid was negatively stained with 2% (w/v) uranyl acetate for 1 min. The excess staining medium was drawn off with tissue paper and the grid was then delivered into the TEM chamber for imaging.

### 3.2.6 Cross Section TEM

Before sending the samples for the analysis of cross section TEM, the samples were first carefully ground and then immersed in 100% ethanol for 2 h with three changes of ethanol. The ethanol was then removed and replaced with a 50/50 (v/v) mixture of ethanol and LR White resin. This was left overnight with mixing. The 50/50 mixture was replaced by pure LR White resin and stirred for 3 h. The sample was then put into a gelatin capsule. Once the sample had sunk to the bottom of the capsule the resin was polymerized at 60 °C overnight. Thin sections around 75 nm thick were cut with an ultramicrotome. The resulting sections were mounted on 100-mesh copper grids and stained with 2% (w/v) uranyl acetate (7 min) and Reynold's lead citrate (3 min). The prepared samples were viewed using a LEO 912 AB EFTEM.

### 3.2.7 SEM

LEO model DSM 982 Gemini Field Emission Scanning Electron Microscopy (FESEM) at an accelerating voltage of 5 kV (GmbH, Oberkochen, Germany) was employed to study the aggregate morphology of the bulk NBR nanoparticles after coagulation. The NBR latex was first coagulated and purified (as described in section 3.2.2). Then the dried bulk polymer sample was directly affixed on an SEM stub using a conductive carbon tape. A thin layer of gold was sputter-coated on the sample for charge dissipation during FESEM imaging.

### 3.2.8 FTIR

Polymer compositions were determined via Fourier transform infrared spectroscopy (FTIR) analysis using a Bio-Rad FTS 3000MX spectrometer (Bio-Rad Laboratories, Ltd., Massachusetts, US). The polymer solid was first dissolved in MEK, and a polymer film was cast onto a sodium chloride disc for FTIR analysis.

### 3.2.9 Polymer Composition and Hydrogenation Degree

The polymer composition and hydrogenation conversion were determined by FTIR recorded on a Bio-Rad FTS 3000MX spectrometer (Bio-Rad Laboratories, Inc. Philadelphia, US). In a typical run, the latex aliquot with a certain degree of hydrogenation was first isolated to obtain the polymer solid (as described in Section 3.2.2). The dried polymer was then re-dissolved in MEK (around 0.5 wt%) and a polymer film was cast onto a sodium chloride disc for FTIR analysis. The calculation of the degree of hydrogenation is based on the corresponding absorbance ($A$) of the important peaks at 2236, 970, and 723 $cm^{-1}$ from the IR spectrum. The 2236 $cm^{-1}$ peak is assigned to the cyano group (C≡N). The 970 $cm^{-1}$ peak is assigned to the C=C (1,4-trans). The 723 $cm^{-1}$ is a new peak assigned to the $(CH_2)_n$, n > 4.

Let $\bar{A}_{(723)} = A_{(723)} / A_{(2236)}$ and $\bar{A}_{(970)} = A_{(970)} / A_{(2236)}$

$F = 1 + \bar{A}_{(723)} / K_{(723)} + \bar{A}_{(970)} / K_{(970)}$

where $K_{(723)}$ (= 0.255) and $K_{(970)}$ (= 2.3) are constants specific to the HNBR polymer.

Then, the relative amount of C=C remaining in HNBR is:

$C(\text{BR}) = \bar{A}_{(970)} / [K_{(970)} F]$

and the relative amount of methylene groups formed through hydrogenation of C=C in NBR is:

$C(\text{HBR}) = \bar{A}_{(723)} / [K_{(723)} F]$

Finally, the degree of hydrogenation can be calculated as:

Degree of hydrogenation (mol%) = $100 - C(\text{BR}) / [C(\text{BR}) + C(\text{HBR})] \times 100$

### 3.2.10 $^1$H NMR

$^1$H NMR spectra recorded on a Bruker 300 MHz Spectrometer (Bruker BioSpin Corp., Massachusetts, US) were used to confirm the degree of hydrogenation. The sample solution was prepared by dissolving 15-20 mg dried polymer solid into 1 mL $CDCl_3$.

### 3.2.11 Zeta-potential

The ζ-potential measurements of core and core-shell latex particles were determined using a Zetasizer Nano ZS (Malvern Instruments, Worcestershire, U.K.) at 25 °C. The latex samples were injected into a disposable cell (folded capillary DTS-1060 from Malvern, Worcestershire, U.K.) with a volume of ~1 mL and analyzed at constant voltage. The ζ-potential distribution (in mV) was automatically calculated from the electrophoretic mobility distribution based on the Smoluchowski formula. For each sample, the ζ-potential measurement was repeated three times and the mean value was reported. The ζ-potentials reported herein correspond to the average of the peak values of the ζ-potential distributions.

### 3.2.12 Cross-linking Examination

The cross-linking was estimated using a solvent extraction technique, which has been described in detail by El-Aasser and coworkers. Briefly, a certain amount of dried latex film of polymer was first cast and then mixed with acetone for 24 h. Afterwards, the mixture was sent for centrifugation at 20,000 rpm for 30 min at ambient temperature. The non-gel part of the sample is determined gravimetrically from the amount of solids remaining in the supernatant after the centrifugation and the gel fraction is the percentage of the insoluble polymer in the total film sample.

### 3.2.13 Glass Transition Temperature

The glass transition temperature ($T_g$) was measured by a differential scanning calorimetry (DSC; Q2000, TA Instruments, New Castle, DE, US). The temperature scan rate was at 10 °C/min. The values of $T_g$ were estimated as the temperature at the midpoint of the transition region from glassy to rubbery, which were given by *Universal Analysis 2000* software (version 4.5A Build 4.5.0.5) from the TA instruments. DSC scans were carried out in triplicate on all samples measured and the values presented are average values (typical error ±0.5 °C).

# Chapter 4
# Development of Micellar Nucleation Mechanism for Preparation of Fine Polymer Nanoparticles

## 4.1 Overview

Polymer nanoparticles below 20 nm with a solid content of more than 13 wt% and a narrow PDI ($\overline{M}_w / \overline{M}_n \sim 1.1$) were prepared using a micellar nucleation semibatch microemulsion polymerization system emulsified by SDS, with SDS/monomer (MMA) and SDS/$H_2O$ weight ratios of up to 1:16 and 1:100 respectively. It was found that for BPO, micellar nucleation is more favorable for the synthesis of smaller polymer nanoparticles than APS which gives rise to homogeneous nucleation and AIBN which involves partially heterogeneous nucleation. In the polymerization process, there exists a critical stability concentration (CSC) of SDS, above which the size of the nanoparticles is to be minimized and stabilized. With an increase in the monomer addition rate, the polymerization system changes from a microemulsion system to an emulsion system. A mechanism was proposed to describe the micellar nucleation process of semibatch microemulsion polymerization. This technique will pioneer a significant new way to use a simple but practical method to synthesize narrow PDI polymers, which is a very meaningful new development.

## 4.2 Introduction

Preparing polymer nanoparticles below 20 nm with a high ratio of polymer/surfactant is a great challenge.[1-21] Conventional microemulsion polymerization has been regarded as an especially suitable technique for producing nano-size polymer latices.[9-14] Nevertheless, there are two major drawbacks which need to be overcome. First, a high surfactant concentration (~15 wt%) is required to emulsify a relatively low monomer content of less than 10 wt%.[6-9] Second, the synthesized nanoparticles have a size above 20 nm, which usually are accompanied by a broad PSD and a wide PDI.[8-14]

The purpose of this work is thereby to prepare polymer nanoparticles of less than 20 nm using a micellar nucleation semibatch microemulsion polymerization system, explore the

initiation nucleation mechanism of the present polymerization system and further to better control the synthesis of polymer nanoparticles. With the MMA polymerization as the model system, we in particularly studied the effect of the BPO initiation mechanism, i.e. micellar nucleation[22] on the properties of PMMA nanoparticles in the present system. For comparison purposes, two types of representative initiators, i.e., water-soluble APS and oil-soluble AIBN were also studied in the semibatch microemulsion polymerization system. Finally, the influence of surfactant concentration and addition rate of the monomers on the properties of nanoparticles was investigated.

## 4.3 Experimental

### 4.3.1 Materials and Apparatus

Methyl methacrylate (MMA; 99%), sodium dodecyl sulfate (SDS; 99%), benzoyl peroxide (BPO; 97%), ammonium persulfate (APS; 98%), 2,2'-azobisisobutyronitrile (AIBN; 98%), ethanol (reagent grade), tetrahydrofuran (THF; reagent grade) were purchased from Sigma-Aldrich Corp. (St. Louis, USA). AIBN was purified by recrystallizing it twice from methanol. The other chemicals were used as received. Distilled water was obtained from the Department of Chemical Engineering, University of Waterloo, Canada.

A three-necked, round bottom 250 mL Pyrex glass flask, equipped with a double jacket reflux condenser, a magnetic stirrer, nitrogen inlet and a dropping funnel was used as the reactor. A HPS-810 Digital Hot Plate Stirrer (VWR International LLC, New Jersey, USA) was used to heat the water bath.

### 4.3.2 Synthesis of PMMA Nanoparticles

The synthetic reaction (Table 4-1) was carried out under a nitrogen atmosphere. The SDS was firstly dissolved in the distilled water at room temperature to form a homogeneous solution in the flask. After subsequent addition of the initiator into the solution, the resulting mixture was subjected to magnetic stirring and heating up to a set temperature for the synthesis. Then, the MMA was added in a semibatch manner at a given rate of addition 0.15±0.02 mL/min via a dropping funnel. After completion of the MMA addition, the

reaction system was aged for an additional hour without changing the temperature. The polymerization was stopped by immersing the flask in an ice/water bath. Polymer was isolated for characterization by addition of ethanol to the microemulsion (which led to coagulation), followed by centrifugation, filtration, washing, and drying at 45 °C under vacuum until constant weight was reached.

**Table 4-1 Formulation of PMMA nanoparticles**

| BPO, g/L | AIBN, g/L | APS, g/L | MMA, mL | SDS, g | Distilled water, mL | T, °C |
|---|---|---|---|---|---|---|
| 1.02 | -- | -- | 14 | 0.15-2.00 | 84 | 83 |
| 1.43 | -- | -- | 14 | 0.10-1.50 | 60 | 83 |
| -- | 0.95 | -- | 14 | 0.11-1.40 | 84 | 70 |
| -- | 1.33 | -- | 14 | 0.09-1.10 | 60 | 70 |
| -- | -- | 0.95 | 14 | 0.40-2.10 | 84 | 80 |

## 4.4 Results and Discussion

### 4.4.1 Effect of SDS Concentration and Nucleation Mechanism on the Size of PMMA Nanoparticles

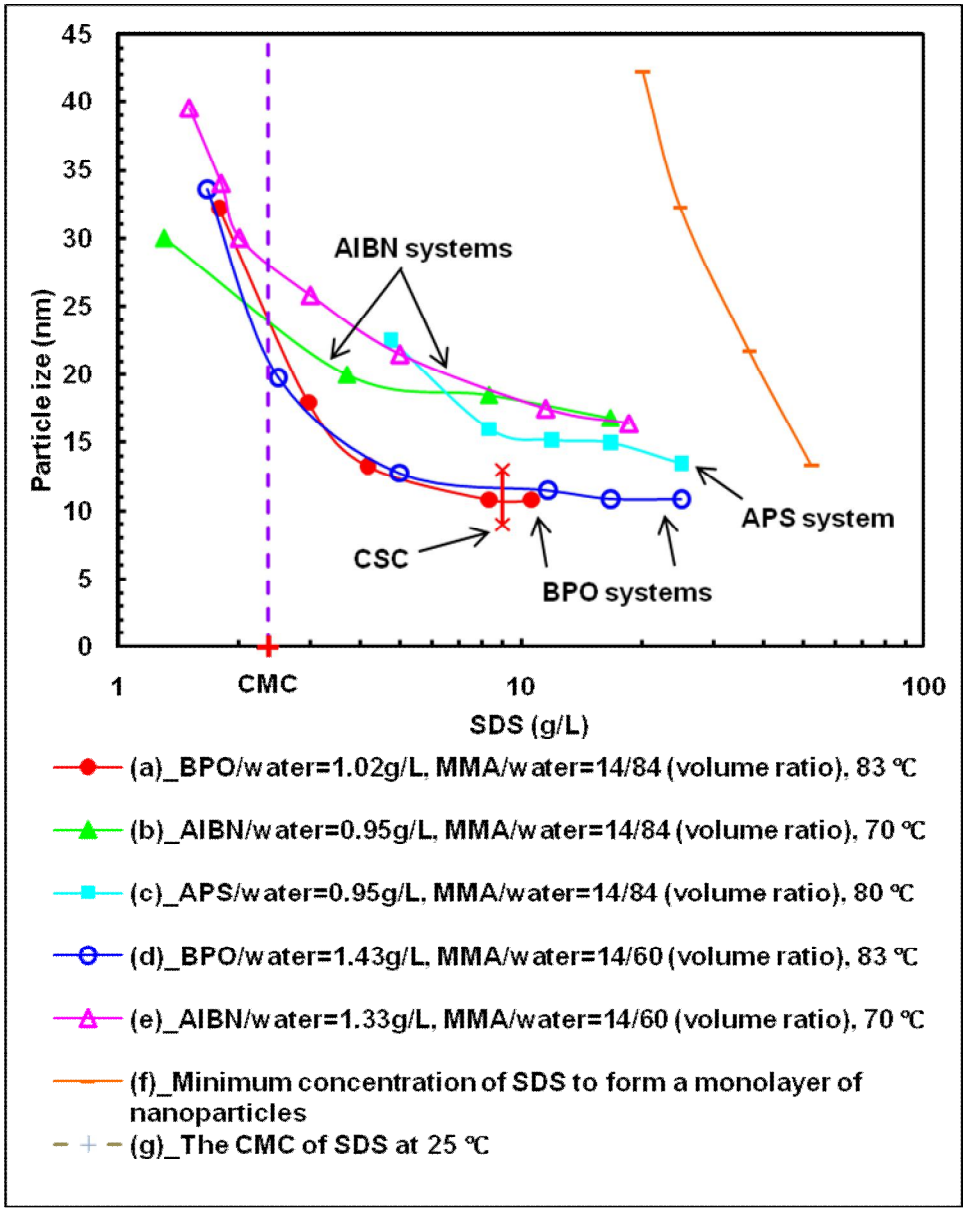


**Figure 4-1 Dependence of the size of PMMA nanoparticles on the SDS concentration in BPO, AIBN and APS initiation DMP systems respectively.**

The surfactant imposes a great influence on the size of the nanoparticles (Figure 4-1a-e). With an increase in SDS concentration, the particle size of PMMA decreased in three different phases (Figure 4-1a, b, d and e). Initially, a slight increase of SDS concentration could cause a rapid decrease of the particle size before the SDS concentration reached the critical micelle concentration (CMC). Then, the particle size dropped relatively slowly with the SDS concentration increasing from the CMC to a critical stability concentration (CSC). The CSC is defined as the lowest surfactant concentration which can give rise to the smallest and stable nanoparticles. When the SDS concentration reached the CSC, the particle size decreased to a minimum size and was maintained at that size level. The phenomena of the CSC of the surfactant were observed in three types of semibatch microemulsion polymerization systems characterized by initiators BPO, AIBN and APS respectively (Figure 4-1a-e). For the BPO system, the particle size could reach close to 10 nm (Figure 4-1a and d, Figure 4-2) at the CSC, which is in the vicinity of 10 g/L. Figure 4-2 showed the good agreement between the TEM imaging and DLS technique. Figure 4-2 showed the morphology of the PMMA nanoparticles was spherical. In the BPO system, the surfactant/monomer and surfactant/water weight ratios required in order to reach a stable particle size are as low as 1:16 and 1:100, respectively, and the surfactant amount is much lower than the required minimum concentration of SDS to give a monolayer around the nanoparticles (Figure 4-1f).[8]

Benefiting from a small amount of surfactant in the final latex, expensive processing required to remove surplus surfactant, concentrate the latices and purify polymer nanoparticles is reduced to a large extent. Furthermore, the PMMA nano-size latices obtained through the BPO initiation semibatch microemulsion polymerization system were stable for more than one and a half years.

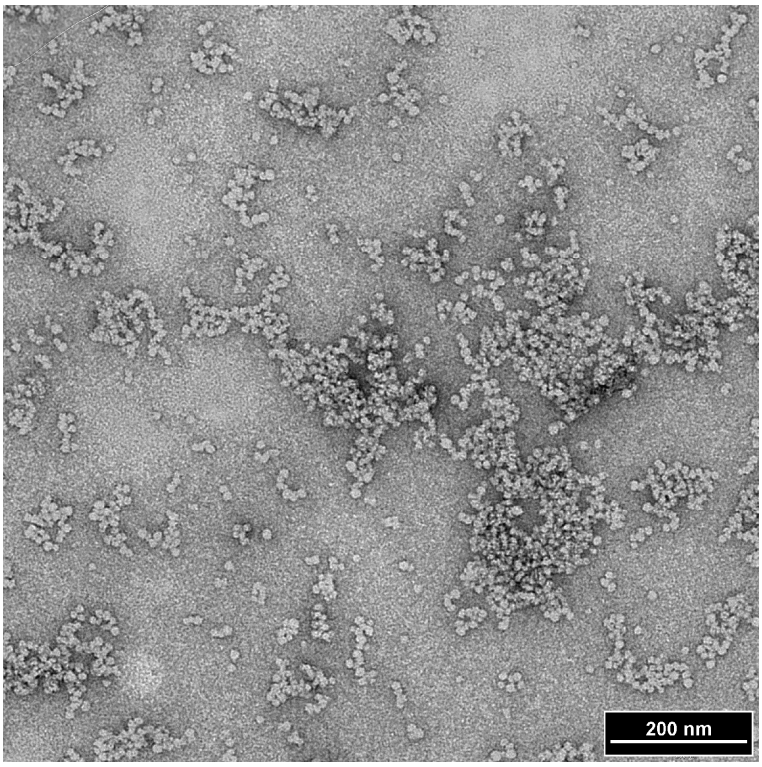


**Figure 4-2 TEM imaging of PMMA nanoparticles. Experiment conditions: BPO/water=1.02g/L, MMA/water=14/84 (volume ratio), SDS concentration=16.7 g/L, 83°C.**

The CSC could be regarded as an intrinsic characteristic of the semibatch microemulsion polymerization system. For a homogeneous nucleation polymerization mechanism, the free radicals were generated in the aqueous phase and then propagated with the joining of the monomer units until the oligomeric radicals exceeded their solubility and precipitated.[23] Precipitated oligomeric radicals would be encapsulated by a micelle to form a polymer precursor. Nevertheless, for the micellar nucleation mechanism, both the monomer initiation and polymer chain growing period occurred inside a micelle. The common traits of these two initiation mechanisms are considered as that the polymer nanoparticle precursors existed in the micelles and require surfactant to be stabilized (Scheme 4-1). If the concentration of the surfactant is adequate to provide a sufficient number of micelles to encapsulate all the generated and newly formed precursors, the particle size will become stable and will be minimized. Thus, the threshold concentration of surfactant at this moment is the CSC.

The nucleation mechanism is another important factor which affects the size of the nanoparticles. Figure 4-1a-e indicated that the initiator BPO exhibited obvious advantages over both AIBN and APS. Xu et al.[22] also reported that a great number of smaller polymer particles would be generated in a BPO micellar nucleation predominated system compared to the potassium persulfate (KPS) homogeneous nucleation polymerization system. As shown in Figure 4-1, first, a particle size around 10 nm that could not be achieved by either AIBN or APS initiation semibatch microemulsion polymerization system has been realized in the BPO system with a surfactant/water weight ratio of 1:125. Second, the BPO system could generate much smaller nanoparticles than that of APS and AIBN under the same surfactant concentration. In addition, the particle sizes of the latices were marginally affected by the ratio of monomer/water in the BPO system (Figure 4-1a and d), different from the AIBN system in which the higher ratio of monomer/water gave rise to larger size nanoparticles (Figure 4-1b and e). These phenomena possibly illustrate three completely different initiation mechanisms represented by micellar nucleation mechanism (BPO),[22] partially homogeneous nucleation mechanism (AIBN)[24] and homogeneous nucleation mechanism (APS)[7,24-26] in the semibatch microemulsion polymerization systems. For the homogeneous nucleation semibatch microemulsion polymerization system, the uniform spherical particles were formed by the absorption of emulsifier on the precipitated oligomeric radicals and continued to grow by accepting monomers from the water phase until termination. In this process, the monomer transfer was inevitable and led to the formation of larger particles than that of the micellar nucleation system, in which mass transfer should be prevented. Accordingly, because the initiation by AIBN occurred in both the micelle and water phase,[24] the monomer/water ratio imposed a considerable effect on the particle size (Figure 4-1b and e). Compared with the AIBN system, in the BPO system, the particle size was independent of the monomer/water ratio due to the micellar nucleation mechanism (Figure 4-1a and d). BPO's water-insolubility is much smaller than AIBN's and the different water solubility affects the formulation mechanism of PMMA nanoparticles to some extent (Table 4-2). Due to the relatively more hydrophobic property of BPO compared to AIBN, under a similar initiator concentration, the free radicals resulting from decomposition of

BPO's molecules will occupy more micelles than AIBN's to form much more valid micelle nanoreactors, i.e. particle precursors. On the contrary, the free radicals produced from APS would attack the monomers in water rather than penetrating into the micelles, which is attributed to the water solubility of APS.

**Table 4-2 Parameters of two oil-soluble initiators under experimental conditions[27]**

| | BPO | AIBN |
|---|---|---|
| Types of Initiators | oil-soluble | oil-soluble |
| water solubility(g/100g of $H_2O$) | $3\times10^{-4}$ | $4\times10^{-2}$ |
| $k_d$ ($cm^3\cdot mol^{-1}\cdot s^{-1}$) | $1.83\times10^{-5}$ | $9.25\times10^{-5}$ |
| F | 0.6 | 0.6 |

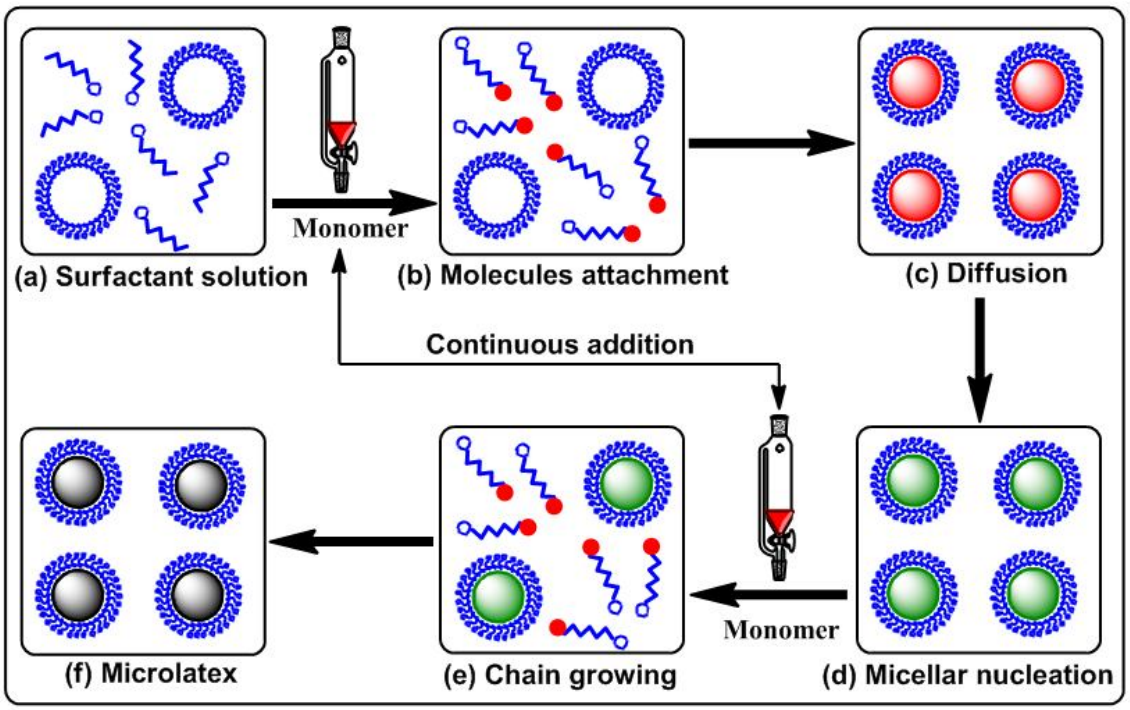


**Scheme 4-1 Schematic illustration of functional mechanism of the BPO initiation semibatch microemulsion polymerization system. Blue color stands for the surfactant molecules. Red color stands for the monomer molecules. Green color stands for the growing polymer chains. Black color stands for the polymer nanoparticles.**

## 4.5 Mechanism of Micellar Nucleation Semibatch Microemulsion Polymerization

The principle of the semibatch microemulsion polymerization system lies in producing and maintaining monomer starved conditions to ensure that the empty micelles will be utilized to a major extent during the polymerization and no empty micelles exist at the end of the polymerization as a result of the semibatch addition technique (Scheme 4-1). In order to reach this purpose, the reaction rate must be faster than the monomer addition rate. Therefore, it is necessary to use a higher polymerization temperature to accelerate the decomposition rate of initiator and thus the polymerization rate. Meanwhile, it is advantageous to produce monodisperse seed polymer particles at high temperatures during the nucleation stage.[28] However, if the temperature is too high, for example 92 °C, the half

life of BPO is only 1 h, less than the whole polymerization time. Based on the discussion above and our previous studies,[7,8] the polymerization temperature for BPO initiation system is chosen as 83°C.

In order to interpret the functional mechanism of the BPO initiation semibatch microemulsion polymerization system, the reaction process of one drop of monomer ($0.05 \pm 0.01$ ml) is analyzed after it is added into the system, shown from Scheme 1b-d. When the monomer molecules contained in one drop enter the surfactant aqueous solution (Scheme 4-1a), they will be captured competitively by the relatively much higher number of surfactant molecules simultaneously (Scheme 4-1b). Because of the active equilibrium between the micelles and surfactant molecules, the surfactant molecules attached with the newly-added monomer molecules would statistically assemble into the micelles. Therefore, no monomer transfer among particles occurred during the entire micelles nucleation period. Through this manner, not only can the monomer diffuse into the micelles evenly, but also the micelles can be used to a maximum extent (Scheme 4-1c). The monomer which will dissolve into the water is negligible and the probability of occurrence of homogeneous polymerization is reduced to a large extent. Then, the free radicals decomposed from the BPO will attack the monomers inside the micelles and initiate the micellar nucleation (Scheme 4-1d). The successive addition of monomer molecules is continuously transported into the micelles through the surfactant molecules to maintain the growing polymer chain (Scheme 4-1e). The final nanoparticles are produced after the monomer addition is completed (Scheme 4-1f).

On the other hand, the dependence of molecular weight and polydispersity of PMMA nanoparticles over the reaction time, i.e. addition time, in the BPO initiation semibatch microemulsion polymerization system was examined. As shown in Figure 4-3, the molecular weight represented by number-average molecular weight $\overline{M}_n$ and weight-average molecular weight $\overline{M}_w$ were observed to increase gradually as a function of reaction time up until the completion of addition at 90 minutes. In addition, over a 30 min aging time, the molecular weight was essentially unchanged. The polydispersity index (PDI) characterized by $\overline{M}_w / \overline{M}_n$ was found to follow a decreasing trend and leveled off at around 1.2 after completion of

reaction. Figure 4-3 not only confirmed the proposed functional mechanism of the BPO initiation semibatch microemulsion polymerization system from the perspective of molecular weight, but also indicated that the BPO initiation semibatch microemulsion polymerization system had a living polymerization property.

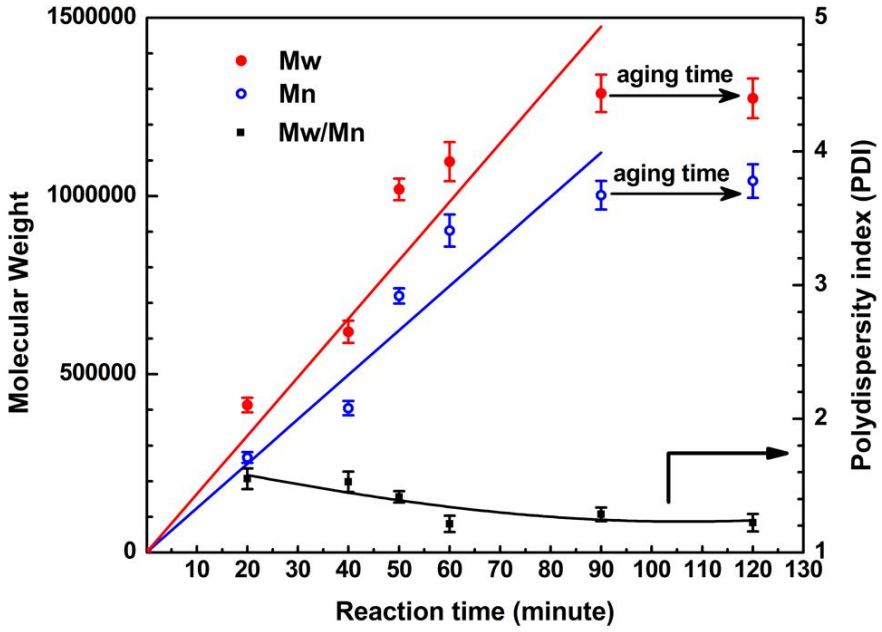


**Figure 4-3 Changing trend of molecular weight and polydispersity of PMMA nanoparticles with the polymerization reaction time. Experiment conditions: BPO/water=1.02g/L, MMA/water=14/84 (volume ratio), SDS concentration= 12 g/L, addition time=90 minutes, aging time=30 minutes, 83°C.**

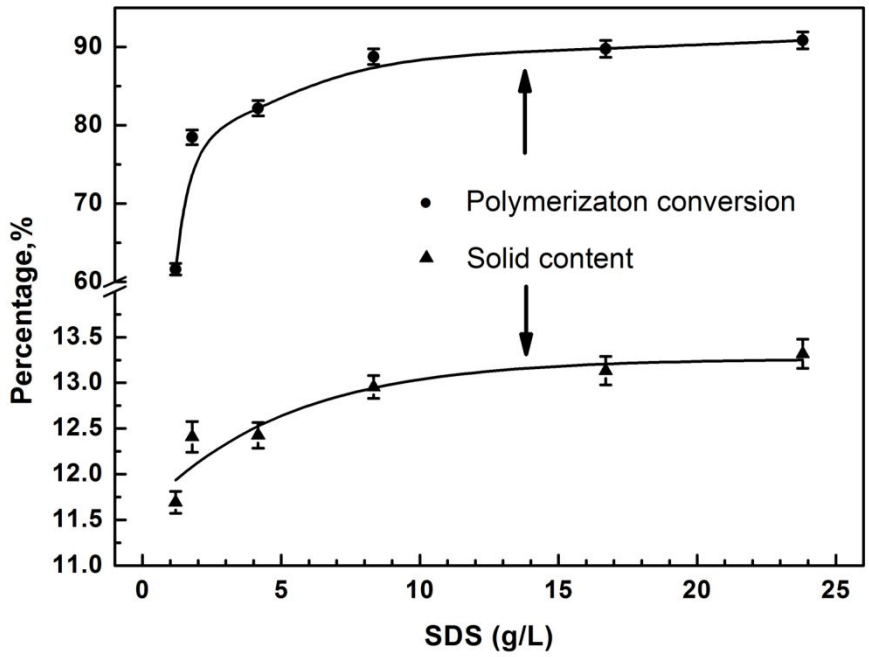


**Figure 4-4 Effect of the SDS concentration on the conversion and solid content of PMMA nano-size latices. BPO/water=1.02g/L, MMA/water=14/84 (volume ratio), 83°C.**

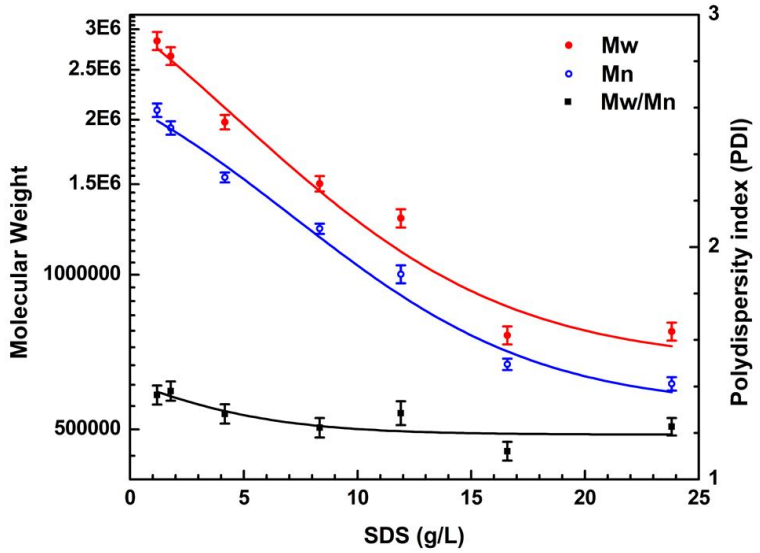


**Figure 4-5 Effect of the SDS concentration on the molecular weight and polydispersity of PMMA nanoparticles. BPO/water=1.02g/L, MMA/water=14/84 (volume ratio), 83°C.**

### 4.6 Effect of SDS Concentration on the Conversion and the Solid Content

Figure 4-4 shows the dependence of the conversion and solid content of PMMA nanoparticles on the SDS concentration using the BPO initiation semibatch microemulsion polymerization system. The conversion and solid content showed a similar change trend with an increase of the SDS concentration (Figure 4-4), which confirmed the theoretical calculation prediction. With increasing SDS concentration, the conversion and solid content initially increased since a greater number of micelles were provided. When the SDS concentration was above the CSC around 10 g/L, the number of micelles was sufficient to encapsulate all the polymer nanoparticle precursors. Therefore, the conversion and solid content arrived at a relatively stable level.

### 4.7 Effect of SDS Concentration on the Molecular Weight and PDI

Scheme 1 indicated that each polymer particle was formed in a single nucleation step. It is, therefore, anticipated that the molecular weight would decrease along with a drop in the particle size. As shown from Figure 4-1a and Figure 4-5, in the BPO initiation semibatch microemulsion polymerization system, the particle size and molecular weight followed a consistent trend, and the polydispersity index (PDI) characterized by $\overline{M}_w / \overline{M}_n$ was within the range of 1.1-1.4 over the varied range of the SDS concentration.

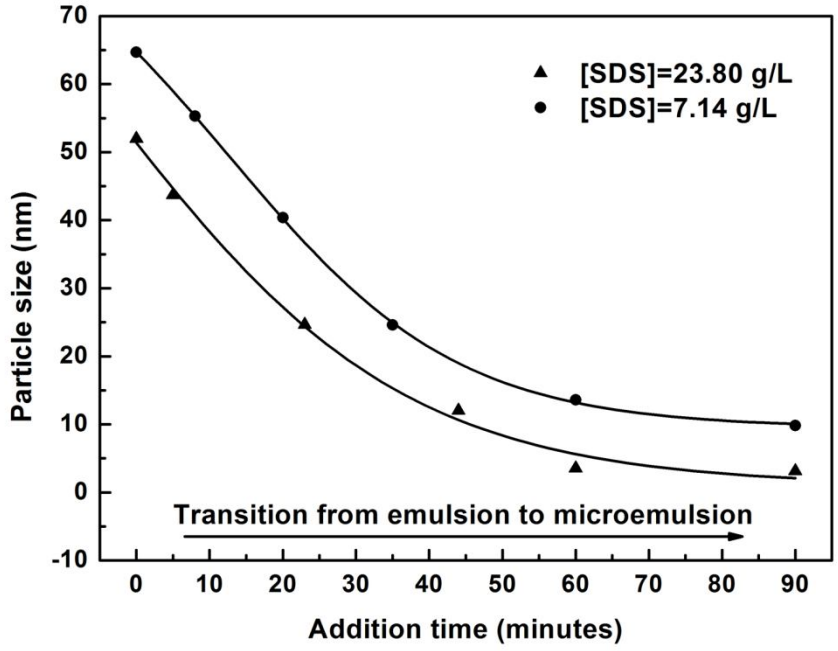


(a)

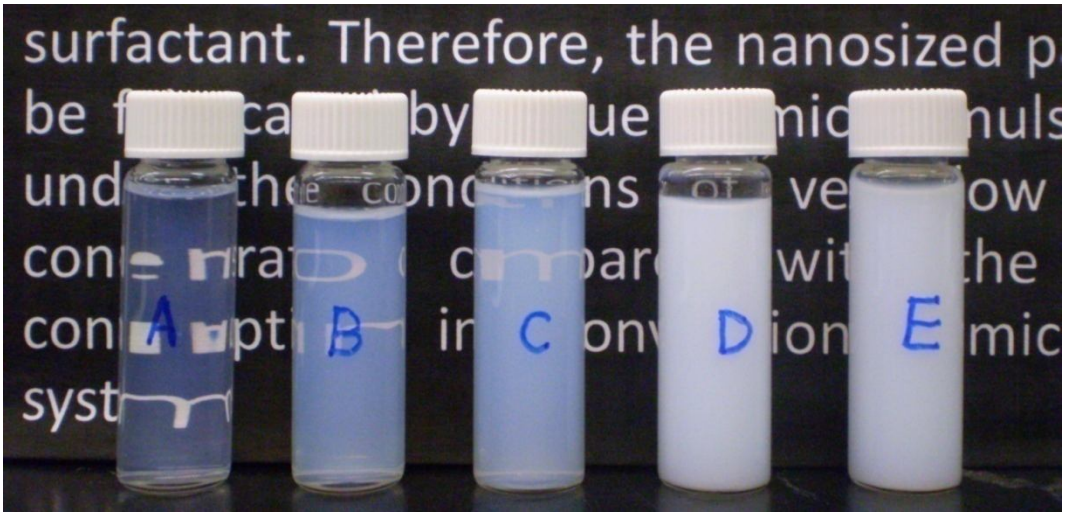


(b)

**Figure 4-6 Effect of the MMA addition time on the nano-size PMMA latices. (a) Effect of the monomer addition time on the size of PMMA nanoparticles. (b) Appearance of the latices with different addition time. A: 60 minutes, B: 44 minutes, C: 23 minutes, D: 5 minutes, E: 0 minute.**

**Experimental conditions: BPO/water=1.02g/L, MMA/water=14/84 (volume ratio), SDS concentration= 16.7 g/L, 83°C.**

## 4.8 Effect of the Monomer Addition Rate on the Nano-Size Latex

The addition time of the monomer is the key factor to ensure the semibatch microemulsion polymerization system works effectively. The influence of monomer addition rate and concentration of surfactant on the particle size of polymer nanoparticles has been studied extensively by Sajjadi et al.[28-31] for the KPS initiation semibatch emulsion polymerization system. Herein, the effect of the MMA addition time on the nano-size PMMA latices of the BPO initiation polymerization system was studied and is shown in Figure 4-6. Figure 4-6a suggested that the size of the nanoparticles became smaller with a reduction in the monomer addition rate. The size of the nanoparticles became stable and minimized when the addition time exceeded 60 minutes (Figure 4-6a). Mass transfer is believed to be the main reason for the size increase as the addition time decreased. When the addition rate is very low, the monomer molecules entering the system will be surrounded and encapsulated by the comparatively higher number of void micelles (Scheme 4-1). In this case, the monomers will be dispersed into the micelles uniformly. So, the mass transfer of the monomers between the aqueous phase and oil phase can be avoided to the largest extent. In this situation, microemulsion is the dominant pathway for the polymerization. However, as the addition rate becomes faster, the interval between two addition actions will be lower than the time needed to transfer the monomer molecules into the micelles. The monomer molecules will form the monomer droplets stabilized by the SDS inside the reaction system, resulting in the monomer-flooded condition. At this stage, emulsion polymerization starts to occur. It can be deduced that the polymerization system undergoes a transition from the microemulsion to the emulsion with an increase in the monomer addition rate and the appearance of the latices also showed a variation from transparent to translucent, Figure 4-6b.

## 4.9 Conclusions

In this chapter, we systematically studied the semibatch microemulsion system and further extended the benefits of the system to a considerable extent by introducing the BPO initiator

which resulted in a micellar nucleation mechanism. With BPO as the initiator, PMMA nanoparticles below 20 nm with narrow size distribution and molecular weight distribution ($\overline{M}_w / \overline{M}_n \sim 1.1$) were prepared and stabilized with a very low SDS/MMA and SDS/$H_2O$ weight ratio of 1:16 and 1:100 respectively as well as with a high solid content of more than 13 wt%. The size of PMMA nanoparticles initiated by BPO is much smaller than that of AIBN and APS at the same SDS concentration in the semibatch microemulsion polymerization systems. In addition, the monomer addition experiments indicate that there exists a minimum required addition time to obtain the minimized particle size. As the addition time was decreased, the polymerization changed gradually from microemulsion polymerization to emulsion polymerization. This technique will pioneer a significant new way to use a simple but practical method to synthesize narrow PDI polymers, which is a very meaningful new development.

# Chapter 5
# Preparation of Poly(butadiene-*co*-acrylonitrile) Nanoparticles

## 5.1 Overview

Poly(butadiene-*co*-acrylonitrile) nanoparticles were synthesized in a semibatch microemulsion polymerization system using Gemini surfactant trimethylene-1,3-bis (dodecyldimethylammonium bromide), referred to as GS 12-3-12, as the emulsifier. The main characteristic of this GS emulsified system lies in that the decomposition rate of initiator was increased considerably at a low reaction temperature of 50 °C because of the acidic initiation environment induced by GS 12-3-12. The particle size can be controlled by the surfactant concentration and monomer/water ratio and a particle size below 20 nm can be reached. The obtained latex particles exhibit a spherical morphology. The microstructure and copolymer composition of the polymer nanoparticles was characterized by FT-IR and $^{1}$H NMR spectroscopy. The effects of the surfactant concentration on the particle size, Zeta-potential, polymerization conversion, copolymer composition, molecular weight, and $T_g$ were investigated. A kinetic study of the copolymerization reaction was carried out, which indicated that an azeotropic composition was produced. The relationship between $T_g$ and number-average molecular weight can be well represented by the Fox-Flory equation. Finally, the semibatch process using conventional single-tail surfactant SDS was compared.

## 5.2 Introduction

Over the past decade, there has been an increasing amount of interest and enhanced research into the design and preparation of polymer nanoparticles.[1-8] As one of the most important members of the polymer family, NBR has been drawing much attention for its synthesis, modification, and applications.[9-11] With the availability of double bond (C=C) units of differing microstructures in NBR polymer chains, the selective reduction of C=C to different levels offers a route to extensively optimize the physical properties of NBR such as elongation, tensile strength, thermal stability, and solvent resistance.

NBR is usually synthesized using the conventional emulsion polymerization technique.[12] However, the emulsion polymerization is known to suffer from several drawbacks, including relatively large particle size and broad polydispersity index (PDI) of molecular weight.[13-15] For example, the VPKA 8817 commercial NBR produced by LANXESS Inc. has a broad PDI of 3.6.[16] The microemulsion polymerization is an effective method to prepare the fine nanoparticles with both high molecular weight and interesting morphologies, which however requires a high surfactant concentration to emulsify relatively low monomer content.[17] Large amounts of retained surfactant in the latex have a considerable negative impact on the properties of the synthesized polymers. However, the separation process is tedious and costly. This is one important reason hindering the wide application of microemulsion polymerization in industry. In order to alleviate this drawback, a monomer-starved semibatch microemulsion polymerization has been put forward and studied extensively by many investigators.[14,17,18] The semibatch microemulsion polymerization is a unique process for manufacturing fine nanoparticles using a high weight ratio of polymer to surfactant. It has been recently shown that this process can produce a large number of small particles and high molecular weight with narrow distributions.[14,18] While comparing to the considerable efforts that have been made to prepare a variety of polymer nanoparticles using the semibatch system, as yet, there has been no report involving the synthesis of NBR Nanoparticles through this semibatch process.

Besides the polymerization process, the development of new surfactant systems with improved emulsifying capability is another important aspect for technical applications. Gemini-type surfactant (GS) is such an unique surfactant, which is made up of two conventional surfactant molecules linked by a spacer.[19,20] It has significantly lower CMC and can greatly increase surface activity compared to the conventional single-tail surfactants with similar chain length and head groups.[20,21] GS trimethylene-1,3-bis(dodecyldimethylammonium bromide), denoted as GS 12-3-12, is one of the most comprehensively characterized GSs and shows many interesting properties in aqueous solution. For example, at ambient conditions, the CMC of GS 12-3-12 is about 1 mM (~0.63 g/L), which is much lower than that of the corresponding monomeric surfactant of

dodecyltrimethylammonium bromide (DTAB, CMC~16 mM, or ~ 4.93 g/L) and the most commonly used single-tail surfactant sodium dodecyl sulphate (SDS, CMC~8 mM, or 2.31 g/L). Most of the studies involving GS self-assembly have been focused on their phase behavior,[22,23] determination of CMC,[23-25] aggregation number and composition of the aggregates.[24,25] However, very few examples have been reported which focus on the use of the assemblies of GS molecules as a platform for the polymerization reactions [26,27] and no research has been carried out on the synthesis of NBR. Therefore, in the present study, GS 12-3-12 was selected as the emulsifier to prepare the NBR nanoparticles and was found to play an interesting and important role in the formation of NBR nanoparticles.

In line with above, the objective of the study in this Chapter was thus to develop an economical and robust viable process to prepare fine NBR nanoparticles, which can be employed as a unique nano-substrate for NBR polymer modifications and other applications based on their superior physiochemical properties. The GS 12-3-12 emulsified semibatch system presented here can be extended to the other latices containing different polymers.

## 5.3 Experimental Section

### 5.3.1 Materials

Acrylonitrile (AN, 99+%), ammonium persulfate (APS, 98%), and methyl ethyl ketone (MEK, reagent grade) were purchased from Aldrich. The inhibitors were removed prior to polymerization by passing the monomer AN through an alumina column. The initiator APS was purified by recrystallization from ethanol and dried under vacuum at room temperature. Deuterated chloroform ($CDCl_3$) with 0.03% v/v tetramethylsilane (TMS) was purchased from Cambridge Isotope Laboratories, Inc. (Massachusetts, US) and used as received. 1,3-Butadiene (BD) was provided by LANXESS Inc. The ethanol, methanol, acetone, and ethyl acetate were all reagent grade and used without further purification. These four organic solvents and distilled water were obtained from the Department of Chemical Engineering, University of Waterloo, Canada. Gemini surfactant trimethylene-1,3-bis (dodecyldimethylammonium bromide) (GS 12-3-12, molar mass = 628.69 g/mol) was synthesized in the authors' laboratory by known procedures[28] and used after repeated

recrystallization from acetone-ethyl acetate (1:1 volume, reagent grade). The yield was 56~58 wt%. GS 12-3-12 with a melting point of 195±5 °C, as determined by differential scanning calorimetry (DSC; Q2000, TA Instruments, New Castle, DE, US) with a scanning rate of 10 °C/min, was obtained.

### 5.3.2 Synthesis of NBR Nanoparticles

Semibatch microemulsion copolymerization was performed in a Parr 316 Stainless Steel Parr reactor. A certain amount of GS 12-3-12 was first dissolved in a measured volume of distilled water (20, 40, 60, or 80 mL) at room temperature to form a homogeneous solution (Scheme 5-1). After the subsequent addition of the initiator APS (0.2 g), the resulting mixture was degassed by bubbling nitrogen gas under about 0.172 MPa for half an hour at room temperature under constant agitation (200 rpm). The system was then subjected to heating up to 50 °C. After the temperature was stabilized, the mixture of AN and BD (1:3 v/v, BD is liquid under 22 psi at room temperature) was added in very small drops at a given rate of 0.075±0.005 mL/min into the prepared micellar solution (surfactant and initiator solution). After the addition of monomers was completed, the polymerization system was allowed to age for six hours to obtain a proper conversion of the polymer before the cooling operation was applied.

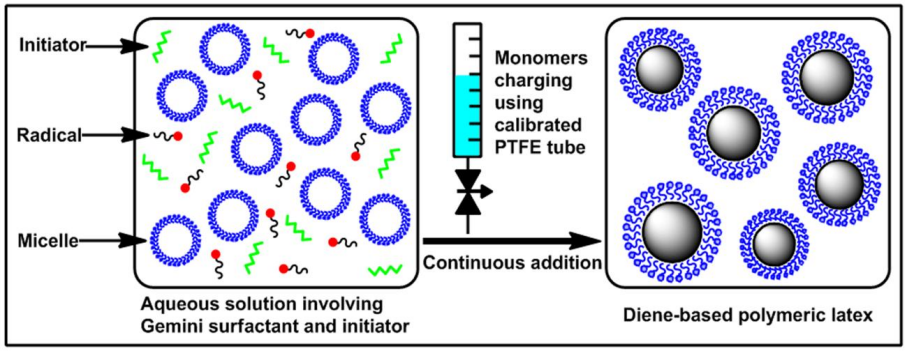


**Scheme 5-1. Schematic diagram illustrating the preparation of diene-based polymer nanoparticles (e.g., NBR) via semibatch microemulsion polymerization.**

## 5.4 Results and Discussion

### 5.4.1 FT-IR and $^1$H NMR Spectra Analysis

FT-IR is a fast, convenient and accurate tool to determine the compositions and microstructures of the polymers.[29,30] Figure 5-1a shows a typical FT-IR spectrum of synthesized NBR nanoparticles with an average particle size of 35.3 nm. The distinct peak exhibited at 2236 $cm^{-1}$ clearly shows the existence of the cyano group (C≡N), which indicates that monomer AN has been polymerized into the obtained nanoparticles. The polymerization of BD usually gives rise to products which have a mixture of 1,4 and 1,2 structural units, and the 1,4 addition products consist of *trans* and *cis* isomers. The intense peak shown at 970 $cm^{-1}$ is characteristic of the level of olefin by the proton vibration on the 1,4-*trans* double bonds. The absorbance at the peak of 917 $cm^{-1}$ corresponds to the 1,2-vinyl terminal bonds, which is much weaker than that of 1,4-*trans* double bonds. There is no notable absorbance in the vicinity of 750 $cm^{-1}$ peak, which is assigned to the 1,4-*cis* double bonds. Taking into account the absorption factors ($k$) of 1,4-*trans* ($k$ = 2.3) and 1,2-vinyl ($k$ = 2.24) configurations, it can be seen that the 1,4-*trans* double bonds account for a major percentage of the olefin units in the synthesized nanoparticles due to the fact that the peak area of 1,4-*trans* units is much larger than that of 1,2-vinyl units. The absorption factor of each functional group is a relative value based on the condition that the absorption factor of AN is equal to one ($k$ = 1). Based on that, the level of bound AN in the copolymer can be calculated according to the ASTM D5670-95 test method (2009), and the results are given in Figure 5-1.

Figure 5-1b shows the chemical shifts of the protons of the different microstructures by $^1$H NMR characterization. Aliphatic protons display signals between 0.9 and 2.8 ppm and the peaks around 2.58 ppm indicate the presence of acrylonitrile methine units. The peaks appearing in the region of 4.9-5.1 ppm are assigned to the 1,2-vinyl terminal units and the double peaks exhibited in the vicinity of $\delta$ = 5.5 ppm are attributed to the protons of 1,4-olefin units. In addition, Figure 5-1b suggests a consistent result with the FT-IR analysis that the 1,4-olefin units account for the majority in all of the olefins units. In short, FT-IR and $^1$H

NMR analysis demonstrate that both the AN and BD units have been incorporated into the obtained NBR nanoparticles.

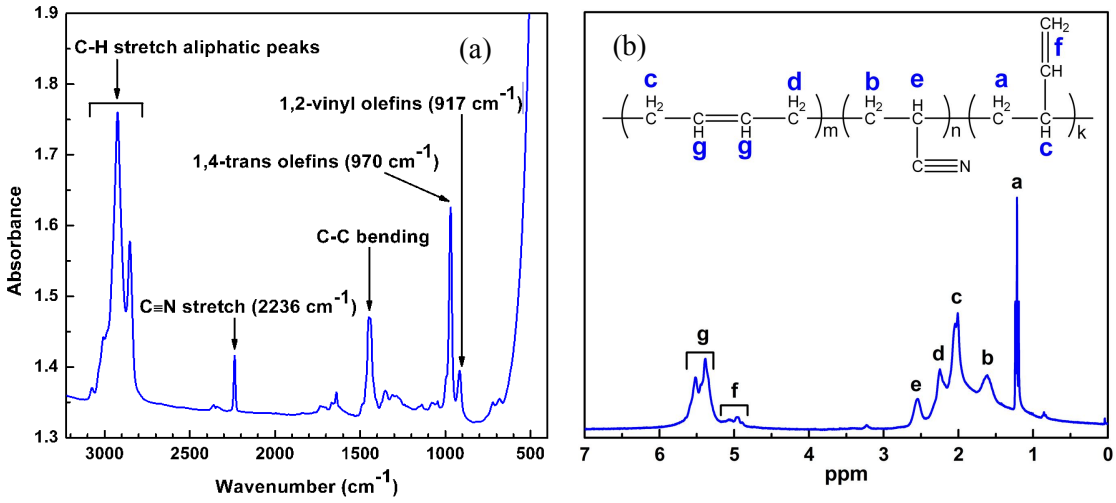


**Figure 5-1 Typical FT-IR (a) and $^{1}$H NMR (b) spectra of NBR nanoparticles. The samples of Nanoparticles for spectra analysis was synthesized in the semibatch microemulsion polymerization system using 0.02389 mol/L GS 12-3-12 surfactant in 80 mL distilled water. m, n, and k are the number of repeating units. Polymerization conditions: AN = 2.5 mL, BD = 7.5 mL, APS = 0.2 g, T = 50 °C.**

### 5.4.2 Effects of GS 12-3-12 Concentration and Monomer/Water Ratio on the Size of NBR Nanoparticles

In order to study the effect of the monomer/water ratio on the particle size, four synthetic systems were implemented differing in the way in which the 20, 40, 60, and 80 mL distilled water were used, respectively (Figure 5-2). Large scale agglomeration was observed in the 20 mL water experimental runs, which indicated that the stability of the emulsion latex was difficult to maintain when the volume of the continuous phase was reduced by a certain extent. This is because in the 20 mL water system, the monomer/water weight ratio was too high to result in significant collisions and aggregation of the nanoparticles. With respect to the other three water systems, there were no precipitates found in the produced latices. Figure 5-2 shows that under the same surfactant concentration, the sizes of the nanoparticles

obtained in the three water systems are different. The particle sizes are found to increase with increasing of the monomer/water ratios because the solid content was increased. A detailed discussion relevant to the influence of solid content on the particle size is provided by He et al.[14]

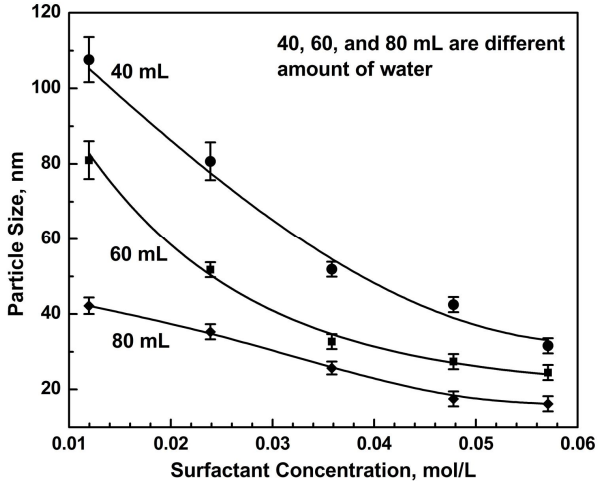


**Figure 5-2 Dependence of the particle size on the monomer/water ratio and the concentration of GS 12-3-12. Polymerization conditions: AN = 2.5 mL, BD = 7.5 mL, APS = 0.2 g, T = 50 °C, distilled water = 40, 60, and 80 mL, respectively. The large scale agglomerations of Nanoparticles were observed when 20 mL distilled water was used. The particle size was determined by DLS and reported as number average.**

Particle nucleation is probably the most important phenomenon in (micro)emulsion polymerization. Up until now, the formation of latex particles involves three well-established particle nucleation mechanisms represented by micellar nucleation,[31] homogeneous nucleation,[32,33] and coagulative nucleation.[34] Micellar nucleation occurs when primary radicals or, much more likely oligomeric radicals are captured by micelles, and this absorption process is commonly described by the collision-controlled model, diffusion-controlled model, and propagation-controlled model.[35] While homogeneous nucleation occurs when the solution-polymerized oligomeric radicals grow in the continuous phase to a critical chain length ($j_{cr}$) at which they become insoluble and precipitate into a primary

particle, which is also called a precursor particle. However, when the surfactant amount is insufficient such as below the CMC to stabilize a larger number of precursor particles, these smaller-sized particles will coagulate rapidly with each other (not polymerization of monomer) to form the mature latex particles whose subsequent growth occurs entirely by polymerization. This coagulation is the so-called coagulative nucleation, which can be considered as part of the overall nucleation process for the formation of mature polymer particles. While, not all radicals are finally absorbed by micelles or stabilized in the aqueous phase, as a certain fraction of the radicals in the water phase will be competitively captured by the existing particles. Nevertheless, when the emulsifier is sufficient such as well above CMC, most of generated radicals will be stabilized by the surfactant thereby reducing the chances of radicals captured by the particles. Concurrently, the coagulative nucleation will become much less important, since there is adequate surfactant to encapsulate and stabilize precursor particles.[36] In the present study, the fraction of homogeneous nucleation occurring in the system will probably be large due to the high water solubility of AN. Meanwhile, because the concentration of GS 12-3-12 is well above CMC along with the BD units added upon the oligomeric radicals, micellar nucleation needs to be taken into account while the coagulative nucleation can be neglected. Therefore, homogeneous and micellar nucleation mechanisms will coexist in the present emulsion polymerizations and must be considered in the case of developing a mathematical model to simulate this semibatch polymerization process.

Figure 5-2 also shows that the surfactant concentration has a significant effect on the size of nanoparticles. It can be seen from Figure 5-2 that in each of the 40, 60, and 80 mL water systems, there is a smooth decrease in the particle size with an increase in the surfactant concentration.

The results in Figure 5-2 including those mentioned previously indicate that: 1) the particle size can be controlled through adjusting surfactant concentration and monomer/water ratio according to the requirements in a real application; 2) the different solid contents of latices can be prepared depending on the amount of water employed; 3) the 80 mL water system investigated in the present study can be economical if the nanoparticles with a particle size of

around 42 nm is acceptable for certain uses, because the surfactant/monomer and surfactant/water weight ratios required are as low as 0.088 and 0.0075, respectively. Benefiting from a low surfactant concentration in the final latex, expensive processing cost required to remove surplus surfactant, concentrate the latex, and purify the polymer nanoparticles is reduced to a large extent, which has significant implications for the latex manufacturing industry. Furthermore, the synthesized latices exhibit a comparable stability to the conventional microemulsion, although the stability varies with the different surfactant concentrations and solid contents. For example, in the 40 mL water system emulsified by 0.04779 mol/L surfactant, the latex can maintain its stable for more than half a year. This further confirms that the GS 12-3-12 emulsified semibatch polymerization is a promising method for synthesizing NBR nanoparticles. Note that in the following sections, the 80 mL water system will be used as the model to show the main characteristics of the GS 12-3-12 semibatch microemulsion polymerization system due to the fact that the 80 mL water system provided the smallest particles under the same surfactant concentration. Meanwhile, a similar discussion between the systems with differing water amounts can be avoided.

### 5.4.3 Potential Applications of Small NBR Nanoparticles

Based on the small feature particle sizes, the obtained NBR nanoparticles may provide many promising applications for academic research and commercial applications. First, due to the small size, the physical and mechanical properties of the polymers can be reinforced to a large extent.[37] Second, the NBR nanoparticles can be used to produce other functional polymers through a variety of modification routes. Finally, the extremely small nanoparticles, such as below 20 nm, can offer an opportunity to solve the central challenge in the field of latex hydrogenation of diene-based polymers. As the solution hydrogenation of unsaturated polymers is known to suffer from the major disadvantage of using large amounts of organic solvent, the latex hydrogenation of polymers in emulsion form is becoming the pursuit of industry.[16] However, an obstacle has limited the application of latex hydrogenation in commercial production. This obstacle lies in how to realize the optimal interplay of accelerating the hydrogenation rate, decreasing the demanded quantity of the catalyst, and eliminating the organic solvent. Now, these small-sized diene-based nanoparticles may

provide an opportunity to overcome this challenge replying on the following notable advantages of: 1) increasing the rate of latex particles to capture the catalyst molecules; 2) improving the mass transfer of catalyst molecules inside the entangled polymer chains.

### 5.4.4 Colloidal Stability of the Produced Latex

Table 5-1 presents the ζ-potentials of NBR latex particles after the polymerization in the 80 mL water system, which shows a good agreement with the observed colloidal stability of the produced emulsion. ζ-potential of particles is a good indicator of their emulsion stability: the higher the ζ-potential, the more stability the charged particles. It is generally accepted that particles with ζ-potentials more positive than +30 mV or more negative than -30 mV are normally considered stable. It can be seen from Table 5-1 that in the experimental runs, the ζ-potentials of NBR latex particles are all above +30 mV and rise up with an increase in the cationic surfactant concentration. When the concentration of surfactant reaches above 0.02389 mol/L, the ζ-potentials are higher than +40 mV, which represents a good stability of an emulsion. This trend in the ζ-potential with variation in surfactant concentration is attributed to the following two aspects. The first aspect needs to be paid attention is the introduction of an anionic initiator APS into this cationic surfactant emulsified system. In the absence of surfactant, the generated sulfate free radicals and subsequent addition of few monomer molecules are able to afford a role of a kind of "anionic surfactant" and this role can stabilize particles thus leading to the latex featuring a negative ζ-potential. Thus, a counteract effect induced by the negative charges (e.g., $SO_4^{\bullet -}$) that stems from the decomposition of APS will be imposed on the electrostatic stabilization built up by cationic GS 12-3-12. But, in the present case, a net higher positive ζ-potential of particles was still measured (Table 5-1), which suggests that the amount of cationic surfactant is much higher than that of APS thereby generating a stronger neutralization effect on the negative ζ-potentials. Nevertheless, at the lower surfactant concentration (e.g., 0.01195 mol/L), this counterbalance effect was relatively small, which thus gives rise to a relatively low positive ζ-potential. With addition of more surfactant, more numerous of particles were generated and the effect of negative charges on the ζ-potential for each particle was reduced accordingly as

the amount of APS is identical in all experiment runs, which thus resulted in a higher ζ-potential. On the other hand, the surface charge density is considered to become larger when the particle size is decreased, which can also give a higher ζ-potential. When the surfactant concentration reached a higher level (e.g., 0.03584 mol/L), the ζ-potential was found to attain a maximum and showed a slight difference with a further increase in the surfactant concentration. This is because the particles are globally positively charged and the neutralization effect originating from APS is very weak under a relatively high surfactant concentration.

**Table 5-1 Zeta potentials of NBR latex particles**

| Surfactant concentration in 80 mL distilled water, mol/L | Zeta potential, mV[a] | pH of latex[b] |
|---|---|---|
| 0.01195 | 37.1 | 4.38 |
| 0.02389 | 50.2 | 4.05 |
| 0.03584 | 58.3 | 3.65 |
| 0.04779 | 62.5 | 3.47 |
| 0.05708 | 64.3 | 3.16 |

[a] Mean value of triplicate measurements for each sample is determined using a Zetasizer Nano ZS at 25 °C. [b] pH value is determined using a Corning Scholar 425 pH Meter.

### 5.4.5 Morphology of NBR Nanoparticles

Figure 5-3 shows the morphology of nanoparticles observed by the TEM imaging. As represented by Figure 5-3, the obtained nanoparticles exhibit a uniform spherical shape. The shape of the nanoparticles is an important issue worth exploring from a practical standpoint since it affects the rheological and solubilization properties. The spacer length, i.e. $(CH_2)_s$ unit of the GS (Scheme 5-2) plays an important role in regulating the micelle morphology. Cryo-transmission electron microscopy studies on GS 12-s-12 have produced photos with different morphologies varying with the carbon number (s) of the spacer. It was reported that for the case of s = 2, the entangled, thread-like or worm-like micelles were observed. For s =

4, 8, and 12, the spherical micelles were observed. When s is as high as 16, the micelles show a vesicle pattern. For GS 12-3-12 with s = 3, shorter thread-like micelles will be present in a higher concentration such as a 110 mM solution of GS 12-3-12, whereas a lower concentration like a 30 mM solution of GS 12-3-12 shows only spherical micelles, as observed in Figure 5-3.

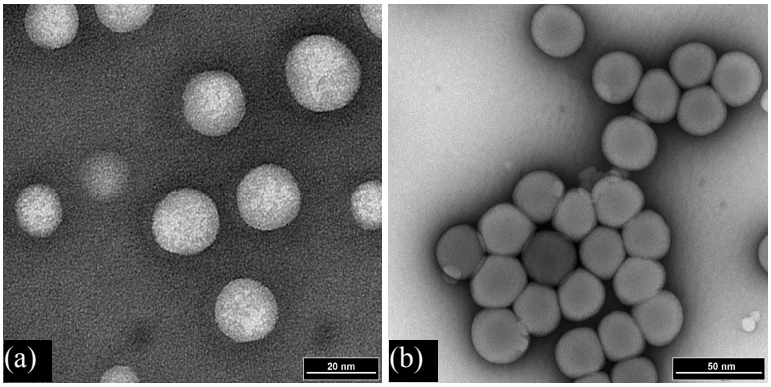


**Figure 5-3 NBR nanoparticles imaged by TEM. (a)-(b) are the NBR nanoparticles prepared under GS 12-3-12 concentrations of 0.04779 and 0.03584 mol/L, respectively. Polymerization conditions: AN = 2.5 mL, BD = 7.5 mL, APS = 0.2 g, distilled water = 80 mL, T = 50 °C.**

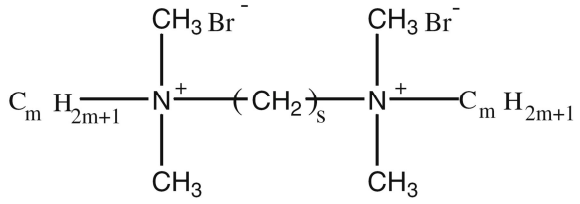


**Scheme 5-2 Chemical structure of bis(quaternary ammonium) Gemini-type surfactant, denoted as *m-s-m*.**

### 5.4.6 Aggregate Morphology of the Bulk NBR Nanoparticles

The aggregate morphology of the bulk NBR nanoparticles after coagulation operation was visualized from SEM image as shown in Figure 5-4. It can be seen from Figure 5-4 that after the coagulation operation, the boundary among the polymer nanoparticles can still clearly be

seen. Nevertheless, the particles were observed to aggregate extensively and a part of particles exhibited the deformed morphology that was different from the spherical shape observed in Figure 5-3a (latex form).

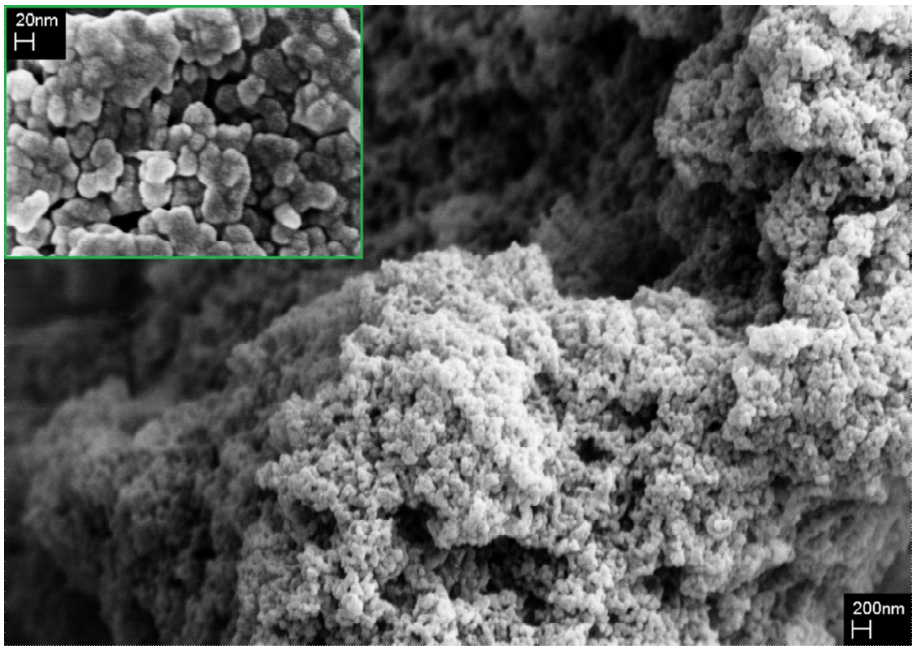


**Figure 5-4 SEM surface images of the bulk NBR. The image of the inset on the left is the higher magnification of part. Experimental conditions of preparation: AN = 5 mL, BD = 15 mL, APS = 0.2 g, distilled water = 80 mL, T = 50 °C, addition time = 200 min, aging time = 8 h, concentration of GS 12-3-12 is 0.050 M.**

### 5.4.7 Composition and Polymerization Conversion of NBR Nanoparticles

Figure 5-5 presents the results of the cumulative copolymer composition ($\overline{F}_{AN}$) and overall polymerization conversions of AN, BD, and NBR, respectively under different surfactant concentrations. The $\overline{F}_{AN}$ shown in Figure 5-5 provides the results measured at the end of the polymerization and are found to be within 31.1-35.2 wt% with variation of surfactant concentration. One can see that the conversions of AN, BD, and NBR increase with an increase in the surfactant concentration. This is because a higher surfactant concentration will generate more micelles which can give birth to more reaction domains in the system thereby resulting in a higher polymerization conversion. On the other hand, the conversions of AN

are found to be always larger than those of BD over the studied surfactant concentrations. This phenomenon can presumably be ascribed to the different solubility of AN and BD in the aqueous phase. Under the reaction temperature (50 °C), the solubility of AN in water is 1.58 M,[38] which is much higher than that of BD of 0.037 M.[39] Therefore, a certain amount of BD vapor will remain in the head space of the reactor.

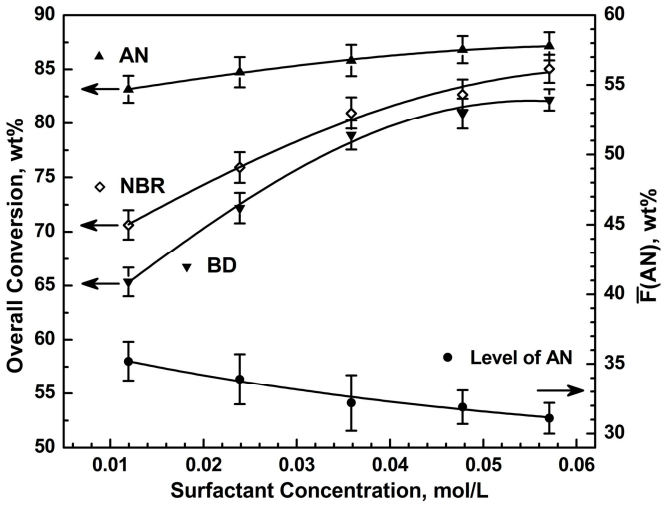


**Figure 5-5 Effects of the GS 12-3-12 concentration on the cumulative copolymer composition and the overall polymerization conversions of AN, BD, and NBR, respectively. Polymerization conditions: AN = 2.5 mL, BD = 7.5 mL, APS = 0.2 g, distilled water = 80 mL, T = 50 °C.**

One big challenge related to the reaction temperature (i.e., 50 °C) is that the decomposition rate of the initiator APS is very slow at this temperature, which means that most of APS will not decompose within 200 min at 50 °C. This no doubt will decrease the rate of polymerization and lead to a lower conversion of monomers. However, as shown in Figure 5-5, a high conversion of NBR above 80 wt% was still achieved in the GS system. This is mainly because the decomposition rate of APS in the aqueous phase is greatly enhanced in the acidic reaction system induced by GS 12-3-12. Koltoff and Miller[40] carried out a detailed study on the rate of decomposition of APS in water at various pH values at 50 °C.

The authors proposed that the persulfate decomposed by two simultaneous reactions, one uncatalyzed and the other catalyzed by hydrogen ion, and the kinetics of the thermal decomposition of the persulfate ion was as described below:

$$-d[S_2O_8^-]/dt = k_1[S_2O_8^-] + k_2[H^+][S_2O_8^-] \qquad (5\text{-}1)$$

where $k_1$ and $k_2$ are the rate constants for the uncatalyzed and catalyzed decomposition, and have been determined to be $6.0 \times 10^{-5}$ $min^{-1}$ and $3.5 \times 10^{-3}$ $min^{-1}\bullet(mol/L)^{-1}$, respectively at 50 °C. The acid-catalyzed term, $k_2$ became dominant when $[H^+]$ is high. As can be seen in Scheme 5-3, GS 12-3-12 is a salt comprised of a weak base (derivative of $NH_3$) and a strong acid (HBr), and the pH of the produced NBR latex is within 3.16-4.38 depending on the level of surfactant concentration (Table 5-1). As reported by Koltoff and Miller,[40] the decomposition rate of APS will increase drastically in the acidic solution compared to a neutral environment. Thus, the radical concentration stemming from decomposition of APS will be much higher in the GS system than in the other neutral or basic systems, such as for the conventional surfactant SDS water system (pH~9 given as the same concentration with GS 12-3-12). Attention should be paid to that the presence of pH drift may affect the stability of the latex. The electrical double layer (EDL) formed by cationic GS 12-3-12 is responsible for what is termed electrostatic stabilization of latex, and this EDL can be adversely influenced by hydrogen ion because a pH drift may promote the solubility of the water soluble portion of the emulsifier molecule. While as already mentioned, the produced latices using GS 12-3-12 exhibit a good stability, which indicates that this pH drift caused by GS does not impose a big effect on the stability of latices. In addition, in industrial production using emulsion polymerization, a pH drift is commonly allowed to occur, and it is usually adjusted at the end of the polymerization.

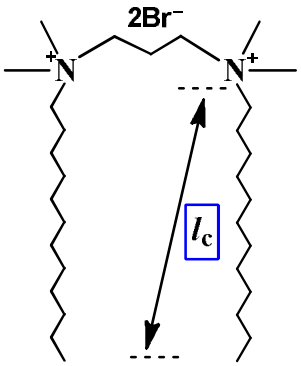


**Scheme 5-3 Chemical structure of GS 12-3-12. The thickness of surfactant layer, $\delta$, was assumed to be the critical length of surfactant molecule, which was thus estimated to be 16.68 Å according to $l_c = (1.5 + 1.265 \times n_c)$, where $n_c$ is the number of carbon atoms in the single alkyl chain.[41]**

The azeotropic composition point is important particularly in industry, because the copolymer composition remains the same with changing conversion in the polymerization thus producing copolymers homogeneous in composition.[42] Figure 5-6 constructs a simulation between the instantaneous compositions of monomer ($f_{AN}$) and copolymer ($F_{AN}$) using the Mayo-Lewis Equation. The reactivity ratios $r_{AN}$ and $r_{BD}$ used for the simulation were obtained from a polymer handbook.[43] Based on three groups of different reactivity ratios, slightly different azeotropic compositions ($F_{AN} = f_{AN}$) were provided. It can be seen from Figure 5-6 that the theoretical azeotropic composition was within the range of 35 to 40 mol% depending on the particular values of $r_{AN}$ and $r_{BD}$ used.

Figure 5-7 shows the changing trend of cumulative copolymer composition $\overline{F}_{AN}$ with the evolution of reaction time. It can be seen that the level of bound AN was relatively high at the early onset of polymerization, and then quickly levelled off at around 32.2 wt%, the percentage of which was then basically unchanged during the rest of the reaction time. This phenomenon has also been observed in other systems involving different surfactant concentrations. These results from Figure 5-7 indicate that the initial monomer feed fraction

($f_{AN}$, 30 mol%) is in the vicinity of azeotropic compositions. For the condition of $f_{AN}$ = 30 mol%, the level of bound AN in the present study was found to be in the range of 31-35 mol% (or wt%, as the mole mass of AN and BD are very similar) depending on the surfactant concentrations (Figure 5-5), which shows a reasonable agreement with the theoretical azeotropic composition (Figure 5-6).

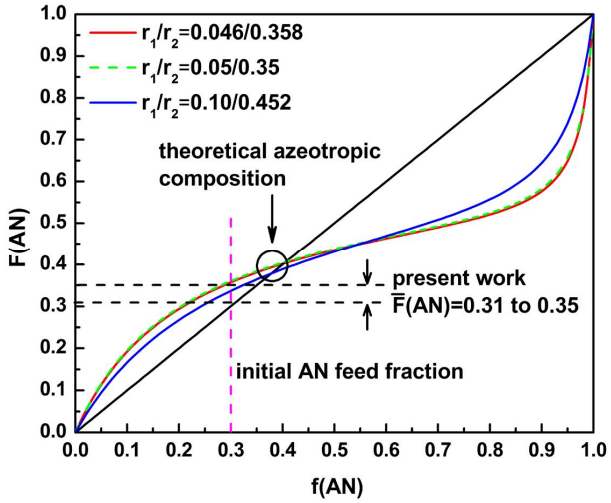


**Figure 5-6 Instantaneous copolymer composition of AN as a function of the mole fraction of AN in reaction system (Mayo-Lewis Equation). The cumulative copolymer composition $\overline{F}_{AN}$ (31-35 mol% or wt% because of the very close mole mass of AN and BD) in Figure 5-6 is the cumulative AN composition obtained at the end of each copolymerization under different surfactant concentrations, which is consistent with the value shown in Figure 5-5.**

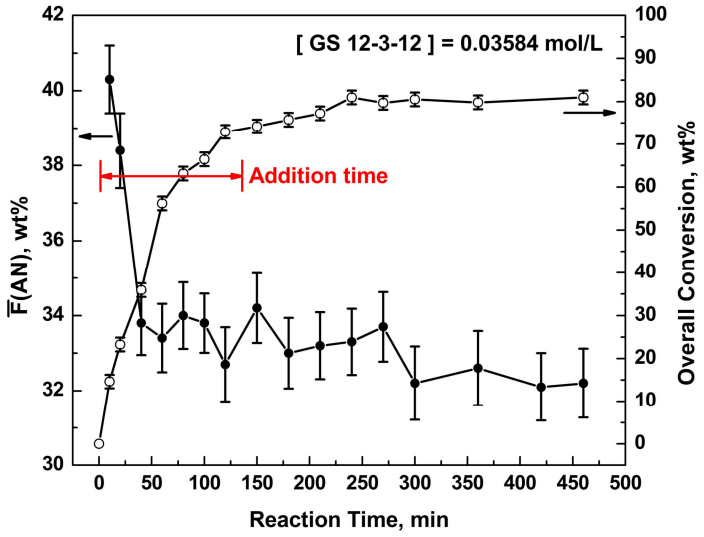


**Figure 5-7 Changing trend of overall copolymerization conversion and cumulative copolymer composition with the reaction time. Polymerization conditions: AN = 2.5 mL, BD = 7.5 mL, APS = 0.2 g, distilled water = 80 mL, T = 50 °C, GS 12-3-12 concentration = 0.03584 mol/L.**

In addition, Figure 5-7 shows the time evolution for the overall conversions for NBR nanoparticles. During the addition stage of the monomer up to around 133 min, the conversion increases almost linearly with the reaction time, which indicates that monomers charged into the system can be consumed to a large extent by the polymerization reaction and the polymerization occurred under starved conditions. Note that even under the starved conditions of monomers, a certain amount of monomer still stay inside the polymer particles over the course of the polymerization. Therefore, after completion of the monomers feeding, an aging time was applied. As shown in Figure 5-7, the conversion continues to grow until it reaches a plateau during the aging period. The rate of polymerization can be estimated using an equation proposed by Sajjadi, as shown below,[18] which is consistent with the results derived from Eq. (2-1):

$$\frac{1}{R_p} = \frac{1}{K} + \frac{1}{R_a} \quad (5\text{-}2)$$

where $R_p$ is the rate of polymerization; $R_a$ is the rate of monomer addition, and $K$ is a constant. According to this equation, the rate of polymerization ($R_p$) was proportional to the rate of monomer addition, and the maximum of the rate of semibatch polymerization is coincidental with that of batch polymerization.

### 5.4.8 Effects of GS 12-3-12 Concentration on Molecular Weight and Glass Transition Temperature ($T_g$) of NBR Nanoparticles

Molecular weight is a key defining property of polymers, as it influences processing characteristics and mechanical properties such as stiffness, strength, and toughness. Figure 5-8 shows the data of $\overline{M}_n$ and $\overline{M}_w$, as well as the molecular weight polydispersity index (PDI = $\overline{M}_w / \overline{M}_n$ ). It can be seen in Figure 5-8 that the molecular weights and PDI decrease gradually with an increase in surfactant concentration. At the high concentration of 0.05708 mol/L, where the particle size is 16.2 nm, the molecular weights are the lowest ($\overline{M}_n$ = 329 900 and $\overline{M}_w$ = 466 702) and PDI is the narrowest being 1.42. This trend in the decrease of molecular weight with increasing surfactant concentration has been observed by many researchers,[14,44-47] and this phenomenon was proposed to be influenced by the following factors. In a semibatch process, the monomer concentration in the particles, $[M]_p$, can impose an effect on the molecular weight of the produced copolymer. At the higher level of surfactant concentration, a high number of polymer particles are produced, and the $[M]_p$ distributed in the latex particles is decreased accordingly. The reduced concentration of monomer at the reaction loci may decrease the rate of polymerization and limit the polymer growth, thereby lowering the molecular weight. In addition, a chain transfer of a growing polymeric radical to surfactant is likely to occur. Because at high surfactant concentration, the size of the obtained particles became smaller, which may increase the proximity of the growing chain radicals to the surfactant adsorbed layer and thus lead to an enhanced chain transfer to the surfactant. Another possible reason is that the average number of free radicals per particle ($\tilde{n}$) varies with the level of surfactant concentration. Under the higher surfactant concentration, $\tilde{n}$ is very small (<< 0.5),[18] which means that the chain transfer of polymeric radicals to monomers will be more important because the resultant monomeric radical will

exit from the micelles very easily thereby reducing the $\tilde{n}$. This chain transfer behavior may reduce the chain growth of particles and thus lead to particles of relatively lower molecular weight. In contrast, the $\tilde{n}$ and $N_c$ (the number of polymer chains per particle) will become larger at the lower surfactant concentration, and the probability of chain transfer to polymer rather than monomer is increased thereby giving as a result of relatively larger molecular weights and higher PDI.

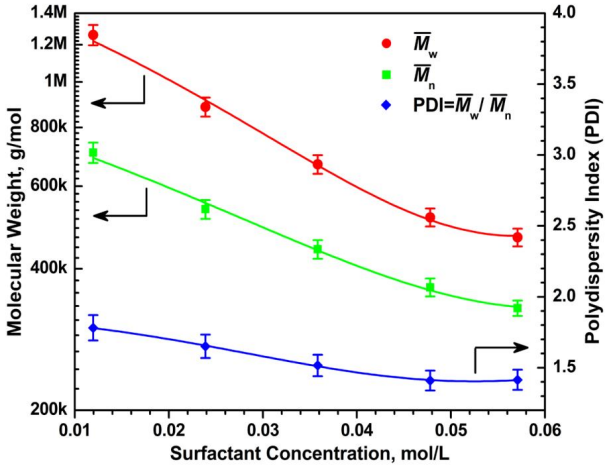


**Figure 5-8 Effects of the GS 12-3-12 concentration on the molecular weight and polydispersity index of NBR nanoparticles. Polymerization conditions: AN = 2.5 mL, BD = 7.5 mL, APS = 0.2 g, distilled water = 80 mL, T = 50 °C**

The glass transition temperature ($T_g$) is an important characteristic of polymers as it determines the range of temperatures for processing and applications. Figure 5-9 shows the DSC curves of polymer nanoparticles prepared using different surfactant concentrations ranging from 0.01195 to 0.05708 mol/L. The $T_g$ values were obtained using the temperatures at the midpoint of the transition region from glassy to rubbery and reported as the mean of three measurements for each sample (±0.5 °C). It can be seen from Figure 5-9 that with an increase in $\overline{M}_n$ from around 329 900 to 707 000 g/mol, there is an increase of $T_g$ from -25.01 to -16.55 °C, which indicates that the $T_g$ values were greatly affected by the molecular

weights. This phenomenon can be explained by the reduction in free volume due to the decrease of the relative volume of the chain ends when the molecular weight increases.[48]

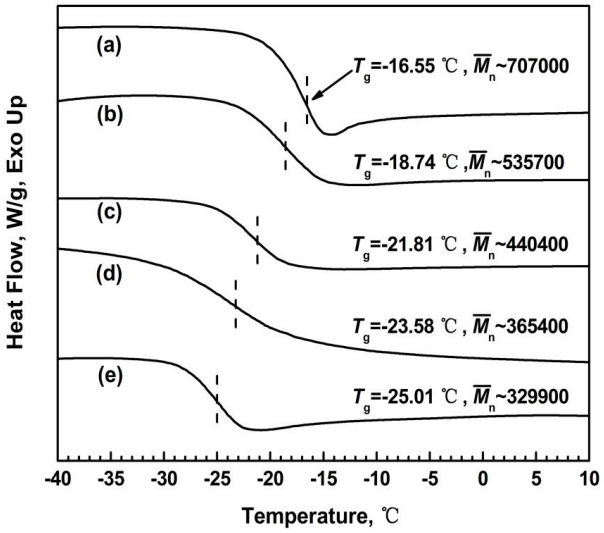


**Figure 5-9 DSC curves of NBR nanoparticles. The nanoparticles were prepared with various surfactant concentrations: (a) 0.01195; (b) 0.02389; (c) 0.03584; (d) 0.04779; (e) 0.05708 mol/L. The values of $T_g$ were estimated as the temperature at the midpoint of the transition region from glassy to rubbery, which were given by the Universal Analysis 2000 software (version 4.5A Build 4.5.0.5) from the TA instruments. The number-average molecular weights shown in Figure 5-9 are consistent with the values presented in Figure 5-8. Polymerization conditions: AN = 2.5 mL, BD = 7.5 mL, APS = 0.2 g, distilled water = 80 mL, T = 50 °C.**

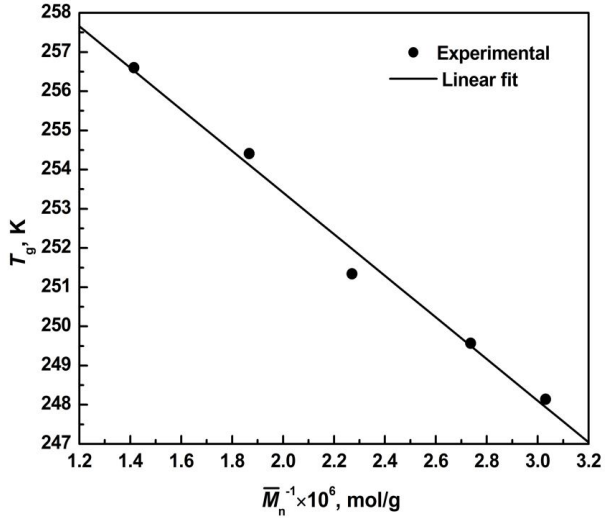


**Figure 5-10 Dependence of the glass transition temperature ($T_g$) on the number-average molecular weight ($\overline{M}_n$). The number-average molecular weights shown in Figure 5-10 are consistent with the values presented in Figure 5-8 and Figure 5-9. Polymerization conditions: AN = 2.5 mL, BD = 7.5 mL, APS = 0.2 g, distilled water = 80 mL, T = 50 °C.**

Further quantitative investigation into the dependence of the $T_g$ upon the molecular weight can be evaluated by the use of the Fox-Flory equation:[49]

$$T_g = T_g^{\infty} - K/\overline{M}_n \qquad (5\text{-}3)$$

where $K$ is a constant, $\overline{M}_n$ is the number-average molecular weight, and $T_g^{\infty}$ is the glass transition temperature for a polymer of infinite chain length.

Figure 5-10 shows the dependence of $T_g$ (Kelvin unit) on the reciprocal of $\overline{M}_n$. A good linear relationship between $T_g$ and $1/\overline{M}_n$ has been found, with $K = (5.31\pm0.32)\times10^6$ g·K·mol$^{-1}$ and $T_g^{\infty} = 264.03\pm0.76$ K, respectively. The $T_g$ of a copolymer is known to steeply depend on both the relative amount of each component and the $T_g$ of the respective homopolymers. As shown in Figure 5-7, the level of bound AN among the different nanoparticles was different ranging from 31 to 35 wt%. However, a linear trend of $T_g$ versus $1/\overline{M}_n$ was still

achieved, which indicates that the discrepancy of cumulative copolymer composition seems too small to produce notable influence on the variation of $T_g$.

### 5.4.9 Effect of Type of Surfactant

#### 5.4.9.1 Particle Size and Morphology of NBR Nanoparticles

The effects of GS 12-3-12 concentration on the particle size and particle size distributions (PSDs) were investigated and are shown in Figure 5-11 (L) and (R). In addition, the single-tail surfactant sodium dodecyl sulfate (SDS) was employed in the polymerization system to replace GS 12-3-12, in order to compare its performance with that of GS 12-3-12 under the same experimental conditions. The particle sizes shown in Figure 5-11 (L) and (R) are reported as the number-average diameter ($D_n$) determined by the DLS technique. For each sample, the size measurement was repeated three times and the mean value was reported.

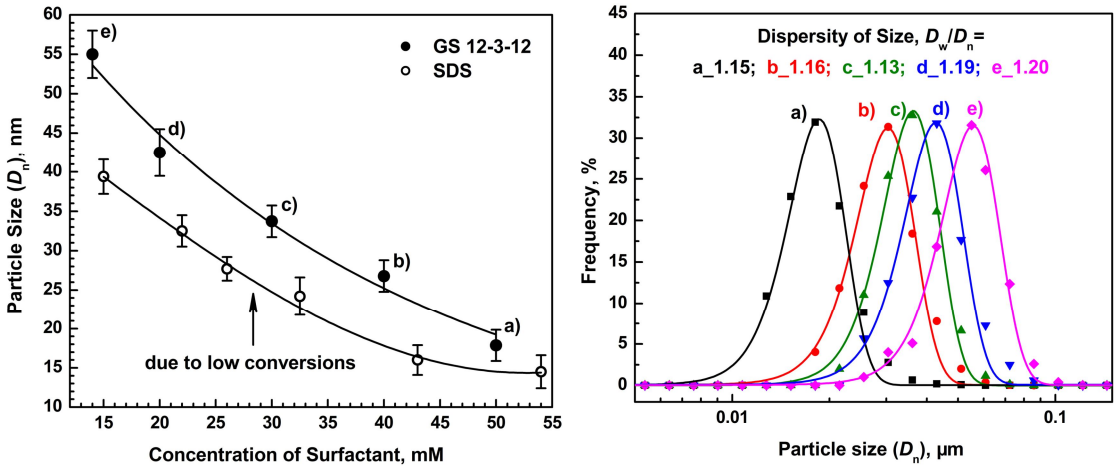


(L) (R)

**Figure 5-11 Dependence of the NBR particle size on the concentrations of GS 12-3-12 and SDS, respectively (left) and a representative set of particle size distributions (PSDs) of NBR nanoparticles prepared under different concentrations of GS 12-3-12 (right). The data of PSDs was fitted with a Gaussian function. The dispersity of particle size ($D_w/D_n$) defined by weight-average diameter ($D_w$) over number-average diameter ($D_n$) was determined by DLS technique. Experimental conditions of preparation: AN = 5 mL, BD = 15 mL, APS = 0.2 g, distilled water =**

**80 mL, T = 50 °C, addition time = 200 min, aging time = 8 h, concentration of surfactant is a variable.**

As shown in Figure 5-11(L), the particle sizes of NBR nanoparticles obtained in the two surfactant systems are plotted as a function of concentrations of GS 12-3-12 and SDS, respectively, which indicates that the type and concentration of surfactant have a great influence on the size of the nanoparticles. On the one hand, Figure 5-11(L) shows that there is a gradual decrease in the particle size with increasing surfactant concentration in each surfactant system. This suggests that the particle size can be well controlled by adjusting the surfactant concentration. In GS 12-3-12 system, the minimized particle size of nanoparticles can reach around 17 nm at the surfactant concentration of 50 mM, while at the relatively low concentration of 14 mM, the particle size is reported as being around 54 nm. At higher levels of surfactant concentration, the particle size is smaller, which indicates that a larger amount of nucleation sites are created.

On the other hand, Figure 5-11(L) shows that the particles prepared in the SDS system are smaller than those obtained in the GS 12-3-12 system. This phenomenon is considered to be due to a much lower polymerization conversion obtained in the SDS system than that in the GS 12-3-12 system (Figure 5-12), as will be discussed later.

Figure 5-11(R) represents the PSDs of NBR nanoparticles obtained via GS 12-3-12 emulsified reaction system. As mentioned, triplicate measurements were performed for each sample, which means that there are three sets of PSDs for each particle size, thus the PSD shown in Figure 5-11(R) is only one of those three sets. Figure 5-11(R) is aimed to provide more detailed information about the frequency of the particle sizes occurring at different size intervals, since the PSDs of particles have a great effect on the processing and properties of the latex polymers. It can be seen in Figure 5-11(R) that a narrow PSD was obtained under each surfactant condition. In the meantime, the PSDs can be quantitatively evaluated by the ratio of $D_w/D_n$ (i.e., dispersity index of size), where $D_w$ and $D_n$ are the weight-average diameter and number-average diameter, respectively. It is commonly accepted that $D_w/D_n$

values ranging from 1.0-1.1 can be regarded as monodisperse, while those ranging from 1.1-1.2 as near-monodisperse.[50] As shown in Fig. 1(R), the $D_w/D_n$ values of the nanoparticles produced using GS 12-3-12 are all within the range from around 1.13 to 1.20, which suggest that near-monodisperse PSDs were obtained, even for the nanoparticles prepared under the very low surfactant to polymer weight ratio. In addition, with increasing surfactant concentration, there is a general decrease in the dispersity index of the particle size. This trend in the PSDs with variation in surfactant concentration is consistent with the results reported by Sajjadi,[51] and a detailed discussion can be found in his report. Based on this small feature particle sizes and narrow PSDs, the obtained NBR nanoparticles may present many promising applications in academic research and commercial applications.

#### 5.4.9.2 Polymerization Conversion, Solid Content, and Copolymer Composition

The effects of the surfactant type and concentration on the polymerization conversion and solid content of NBR emulsion are shown in Figure 5-12a and b, respectively. It can be seen from Figure 5-12a and b that a relatively high polymerization conversion and solid content can be achieved under higher levels of surfactant concentration, e.g., above 30 mM for the GS 12-3-12 system. In an emulsion polymerization system, a certain amount of surfactant no matter whether GS 12-3-12 or SDS can form numerous compact micelles while the inner space of each micelle can be used as a "nanoreactor". A high level of surfactant concentration will provide more numerous micelles thereby giving birth to more “nanoreactors” in the system. Thus, for a given polymerization system, a higher surfactant concentration will result in a higher polymerization conversion and solid content.

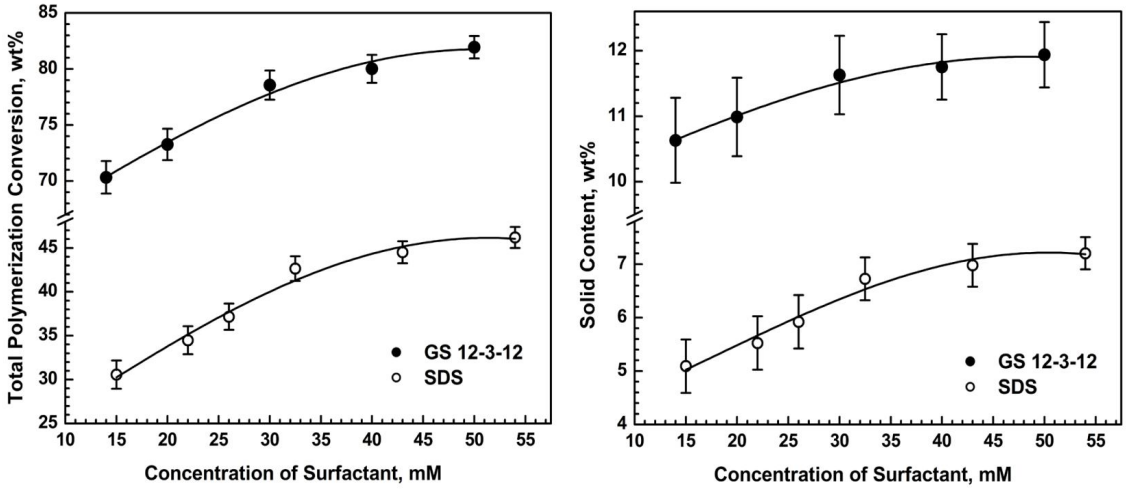


**Figure 5-12 Effects of the type and concentration of surfactant on the polymerization conversion of NBR nanoparticles (a) and solid content of NBR latex (b). Experimental conditions of preparation: AN = 5 mL, BD = 15 mL, APS = 0.2 g, distilled water = 80 mL, T = 50 °C, addition time = 200 min, aging time = 8 h, concentration of surfactant is a variable.**

Figure 5-12a and b clearly show the advantages of GS 12-3-12 over SDS with respect to the polymerization conversion as well as the solid content of the latex. It can be seen from Figure 5-12 that with an increase in the surfactant concentration, the polymerization conversions obtained in GS 12-3-12 system span from 75 to 87 wt%, which are much higher than the conversions ranging from 31 to 46 wt% obtained in the SDS system within the same reaction period. That is why the particle sizes prepared using the GS 12-3-12 system are larger than those obtained from the SDS system, as can be seen from Figure 5-11(L).

Depending on the balance of linear-to-branched configuration desired, it is well-known that the nitrile rubber can be polymerized from 5 to 15 °C (cold NBR, more linear polymer chains) and 30 to 50 °C (hot NBR, highly branched). Redox initiation is used for the production of cold rubber, while a typical thermal decomposition of the initiator is employed in the production of hot rubber. In the present study, a hot rubber recipe was employed, as it can provide a "cleaner" substrate system for subsequent catalytic latex hydrogenation. However, one issue associating with the reaction temperature (i.e., 50 °C) is that the

decomposition rate of initiator APS is slow, which will decrease the rate of polymerization and thus lead to a lower conversion of monomers. However, as shown in Figure 5-12a, a relatively high conversion was still obtained in the GS system compared to the low conversion in the SDS system at the same concentrations of GS and SDS. This is mainly attributed to the following two reasons.

First of all, the decomposition rate of APS in the aqueous phase is greatly enhanced in the acidic reaction system induced by GS 12-3-12, which has been described in Section 5.4.7. On the other hand, GS 12-3-12 can provide more numerous of micelles thereby creating more nucleation loci which increases the polymerization rate. The aggregation number for GS 12-3-12 is 45 determined by pyrene fluorescence quenching,[52] which is around 25% less than the aggregation number of SDS that is usually considered to be 60±2.[53] Therefore, during the polymerization, GS 12-3-12 system can generate more numerous nucleation sites in the reactor and create more reaction domains than the SDS system. In keeping with the above discussion, the GS 12-3-12 system has a faster polymerization rate than that of the SDS system under the same concentration of emulsifier.

In short, the NBR latex obtained using the GS system has a relatively high polymerization conversion/rate under the low reaction temperature of 50 °C and exhibits good colloidal stability. More importantly, this GS emulsion system avoids the use of additional chemicals such as acidic electrolytes to increase the conversion of polymer nanoparticles, which thus simplifies the formulation recipe and circumvents chemicals that may impose negative effects on the stability of the latex and catalytic activity for the subsequent latex hydrogenation.

## 5.5 Conclusions

NBR nanoparticles were successfully synthesized in a semibatch microemulsion polymerization system using GS 12-3-12 as the emulsifier. An enhanced decomposition rate of initiator APS was achieved even under the low temperature of 50 °C, which is attributed to the acidic initiation environment by using GS 12-3-12 as the emulsifier. The FT-IR and $^{1}$H NMR characterizations demonstrate that the monomers have been incorporated into the

produced nanoparticles and the 1,4-*trans* double bonds account for a major percentage of the olefin units in the synthesized polymers. The produced latices show a comparable stability to a conventional microemulsion while the required surfactant/monomer and surfactant/water weight ratios are much lower than those of the microemulsion system. The latex nanoparticles exhibit a spherical morphology and a particle size below 20 nm can be reached. The obtained NBR nanoparticles are spherical in shape and exhibit a near-monodisperse PSDs with $D_w/D_n$ ranging from 1.13 to 1.20. The obtained NBR nanoparticles have high molecular weights and narrow PDIs within the range of 1.42-1.78. The kinetic data suggests that the initial monomer feed fraction ($f_{AN}$ = 30 mol%) is in the azeotropic composition region and the level of bound AN was found to be in the range of 31-35 wt% depending on the surfactant concentrations used. These results agree with the theoretical azeotropic composition simulated by the Mayo-Lewis equation. The $T_g$ values were found to increase from -25.01 to -16.55 °C with an increase in $\overline{M}_n$ from around 329 900 to 707 000 g/mol. The linearity of $T_g$ versus $1/\overline{M}_n$ shows a good agreement with the Fox-Flory equation. The GS 12-3-12 system has notable advantages in providing much higher polymerization conversion and solid content than obtained in the SDS system. The present synthesis process can be extended to latices made from semibatch microemulsion polymerization containing other diene-based polymers. The obtained fine NBR nanoparticles may find many important applications in various fields, particularly in the improvement of the hydrogenation rate of the diene-based polymers in the latex form.

# Chapter 6

# Organic Solvent-Free Catalytic Hydrogenation of Diene Polymer Nanoparticles in Latex: Kinetic Analysis and Mechanistic Study

## 6.1 Overview

The direct catalytic hydrogenation of poly(butadiene-*co*-acrylonitrile) nanoparticles in latex form was carried out under various experimental conditions in the presence of Wilkinson's catalyst without the addition of any organic solvents. In order to appreciate the important factors which influence the nature and extent of this type of hydrogenation, the effects of particle size within the range from 17.5 to 42.2 nm, temperature from 90 to 130 °C, and catalyst concentration from 0.1 to 1.0 wt% (based on the weight of polymer) on the hydrogenation rate were fully investigated. The kinetic study shows that the reaction is chemically controlled with a high apparent activation energy (100 to 110 kJ/mol) under experimental conditions. Mass transfer of both the hydrogen and catalyst involved in the reaction system are discussed. The analysis of mass transfer of reactants coupled with the reaction kinetics indicated that the catalysis of hydrogenation proceeds on the molecular level. The competitive coordination of the active catalyst species $RhH_2Cl(PPh_3)_2$ between the carbon-carbon unsaturation and acrylonitrile units within the copolymer was elucidated based on the reaction kinetics of the hydrogenation.

## 6.2 Introduction

Hydrogenation constitutes an important process of chemical modification as it not only provides a pertinent way to improve the mechanical, chemical, physical and thermal properties of unsaturated polymers, but also offers an efficient synthetic route to synthesize the novel polymers with controlled molecular weight, required microstructure, and unique stereochemistries that are difficult or too expensive to achieve by conventional monomer polymerization.[1-3] The selective hydrogenation of the carbon-carbon double bonds in NBR is such a typical commercial process. The produced HNBR shows more resistant than NBR towards oxidative and thermal degradation while maintaining its elastomeric properties in

chemically aggressive environments, as well as notable improvements in mechanical properties characterized by tensile strength, elongation, abrasion resistance, and hardness.[1] Thus, HNBR has been extensively used for hoses, seals, belts and gaskets for oil exploration and processing and under-the-hood rubber components in automobiles, and so forth.

The current commercial process for the hydrogenation of unsaturated polymers such as NBR, SBR and NR usually involves a number of cumbersome steps, including purifying polymer from the latex, dissolving the polymer in large amounts of organic solvent i.e. solution hydrogenation, and recovering the organic solvent after the hydrogenation operation. This process not only raises environmental concerns but increases the cost of production. It is therefore very desirable to directly hydrogenate the unsaturated polymers in latex or bulk form as such a process would avoid the tedious hydrogenation steps and thereby eliminate the need of large amounts of toxic organic solvents. The pioneer work of bulk hydrogenation of olefinic polymers can be traced to Gilliom and co-worker's reports.[4,5] However, the relevant studies with the bulk hydrogenation appear rare since Gilliom and co-worker's studies, should very slow rates of reactions as a result of severe mass transfer and heat transfer. Thus latex hydrogenation is becoming important, especially when the hydrogenated product in latex form is the desired end-use product or only surface/gradient hydrogenation of a product is required.[6-23]

The challenges associated with latex hydrogenation pertain to how to accomplish the optimal interplay of accelerating the hydrogenation rate, decreasing the demanded quantity of catalyst, and eliminating the need for an organic solvent. It is reported here that through using nanoscale NBR particles, e.g. below 20 nm, as the substrate, the hydrogenation rate can be increased dramatically in the absence of organic solvent while a quite low level of catalyst loading is required. This provides one way to overcome the challenges involved in latex hydrogenation. In addition, the present research is an attempt to appreciate the underlying chemistry of latex hydrogenation of NBR under the conditions that are relevant to industrial applications of this technology. The mass transfer of hydrogen and catalyst in the latex system is considered and discussed extensively. The effects of main factors characterized by particle size, catalyst concentration, and temperature on the hydrogenation rate were

investigated. Based on the kinetic data obtained, the kinetics and mechanism of NBR latex hydrogenation catalyzed by $RhCl(PPh_3)_3$ was examined.

## 6.3 Experimental

### 6.3.1 Materials

Ultra-high purity hydrogen (99.999%, oxygen-free) was used as received (Praxair Inc., Mississauga, CA). Wilkinson's catalyst $RhCl(PPh_3)_3$ was prepared according to the literatures.[24,25] Acetone (reagent grade), methanol (reagent grade), and methyl ethyl ketone (MEK, reagent grade) were purchased from Sigma-Aldrich Corp. (Oakville, CA) and used as received. Triphenylphosphine (TPP, 99%) was obtained from Strem Chemicals, Inc. (Massachusetts, USA) and further purified by recrystallization from ethanol to remove triphenylphosphine oxide. The substrate for the latex hydrogenation is NBR nanoparticles, which were prepared in our laboratory via a semibatch microemulsion polymerization system using Gemini surfactant trimethylene-1,3-bis(dodecyldimethylammonium bromide), denoted as GS 12-3-12, as the emulsifier. The detailed preparation procedure and characterization of NBR nanoparticles can be found in Chapter 5. The principal characteristics of the prepared nanoparticles are summarized and presented in Table 6-1 for convenience and facilitation for subsequent discussion. It should be noted that size measurements using DLS yielded a number-average diameter, which is a mean value from triplicate measurements for each sample and this diameter was found to be consistent with the dimensions of particles viewed by TEM.

**Table 6-1 Principal characteristics of NBR latex particles**

| Surfactant concentration in polymerization, mM[a] | Radius of latex particles, nm | BD conversion, wt% | Bound AN, wt% | $\overline{M}_n$ | Polydispersity= $\overline{M}_w / \overline{M}_n$ | $T_g$, °C |
|---|---|---|---|---|---|---|
| 12 | 42.2 | 65.36 | 35.2 | 707000 | 1.78 | -16.55 |

| | | | | | | |
|---|---|---|---|---|---|---|
| 24 | 35.3 | 72.18 | 33.9 | 535700 | 1.65 | -18.74 |
| 36 | 25.7 | 78.89 | 32.2 | 440400 | 1.52 | -21.81 |
| 48 | 17.5 | 80.90 | 31.9 | 365400 | 1.41 | -23.58 |

[a] The surfactant used was Gemini surfactant trimethylene-1,3-bis (dodecyldimethylammonium bromide), denoted as GS 12-3-12.

### 6.3.2 Typical Protocol of Latex Hydrogenation of Diene-based Polymers

The latex hydrogenation of NBR nanoparticles was carried out in a 300 mL Parr 316 Stainless Steel reactor. A catalyst pre-dispersion approach was employed. It is called the catalyst pre-dispersion method because there was an introduction period allowing for mass transfer of catalyst into the latex particles before the initiation of hydrogenation. In a typical run, a measured volume of the NBR latex was first mixed with a certain amount of accurately weighed Wilkinson's catalyst and the required additive triphenylphosphine (TPP) with an accurate weight ratio of 10:1 catalyst. TPP is a key component and plays a vital role in a "green" latex hydrogenation, by which the alien solvent required in most of latex hydrogenation can be eliminated. The optimum weight ratio of 10:1 of TPP over catalyst is determined from our previous experiments,[23] under which the catalyst exhibits a high activity and a conversion above 95 mol% can be reached. The mixture including the substrate, catalyst, and TPP was degassed with three quick $N_2$ cycles and subjected to bubbling $N_2$ under about 1.38 MPa for 20 min at room temperature with an agitation speed of 200 rpm. The resulting mixture was then heated up to a given reaction temperature and stabilized for 3 h under 600 rpm stirring speed. The hydrogenation reaction was embarked on when the hydrogen gas with a pressure of 1000 psi (6.89 MPa) was introduced into the reactor. The hydrogen pressure (1000 psi), hydrogenation temperature (90-130 °C), and agitation speed (600 rpm) were maintained constant throughout the reaction period. Aliquots were taken at various time intervals through a dip tube and characterized by FT-IR and $^1$H NMR to obtain the degree of hydrogenation. When the degree of hydrogenation reached more than 95 mol%, the system was cooled down to room temperature and depressurized to obtain the final product.

## 6.4 Results and Discussion

### 6.4.1 Analysis of Mass Transfer in the Latex Hydrogenation

The latex hydrogenation of diene-based polymers is carried out in a solid (polymer)-liquid (water)-gas (hydrogen) three-phase system (Scheme 6-1). Different terms, such as biphasic hydrogenation were also used to describe this process.[21] The unique characteristic of this latex hydrogenation system is that each polymer-swollen micelle acts as a nanoreactor and the catalyst and hydrogen are required to transfer into the micelles to access the olefins. The latex hydrogenation of NBR nanoparticles is a complex reaction system involving nanoparticle-water-hydrogen three phases and mass transfers of Wilkinson's catalyst and hydrogen between the different phases. Therefore, it is important to investigate the mass transfer process of hydrogen and catalyst in the reaction system, particularly when kinetics and mechanistic studies are involved.

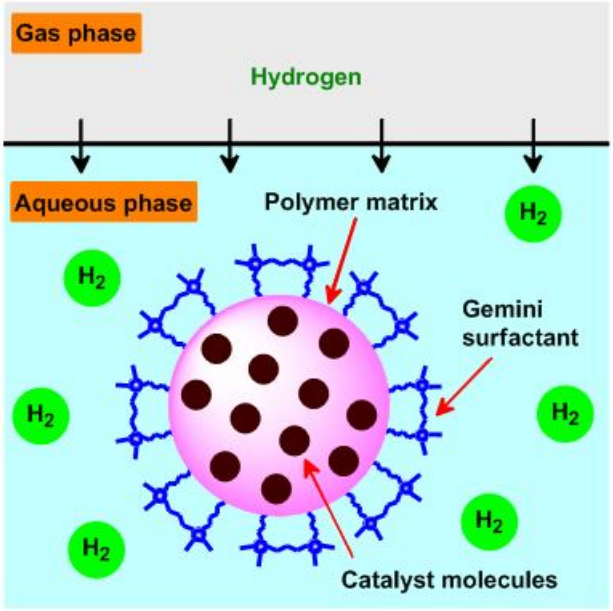


**Scheme 6-1 Illustrative diagram of three-phase latex hydrogenation of unsaturated polymer.**

#### 6.4.1.1 Catalyst Pathway

The mass transfer of catalyst in the latex hydrogenation can be represented by the following steps:

(1) Transport of the catalyst from the bulk water phase to the water-solid interface (surfactant layer) of the latex particles;

(2) The catalyst permeates the surfactant layer surrounding the particles and contacts the polymer chains which are in the outside layer of the particles;

(3) Intraparticle diffusion of the catalyst molecules within the polymer chains.

##### 6.4.1.1.1 Effect of catalyst pre-dispersion on hydrogenation

A catalyst pre-dispersion approach was employed in the present latex hydrogenation. It is called the catalyst pre-dispersion method because there is an introduction period allowing for the mass transfer of catalyst into the latex particles before the initiation of hydrogenation. This addition approach of catalyst before charging hydrogen stems from the important work of Gilliom and coworker who pioneered bulk hydrogenation of olefinic polymers by using molecular catalysts.[4,5] They demonstrated that the hydrogenation can be realized in the unsaturated polymer matrix without the presence of added organic solvent and verified the homogeneous nature of the catalysis during the course of hydrogenation. In their studies, the catalyst was distributed into the butadiene-derived elastomers by dissolving these two materials in a proper solvent and then removing the solvent to yield a homogenous starting mixture. With respect to latex hydrogenation, however, it is a great challenge to disperse the oil soluble catalyst e.g. Wilkinson's catalyst into the latex particles, which is more difficulty if the dispersion is required to reach a molecular level. It is apparent that the solution cast approach used by Gilliom was not applicable in the latex hydrogenation system in terms of dispersing the catalyst within the latex particles. A breakthrough was achieved in this aspect is that through taking advantage of the added TPP, Wilkinson's catalyst was successfully transferred into the polymer particles. What's more important, the catalyst entering into the particles was dispersed homogeneously within the polymers, as shown in the following section.

6.4.1.1.2 TPP's role as a promoter

TPP is an important component for maintaining the activity of the catalyst. In the commercial solution hydrogenation it only works as the required free ligand to keep the high catalytic activity of Wilkinson's catalyst, $RhCl(PPh_3)_3$. However, when the latex hydrogenation system was introduced, the role of TPP played was expanded extensively. The main role of TPP has been changed to a catalyst mass transfer promoter, which means that during the course of latex hydrogenation, the free TPP will act as a continuous phase to dissolve the dispersed catalyst molecules thereby facilitating the phase boundary crossing of the catalyst from the aqueous phase to the polymer phase. The schematic representation of this process has been elucidated in Scheme 6-2. In the present experiments, the catalyst and TPP were first added and suspended in the aqueous phase (Scheme 6-2a) before charging hydrogen gas and the ratio of TPP over catalyst is 10:1 (w/w), which has been reported to be the optimum ratio to guarantee effective mass transfer as well as to maintain the stability of the catalyst.[23] The melting point of TPP purchased from Sigma-Aldrich is 79-81 °C, and thus TPP will be melted and form numerous liquid droplets under reaction temperature above 90 °C (Scheme 6-2b). The catalyst will be then dissolved into the TPP droplets to form a homogenous solution. In parallel with this dissolution process, this mixture will be encapsulated and stabilized by the statistically moving surfactant molecules (Scheme 6-2c). In the micellar solution of surfactant, the micelles are in a dynamic equilibrium state and the surfactant molecules are constantly being exchanged into and out of the micelles in a continuous disintegration and reformation process. This functional mechanism will promote the formation of homogenous droplets comprised of the catalyst and TPP. The surfactant molecules attached to TPP-Catalyst droplets will then assemble into the latex particles by taking advantage of the active equilibrium between the micelles and surfactant molecules (Scheme 6-2d).

When the catalyst and TPP are transferred into polymer phase, these three components are considered to form a homogeneous mixture during the predispersion period under the studied experiential conditions. At the elevated temperate of the reaction system above 90 °C, the NBR nanoparticles are melted and appear to behave as a fluid. Meanwhile, the liquid TPP

can dissolve into NBR, which thus promotes the dissolution of Wilkinson's catalyst into the NBR matrix. In addition, the observed number of turnovers (TON) has particularly interesting implications for the molecular-level homogeneous distribution of catalyst within the polymer matrix.[4] As shown in Table 6-7 (which will be presented later), most of the experimental runs have a high TON above 1000, especially in run 24, an exceptionally high TON of 11065.88 and a high turnover frequency (TOF, ~553.29 $h^{-1}$) were achieved. Assuming that each molecule of catalyst was equally involved in the reaction, obtaining greater than 10,000 turnovers requires sufficient mobility in the reaction medium for the catalyst to encounter more than 10,000 double bonds, which suggest that the mobility of catalyst molecules inside the polymer matrix is very high thereby providing strong evidence that catalysis was carried out at the molecular level. Furthermore, Gilliom pointed out that the effective hydrogenation of a bulk polymer required a soluble catalyst[4] and the fact that the HNBR nanoparticles with more than 95 mol% conversion in the absence of solvent presented here provided additional evidence that the catalytically active species in the polymer matrix is homogenous. Based on the discussion above, it can be stated that the latex hydrogenation can be regarded as "*mini-bulk*" hydrogenation comprised of nano homogenous bulk hydrogenation inside latex particles.

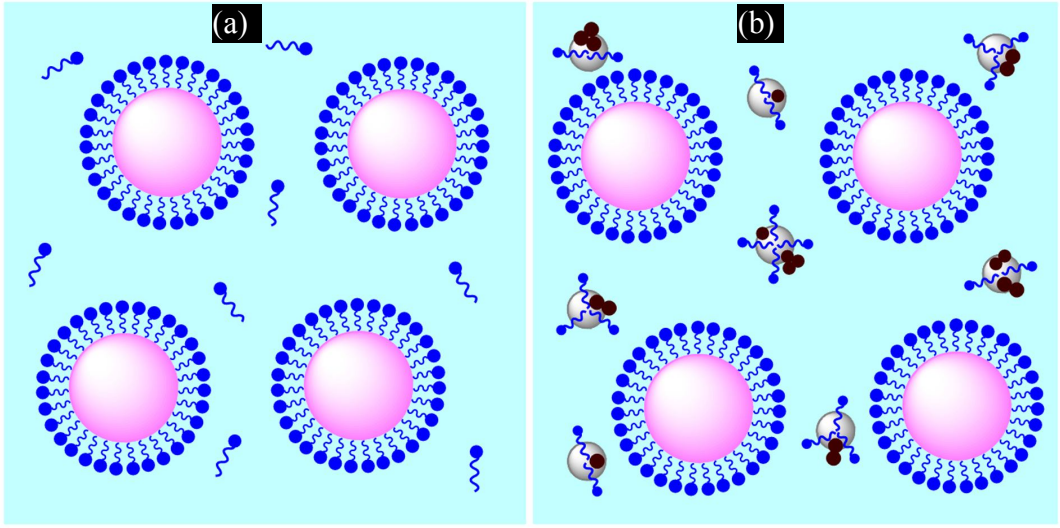

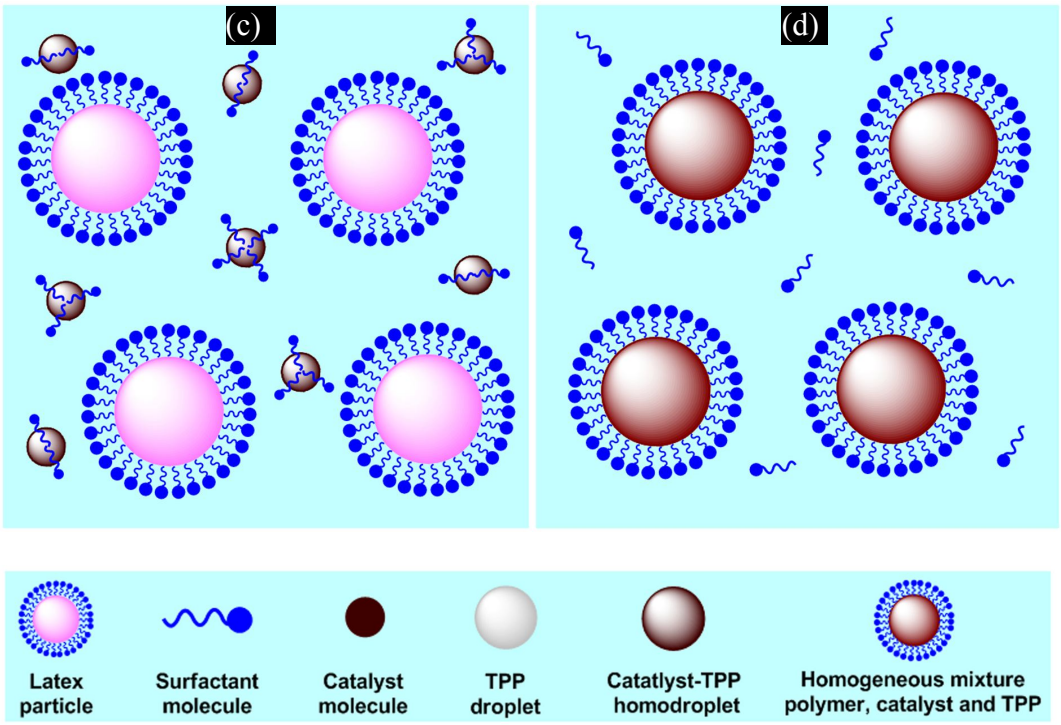


**Scheme 6-2 Mass transfer of catalyst using TPP as the carrier from aqueous to bulk phase.**

### 6.4.1.2 Hydrogen Pathway

The mass transfer of hydrogen in the latex hydrogenation is rationalized to consist of the following events that may occur in a sequence or in a parallel:

(1) Transport of $H_2$ from the bulk gas phase to the gas-water interface (surfactant "membrane").

(2) Mass transfer of $H_2$ from the gas-water interface to the bulk of the aqueous phase.

(3) Mass transfer of $H_2$ from the bulk water phase or directly from the gas-water interface to the water-polymer interface, i.e. surfactant layer surrounding the polymer particles when the colloidal particles appear at the gas-water interface.

(4) Penetration of the hydrogen through the surfactant layer to the surface of polymer particles.

(5) Intraparticle mass transfer of hydrogen inside each polymer particle to access all C=C bonds.

(6) Participate in the catalysis process for the reduction of C=C bonds in the presence of the catalyst.

Due to the vigorous agitation (600 rpm) and high constant charged pressure (1000 psi), the diffusion process of hydrogen in steps 1-3 was insignificant and can be considered as negligible. In addition, the hydrogen concentration in the water phase can be assumed to be constant because the pressure is constant. This means that with respect to the latex particles, the gas phase and water phase can be regarded as "one" phase because of the surrounding constant hydrogenation concentration. Given that the present reaction system was run with very high agitation, the hydrogen contained in the water phase mainly includes two parts: one is the hydrogen dissolved into the water and the other is the hydrogen suspended in the water in the form of gas bubbles, which accounts for the major part of hydrogen in the aqueous phase. Nevertheless, it is very difficult to directly measure the hydrogen concentration in the water phase, thus quantitative estimates can only be considered to be within a range starting from the hydrogen dissolved into the stagnant water without agitation (molecule diffusion) to the hydrogen with very high agitation (turbulent diffusion).

6.4.1.2.1 Concentration of Hydrogen in Agitated Water Phase

The solubility of hydrogen gas in the stagnant water can be determined from the Krichevsky-Kasarnovsky (KK) equation,[31] which is expressed as below:

$$\log\frac{f_{H_2}}{N_{H_2}} = \log K + \frac{P\bar{v}}{2.303RT} \quad \textbf{(6-1)}$$

where $f_{H_2}$ is fugacity of hydrogen gas, which is estimated as 70.703 atm under 1000 psi;[32] $N_{H_2}$ is mole fraction of hydrogen in water; and $K$ is the corrected Henry's Law coefficient based on different temperatures using Eq. (6-2), atm; $\bar{v}$ is the partial molar volume of

hydrogen in water; $P$ is the pressure, atm; $R$ is the gas constant equal to 82.05746 $cm^3 \cdot atm \cdot K^{-1} \cdot mol^{-1}$, and $T$ is the absolute temperature, K.

The Henry's Law constant is commonly used to describe the low solubility of light solutes in a variety of solvents at a moderate partial pressure over a wide range of temperature. Regarding a hydrogen-water pair, the Henry's Law constant was reported to first undergo an increase with increasing of temperature, pass through a maximum, and then decline at higher temperatures.[33] Therefore, at different temperatures, the Henry's Law constant needs to be corrected, which can be determined using the following equation given by Harvey:[33]

$$\ln K_{\mathrm{H}} = \ln P_l^{sat} + (-4.4964)/T^* + 6.0952(1-T^*)^{0.355}/T^* + 5.8390\exp(1-T^*)/(T^*)^{0.41} \quad (6\text{-}2)$$

where $K_{\mathrm{H}}$ is Henry's constant of $H_2$ in water, MPa; $P_l^{sat}$ is the vapor pressure of water at saturation (Table 6-2), which was computed with the equation proposed by Saul and Wagner;[34] $T^* = T/T_c^l$, where $T$ is the absolute temperature and $T_c^l$ is the critical temperature of water which is equal to 647.14 K.

On combining the above two equations, the solubilities of hydrogen in stagnant water at temperatures ranging from 90 to 130 °C under 1000 psi were obtained and are presented in Table 6-2. The calculated hydrogen concentration in the stagnant water is found to be within the range of experimental results reported by Baranenko and Kirov.[35] On the other hand, the hydrogen concentration in the agitated water with infinite fast stirring can be hypothesized to equal to that in the bulk gas phase, which was thus calculated using the ideal gas law and the results are listed in Table 6-2. As stated earlier, the hydrogen concentration in the studied aqueous phase will fall between these two concentrations. It can be seen from Table 6-2 that the agitation can greatly benefit the transport of hydrogen from the gas phase into the aqueous phase. The level of bound hydrogen can be used to evaluate the diffusivity of hydrogen inside the polymer chains.

**Table 6-2. Solubility of hydrogen in agitated water under the studied experimental conditions.**

| temperature | Saturation | Henry's | Mole | concentration | concentratio |
|---|---|---|---|---|---|

| , °C/K | pressure of water vapour, $P_l^{sat}$ ,(MPa) | constant, KH (MPa) | fraction, mol% | in stagnant water, mol/L | n in infinite fast agitation, mol/L[a] |
|---|---|---|---|---|---|
| 90/363.15 | 0.0701 | 7435.89 | 0.0917 | 0.0513 | 2.28 |
| 100/373.15 | 0.101 | 7177.56 | 0.0952 | 0.0532 | 2.22 |
| 110/383.15 | 0.143 | 6874.60 | 0.0995 | 0.0556 | 2.16 |
| 120/393.15 | 0.198 | 6539.12 | 0.105 | 0.0585 | 2.11 |
| 130/403.15 | 0.270 | 6181.88 | 0.111 | 0.0619 | 2.06 |

[a] Calculated based on the ideal gas law $P=C_gRT$, where $P$ is the pressure; $C_g$ is the concentration of hydrogen in gas phase ($mol \cdot m^{-3}$); $R$ is the gas constant using 8.314 $J \cdot K^{-1} \cdot mol^{-1}$ and $T$ is absolute temperature.

6.4.1.2.2 Estimation of Mass Diffusivity of Hydrogen in NBR Nanoparticles

The mass diffusion in solids is often not well represented by Fick's law, thus the diffusion coefficient might not be well-defined. It is desirable to adopt other (empirical) correlations instead of Fick's law to describe the mass diffusion of the hydrogen inside the NBR nanoparticles. Numerous studies have shown that the diffusion coefficients for gases in polymers exhibited an Arrhenius behavior dependence on temperature, which can be represented as:[36-40]

$$D = D_0 \exp(\frac{-E_d}{RT}) \qquad (6\text{-}3)$$

where $D$ is the diffusion coefficients, $cm^2/sec$; $D_0$ is the pre-exponential factor, $cm^2/sec$ and is a constant; $E_d$ is the activation energy of diffusion, J/mol; $R$ is the universal gas constant equal to 8.314 $J \cdot K^{-1} \cdot mol^{-1}$, and $T$ is the absolute temperature, K.

A careful examination of the mass diffusion coefficients of gas in various types of rubbers was conducted by Van Amerongen.[37] The diffusion coefficient has a close relationship with the bound level of nitrile in NBR, which was found to decrease with an increase in the

level of bound AN. With respect to the nitrile butadiene rubber containing 68 wt% BD and 32 wt% AN, the $E_d$ and $D_0$ are determined to be 29288 J/mol and 0.52 $cm^2$/sec, respectively. For the studied NBR particles, the bound level of AN is in the range from 31.1 to 35.2 wt% with the variation of surfactant amount in the polymerization stage (Table 6-1). As indicated in Van Amerongen's report, the diffusivity response to the changes of AN content ranging from 30 to 40 wt% is of the same order of magnitude. Therefore, the diffusivity of hydrogen in NBR can be evaluated using the data of 32 wt% of bound level AN. Through applying the values of $E_d$ and $D_0$ into Eq. 6-3, the diffusion coefficients under different temperatures can be obtained, which are provided in Table 6-3. The diffusivity stands for the mass transfer capability of the hydrogen in the polymer matrix and can be used to evaluate whether the mass transfer limitations of hydrogen can account for the rate-determining step in the hydrogenation reaction, which will be discussed in the following section. It can be seen from Table 6-3 that the diffusion coefficients of hydrogen in NBR are relatively large and are of the same order of magnitude with the diffusivity of hydrogen in water reported by Ferrell and Himmelblau.[41] In addition, the diffusivity of hydrogen in NBR is insensitive to the variation of temperature as the coefficient increases only slightly with rising temperature.

**Table 6-3 Diffusivity of $H_2$ in NBR nanoparticles (32 wt% acrylonitrile)**

| temperature, °C/K | Diffusivity ($cm^2$/sec) |
|---|---|
| 90/363.15 | 3.18518E-05 |
| 100/373.15 | 4.1308E-05 |
| 110/383.15 | 5.28496E-05 |
| 120/393.15 | 6.67736E-05 |
| 130/403.15 | 8.3393E-05 |

6.4.1.2.3 Modeling of Hydrogen Diffusion in NBR Nanoparticles

Gilliom and Honnell carried out a bulk hydrogenation study using a polystyrene-polybutadiene-polystyrene (PS-PB-PS) pellet with dimensions of ~2 mm thick and ~2.5 cm

in diameter as the substrate, in which the reaction rate was observed to be controlled by the diffusion of hydrogen through the pellet.[5] They proposed a one-dimensional, moving boundary model to describe this diffusion process, where the concentration of hydrogen at the pellet surface is equal to that in the surrounding gas phase and the concentration at the reaction front is zero. However, when the size of the substrate was reduced significantly, even to the nanoscale as shown in the present study, it will become unclear whether the diffusion of hydrogen is still the rate-determining step or not. In order to make it clear, the following analysis was conducted.

The diffusion distance starting from the particle surface as a function of time can be related through the following expression:[5]

$$d(t) = \xi(2Dt)^{1/2} \quad \textbf{(6-4)}$$

where $d$ is the distance taken from the outside boundary of the particle; $D$ is the hydrogen diffusivity in the polymer, $t$ is the diffusion time of hydrogen and $\xi$ is given by the transcendental equation:

$$C_0 e^{-\xi^2/2} = (2\pi)^{1/2} b\xi \, \mathrm{erf}\left(\frac{\xi}{\sqrt{2}}\right) \quad \textbf{(6-5)}$$

where $C_0$ denotes the concentration of hydrogen at the outer surface of NBR nanoparticles and $b$ is the concentration of reactive double bonds, as shown in Table 6-1.

The hydrogen concentration $C_0$ has been stated to be within a range (Table 6-2) and it is unlikely to obtain an accurate value of $\xi$ according to Eq. (6-5). However, the range of $\xi$ can be determined using the two boundary values of hydrogen concentration as shown in Table 6-2. The higher the hydrogen concentration, the larger the $\xi$ values, and the faster the hydrogen diffuses in the polymer. The modeling under the condition of the slowest diffusion rate of hydrogen was first investigated. Table 6-5 presents the $\xi$ values obtained using the minimum hydrogen concentration. Combined with the diffusion coefficients shown in Table 6-3, the position of hydrogen diffusing in the particles as a function of time can be modeled using Eq. (6-4) as shown in Figure 6-1.

**Table 6-4 Concentration of olefins in NBR with different radii of particles**

| Surfactant concentration used in the synthesis, mM[a] | Radius of latex particles, nm | Concentration of C=C in the NBR particles, mM |
|---|---|---|
| 12 | 21.10 | 181.547722 |
| 24 | 17.65 | 200.4955 |
| 36 | 12.85 | 219.149472 |
| 48 | 8.75 | 224.711583 |

[a] The surfactant used was Gemini surfactant trimethylene-1,3-bis (dodecyldimethylammonium bromide), denoted as GS 12-3-12.

**Table 6-5 $\xi$ values calculated using the minimum hydrogen concentration**

| temperature, °C/K | concentration of hydrogen in stagnant water, mol/L | $\xi$ |
|---|---|---|
| 90/363.15 | 0.051276 | 0.351 |
| 100/373.15 | 0.053191 | 0.357 |
| 110/383.15 | 0.055604 | 0.365 |
| 120/393.15 | 0.058526 | 0.374 |
| 130/403.15 | 0.061978 | 0.384 |

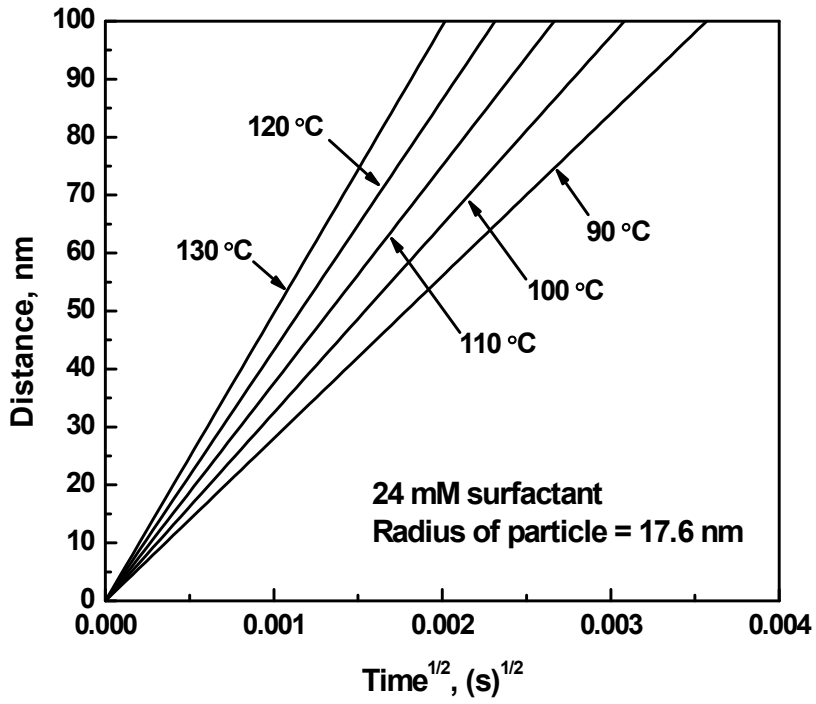


**Figure 6-1 The diffusion position of the hydrogen gas in the bulk particles with the evolution of the squire root of time. The original distance (d) = 0 is taken as the particle outside boundary.**

It can be seen form Figure 6-1 that for the latex particles with an average radius of 17.6 nm, the time taken to reach the core of the particles with temperatures rising from 90 to 130 °C is around $10^{-6}$ seconds. With respect to other systems with different particle sizes (Table 6-1), the time required for the hydrogen gas to completely penetrate the polymer nanoparticles is all of the same order of magnitude of -6. It should be noted that these model results shown in Figure 6-1 are obtained based on the hydrogen concentration in stagnant water, while the real hydrogenation concentration is larger than that. Therefore, it can be deduced that the time required to penetrate the nanoparticles under the real conditions is less than that modeled in the stagnant water (Figure 6-1). To be contrast, during the course of the latex hydrogenation, the reaction time as shown in Table 6-7 is evaluated at the level of hours, which is

significantly longer than the time for the hydrogen to diffuse from the outside boundary to the core of particles. Therefore, the mass transfer problem of hydrogen gas in the present particles can safely be regarded as being negligible. Compared to the study of Gilliom and Honnell where the diffusion of hydrogen in PS-PB-PS is the rate-determining step, the present results suggest that the variation of the size of substrate can impose profound influence on the essence of the reaction, which shows the great advantages in the design and synthesis of nanoscale materials. Note that though the diffusivity of hydrogen in PS-PB-PS ($1.77 \times 10^{-7}$ $cm^2$/sec at 295 K) is two orders of magnitude smaller than that of NBR (Table 6-3). This discrepancy however could not induce a large difference on the modeling results according to Eq. (6-4). The time required to diffuse through the substrate is still determined by their size.

6.4.1.2.4 Mass Transfer of Hydrogen across the Interfacial Surfactant layer

The NBR nanoparticles employed in the present study were prepared using Gemini surfactant trimethylene-1,3-bis (dodecyldimethylammonium bromide) (GS 12-3-12) as the emulsifier (Chapter 5). The structure of GS 12-3-12 was schematically illustrated in the right image of Scheme 6-3. To the best of our knowledge, there has been no report describing the diffusion process of gas through the Gemini surfactant layers. One of our previous studies showed that the obtained NBR nanoparticles present a spherical morphology when the surfactant concentration is in the range from 12 to 48 mM. This is consistent with the report by Zana that the micelles of GS 12-3-12 exhibit spherical morphology at lower surfactant concentrations, such as 30 mM.[42] Coupled with the reported possible arrangements of Gemini surfactant molecules in water,[43,44] a structure of latex particles was proposed and is represented in Scheme 6-3. The thickness of the surfactant layer, $\delta$, was assumed to be the critical length of a surfactant molecule, which was estimated to be 16.68 Å according to Eq. (6-6). It can be seen that this interfacial layer is very thin.[45]

$$\boldsymbol{l}\mathbf{c} = \mathbf{(1.5 + 1.265}\boldsymbol{n}_{\mathbf{c}}\mathbf{)} \quad \text{(6-6)}$$

where $n_c$ is the number of carbon atoms in the single alkyl chain.

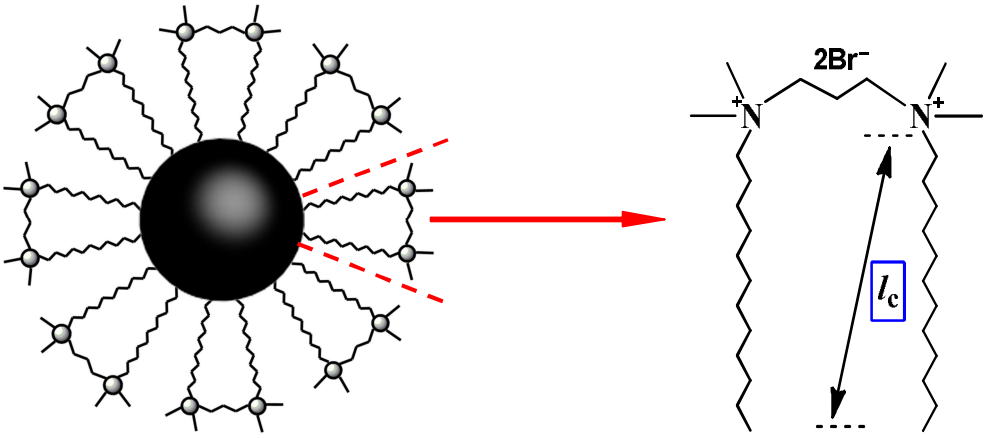


**Scheme 6-3 Proposed structure of NBR colloidal particles stabilized by GS 12-3-12**

The mass transfer of hydrogen diffusing through the surfactant layer can be examined from the perspective of the interface area ***A*** per surfactant molecule at the latex particles. The area ***A*** occupied by one surfactant at the interface is an important characteristic of the surfactant, which is determined by the amphiphile structure of the surfactant, the degree of hydration, temperature, and degree of counterion binding to micelles for ionic surfactants.[46] Antonietti et al. provided a simple spherical geometric approach to correlate ***A*** with the particle size and the calculated values of ***A*** are presented in Table 6-6.[47] Han et al. reported that the value of ***A*** of GS 12-3-12 at the crude oil-water interface is 121 $Å^2$,[48] which shows a reasonable agreement with the results listed in Table 6-6. On the other hand, the area produced by the repulsive force between the two ionic head groups of a Gemini surfactant molecule is reported to be 40 $Å^2$,[49] which is much smaller than the interface area ***A*** . This indicates that the surfactant molecules absorbed on the particles may stay in a gaseous-like state rather than form a condensed layer absorbed on the particles. It is thereby to be concluded that the mass transfer of hydrogen through the surfactant layer can be regarded as being negligible.

**Table 6-6 The interface area *A* occupied by one Gemini surfactant molecule at the water/oil interface under different surfactant concentrations.**

| Surfactant concentration used in the synthesis stage, mM | Radius of latex particles, nm | Interface area per surfactant molecule *A*,[a] Å$^2$ |
|---|---|---|
| 12 | 21.1±1.1 | 133.95 |
| 24 | 17.65±1 | 94.28 |
| 36 | 12.85±0.85 | 99.11 |
| 48 | 8.75±1 | 119.84 |

[a] Interface area per surfactant molecule occupied on the latex particle ***A*** is estimated based on the following conditions: the density of polymer particles is maintained constant during the hydrogenation and used as 0.98 g/cm$^3$. The hydrodynamic radius used in the Antonietti's equation is the number-average radius of latex nanoparticles determined by DLS.[47]

## 6.5 Results

One typical TEM image of particles after hydrogenation is shown in Figure 6-2. 500 to 1000 particles were counted to give a number-average particle size of 44.1 nm, which agrees well with the results obtained using DLS techniques of 42.2 nm. A spherical morphology was obtained after the hydrogenation, which is consistent with a previous report that latex hydrogenation has no adverse effects on the latex stability, particle size, and morphology.[23]

Before the sample was sent for the TEM imaging, a heavy metal salt, e.g. uranyl acetate was used to stain the polymer samples. Uranyl acetate is most often employed as a contrast agent, which can enhance the contrast of sample through shadowing the product by a metallic deposit. The technique is widely applied to materials containing light elements, fine particles, or single layers, and especially to polymers and biological materials.[50] As can be seen in Figure 6-2, the dark halo that appeared surrounding the white color polymer nanoparticles is the domains covered by the uranyl acetate and a sharp demarcation between the body of particles (white color) and the background regions was achieved.

In addition, the acceleration voltage of TEM used for the observation is 100 kV, which is high enough for the electron beam to penetrate straight through the studied polymer particles (< 50 nm) with little energy transfer. Therefore, the TEM imaging can be used to examine whether there exists an accumulation of catalyst clusters on the surface or inside of the particles. If the catalyst molecules are accumulated, the darker region induced by the assembling of heavy metal salt or the heavy metal particles will appear, rather than a pure white color represented throughout each particle. Thus, one conclusion can be made based on the observation of Figure 6-2 that the catalyst molecules have a quite even distribution throughout the particles. In addition, Figure 6-2 was imaged at the larger particle of 42.2 nm with a relatively small specific surface area (SSA) and high catalyst loading of 1 wt%. Therefore, it can be inferred that the other smaller particles having larger SSA and less catalyst loading will result in a better dispersion. In order to confirm this point: the other hydrogenated particles were also imaged by TEM and no dark area was found throughout the nanoparticles.

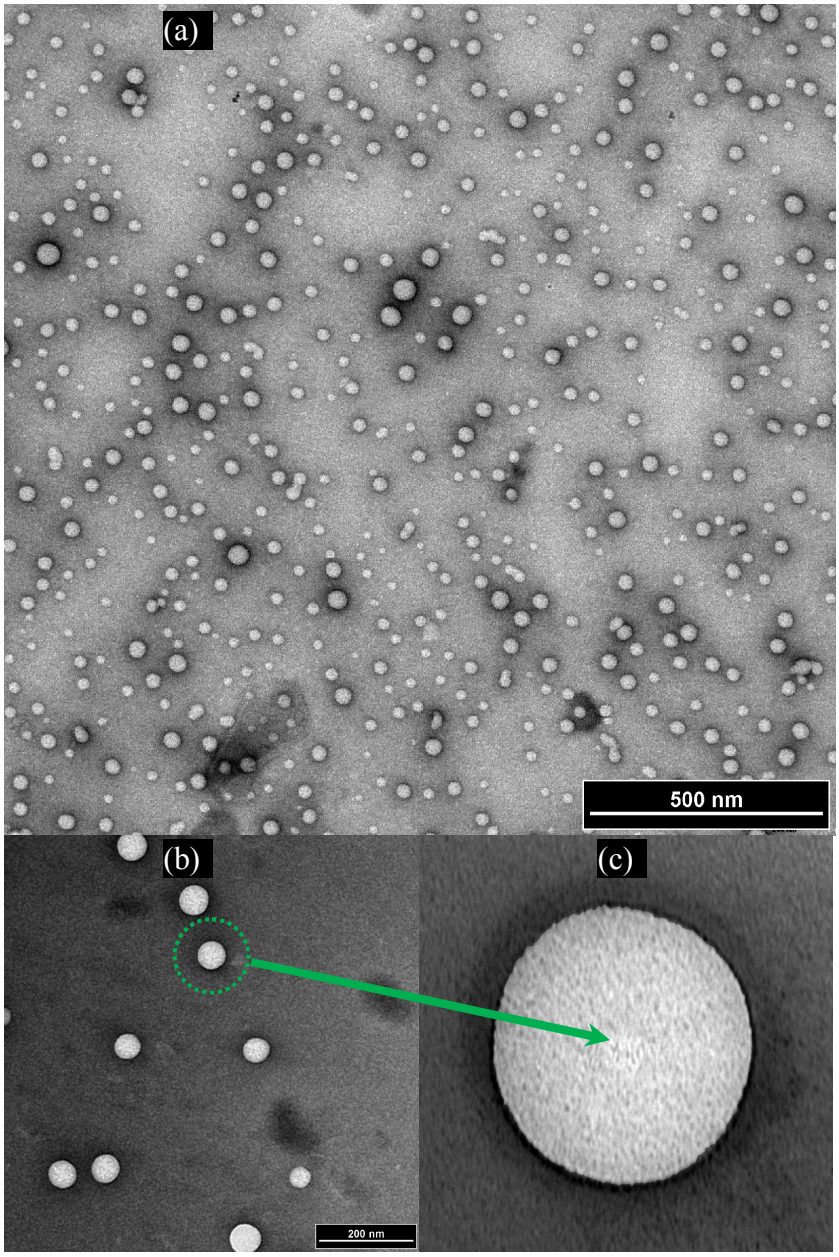


**Figure 6-2 TEM imaging of HNBR nanoparticles with conversion above 95 mol% (run 13). (b) The higher magnification of part of (a). (c) One particle in (b). Experimental conditions of latex hydrogenation: $RhCl(PPh_3)_3$/NBR = 1:10(w/w), $RhCl(PPh_3)_3$/TPP = 1:10 (w/w), agitation = 600 rpm, T = 130 °C, $P_{H2}$ = 1000 psi.**

**Table 6-7 Univariate experimental design and principal kinetic data of hydrogenation reaction**

| Run No. | Particle size ( nm) | Wilkinson's Catalyst (wt%) | Temperature [a] (°C) | Time required to reach 95 mol% conversion (h) | Rate constant [b] k ($h^{-1}$) | Apparent Activation energy [b] (J/mol) | Butadiene concentration (mM) | TON [c] (reach 95 mol%) | TOF [d] (reach 95 mol%) ($h^{-1}$) |
|---|---|---|---|---|---|---|---|---|---|
| 1 | 17.5±1.8 | 1.0 | 90 | 67.11 mol% at 50 h | -- | -- | 224.71 | -- | -- |
| 2 | 17.5±1.8 | 1.0 | 100 | ~38 | 0.13 | 103760.5 | 224.71 | 1106.59 | ~29.12 |
| 3 | 17.5±1.8 | 1.0 | 110 | ~11 | 0.30 | 103760.5 | 224.71 | 1106.59 | ~100.60 |
| 4 | 17.5±1.8 | 1.0 | 120 | ~5.5 | 0.68 | 103760.5 | 224.71 | 1106.59 | ~201.20 |
| 5 | 17.5±1.8 | 1.0 | 130 | ~3 | 1.56 | 103760.5 | 224.71 | 1106.59 | ~368.86 |
| 6 | 25.7±1.7 | 1.0 | 100 | stabilized at 75 mol% from ~70 h | -- | -- | 219.15 | -- | -- |
| 7 | 25.7±1.7 | 1.0 | 110 | ~ 40 | 0.10 | 106939.2 | 219.15 | 1101.71 | ~27.54 |
| 8 | 25.7±1.7 | 1.0 | 120 | ~16 | 0.21 | 106939.2 | 219.15 | 1101.71 | ~68.86 |
| 9 | 25.7±1.7 | 1.0 | 130 | ~5 | 0.52 | 106939.2 | 219.15 | 1101.71 | ~220.34 |
| 10 | 35.3±2.1 | 1.0 | 110 | stabilized at 87 mol% from ~50 h | -- | -- | 200.50 | -- | -- |
| 11 | 35.3±2.1 | 1.0 | 120 | ~31 | 0.11 | -- | 200.50 | 1074.09 | ~34.65 |
| 12 | 35.3±2.1 | 1.0 | 130 | ~16 | 0.30 | -- | 200.50 | 1074.09 | ~67.13 |
| 13 | 42.2±2.8 | 1.0 | 130 | ~26 | 0.09 | -- | 181.55 | 1052.96 | ~40.50 |

| | | | | | | | | | |
|---|---|---|---|---|---|---|---|---|---|
| 14 | 17.5±1.8 | 0.5 | 110 | 92.33mol% at 58h | 0.068 | 108172.7 | 224.71 | -- | -- |
| 15 | 17.5±1.8 | 0.5 | 120 | ~20 | 0.15 | 108172.7 | 224.71 | 2213.18 | ~110.66 |
| 16 | 17.5±1.8 | 0.5 | 130 | ~10 | 0.37 | 108172.7 | 224.71 | 2213.18 | ~221.32 |
| 17 | 25.7±1.7 | 0.5 | 110 | 85.36 mol% at 105 h | 0.022 | -- | 219.15 | -- | -- |
| 18 | 25.7±1.7 | 0.5 | 120 | ~44 | 0.062 | -- | 219.15 | 2203.43 | ~50.08 |
| 19 | 25.7±1.7 | 0.5 | 130 | ~30 | 0.13 | -- | 219.15 | 2203.43 | ~73.45 |
| 20 | 35.3±2.1 | 0.5 | 120 | 70.56 mol% at 60 h | -- | -- | 200.50 | -- | -- |
| 21 | 35.3±2.1 | 0.5 | 130 | ~47 | 0.069 | -- | 200.50 | 2148.18 | ~45.71 |
| 22 | 17.5±1.8 | 0.1 | 110 | 68.65 mol% at 70h | -- | -- | 224.71 | -- | -- |
| 23 | 17.5±1.8 | 0.1 | 120 | ~45 | 0.077 | -- | 224.71 | 11065.88 | ~245.91 |
| 24 | 17.5±1.8 | 0.1 | 130 | ~20 | 0.16 | -- | 224.71 | 11065.88 | ~553.29 |
| 25 | 25.7±1.7 | 0.1 | 130 | 80.94 mol% at 142 h | 0.011 | -- | 219.15 | -- | -- |

[a] When the set up temperature for the hydrogenation was higher than 140 °C, large amounts of exothermic heat were generated from the initially fast hydrogenation (the *in-situ* temperature will rise up to 145-150 °C in a very short time), and the latex particles will lose their stability to form the precipitate. However, the latex is maintained stable at 140 °C before the initiation of hydrogenation. Therefore, the upper limit of temperature for the hydrogenation is set up at 130 °C.

[b] The rate constant and activation energy are determined based on the apparent first-order reaction in the olefinic substrate.

[c] TON is defined as the moles of double bonds hydrogenated per moles of rhodium.

[d] TOF is defined as the moles of double bonds hydrogenated per moles of rhodium per hour.

The experimental conditions of the hydrogenation are designed to be controlled at a level where it is rigorous enough: such as high temperature and catalyst loading to reach a high conversion e.g. 95 mol%. On the other hand, one should minimize the cost of the hydrogenation without sacrificing the hydrogenation rate to a large extent. Therefore, it is important to optimize the reaction conditions in which the temperature, catalyst loading, particle size, hydrogenation conversion, as well as the reaction rate can be optimally cooperated. Based on this principle, a series of experiments are designed and performed. All the experimental parameters and the principal characteristics of reactions are presented in Table 6-7.

The hydrogenation experiments were performed in a semibatch reactor for the purpose of matching possible industrial operations, which are operated under isothermal and isobaric conditions through admitting the hydrogen flow continuously into the reactor. During the course of hydrogenation, the concentration of olefin will decrease gradually with the evolution of the reaction time. 95 mol% conversion without the cross linking in the resultant HNBR is an important indicator that safeguards the high-performance applications of HNBR. This high conversion can be interpreted from the substantial incorporation of hydrogen into the polymer via the spectroscopic data, as shown in Figure 6-3(a-b). The proton NMR

spectrum of the product showed near-complete reduction of the double peaks attributable to olefinic protons (δ = 5-6 ppm) (Figure 6-3a). Infrared spectra also indicated substantial hydrogenation of the polymer from the significant decrease of peak intensity at 970 $cm^{-1}$ (1,4-*trans*) and 917 $cm^{-1}$ (vinyl terminal bonds), and the increase in 723 $cm^{-1}$ assigned to the $(CH_2)_n$, n> 5 (Figure 6-3b).

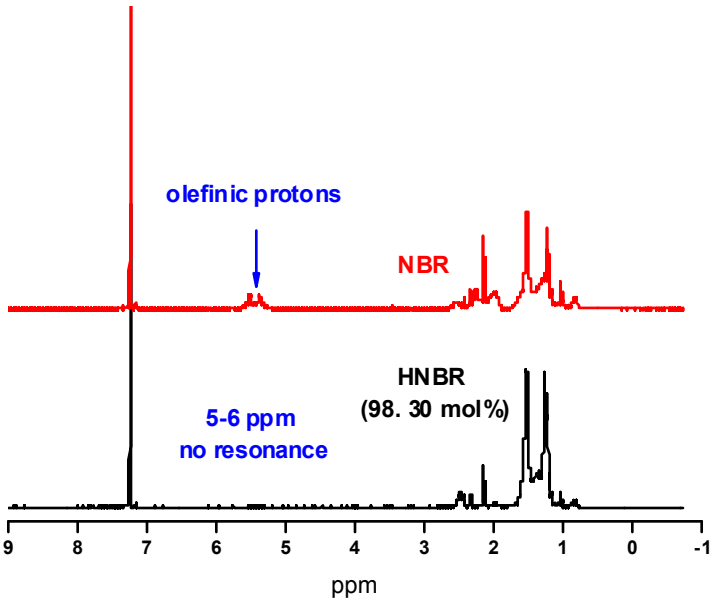


(a)

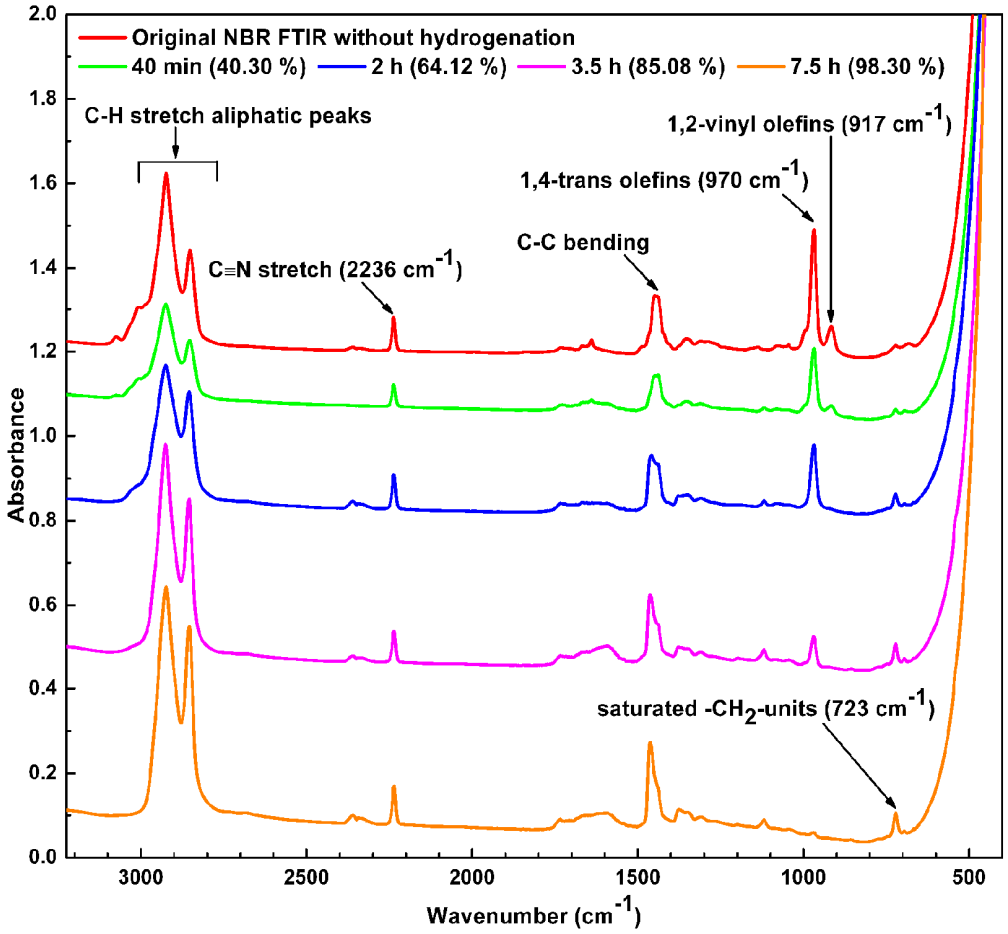


(b)

**Figure 6-3 Representative $^{1}$H NMR (a) and FT-IR (b) spectra of both original NBR (25.7 nm) and HNBR with a conversion of 98.30 mol%. Experimental conditions of latex hydrogenation: $RhCl(PPh_3)_3$/NBR = 1:10 (w/w), $RhCl(PPh_3)_3$/TPP = 1:10 (w/w), agitation = 600 rpm, T = 130 °C, $P_{H2}$ = 1000 psi.**

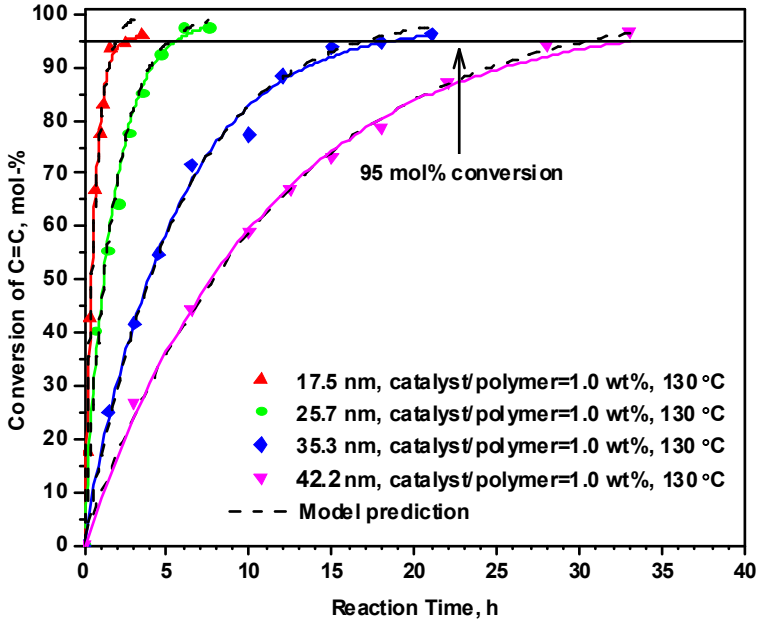
Conversion of C=C, mol-%
Reaction Time, h
95 mol% conversion
17.5 nm, catalyst/polymer=1.0 wt%, 130 °C
25.7 nm, catalyst/polymer=1.0 wt%, 130 °C
35.3 nm, catalyst/polymer=1.0 wt%, 130 °C
42.2 nm, catalyst/polymer=1.0 wt%, 130 °C
Model prediction

(a)

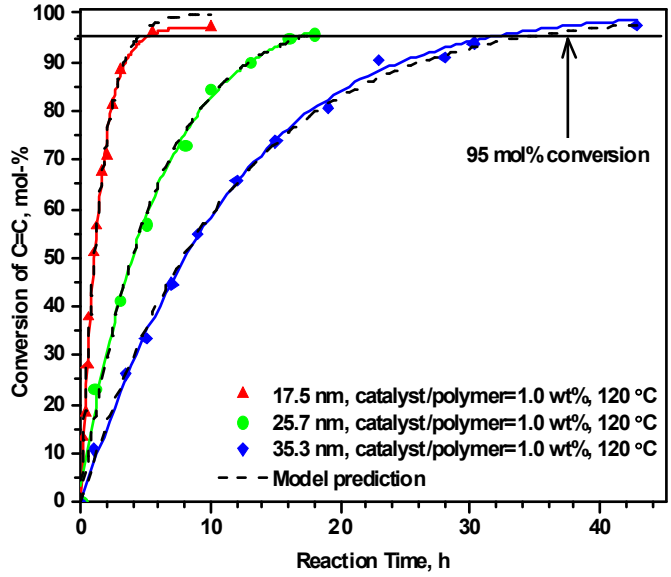
Conversion of C=C, mol-%
Reaction Time, h
95 mol% conversion
17.5 nm, catalyst/polymer=1.0 wt%, 120 °C
25.7 nm, catalyst/polymer=1.0 wt%, 120 °C
35.3 nm, catalyst/polymer=1.0 wt%, 120 °C
Model prediction

(b)

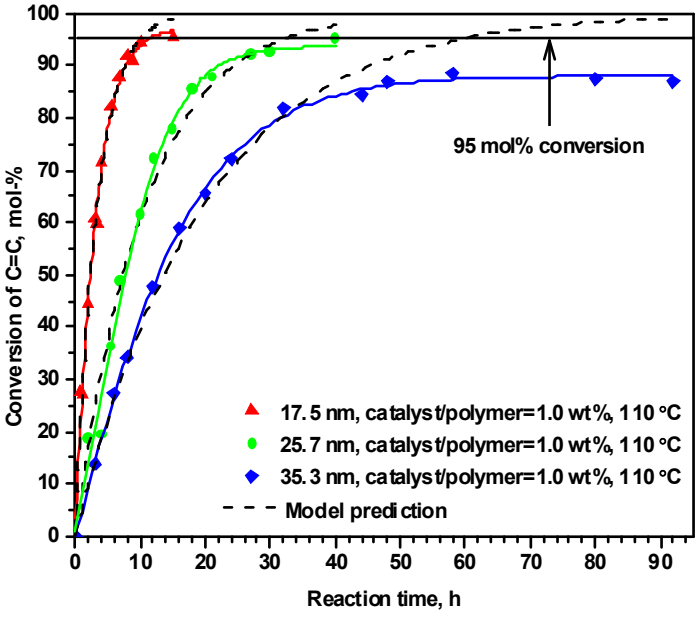
Conversion of C=C, mol-%
Reaction time, h
95 mol% conversion
17.5 nm, catalyst/polymer=1.0 wt%, 110 °C
25.7 nm, catalyst/polymer=1.0 wt%, 110 °C
35.3 nm, catalyst/polymer=1.0 wt%, 110 °C
Model prediction

(c)

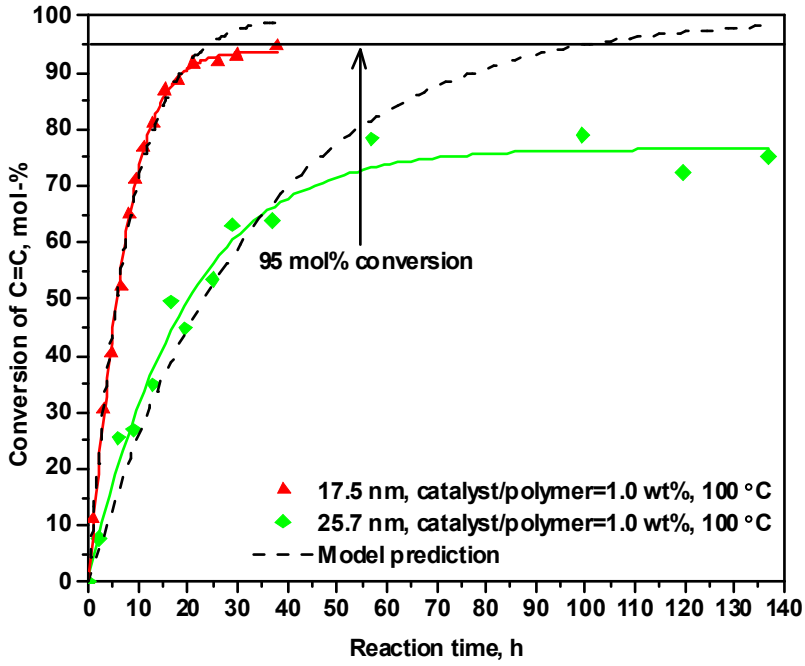
Conversion of C=C, mol-%
Reaction time, h
95 mol% conversion
17.5 nm, catalyst/polymer=1.0 wt%, 100 °C
25.7 nm, catalyst/polymer=1.0 wt%, 100 °C
Model prediction

(d)

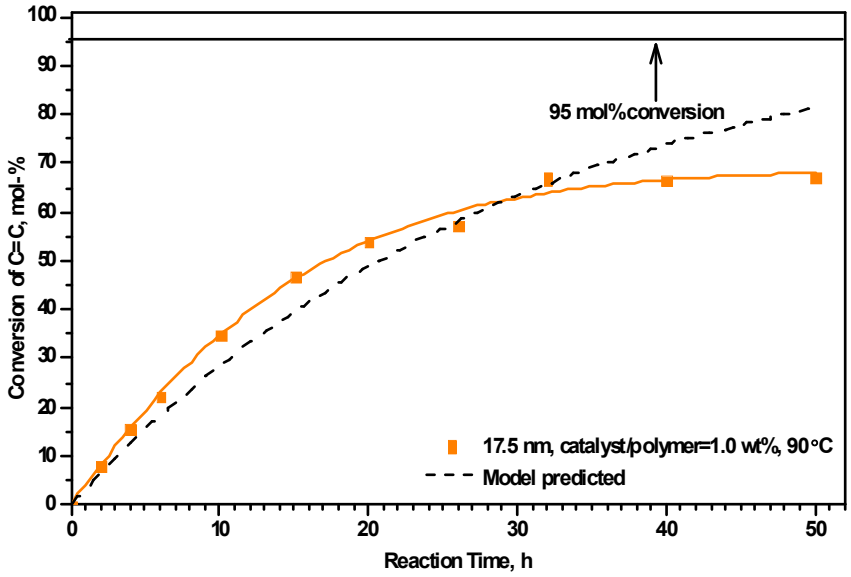
Conversion of C=C, mol-%
Reaction Time, h
95 mol%conversion
17.5 nm, catalyst/polymer=1.0 wt%, 90°C
Model predicted

(e)

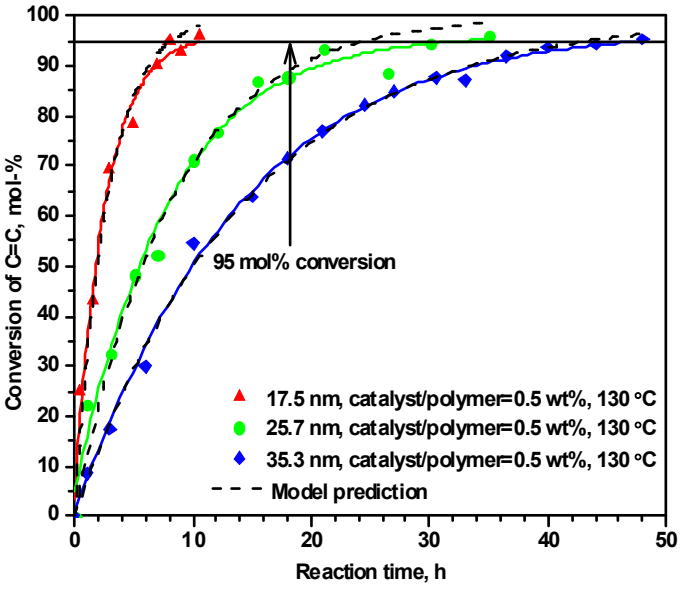
Conversion of C=C, mol-%
Reaction time, h
95 mol% conversion
17.5 nm, catalyst/polymer=0.5 wt%, 130 °C
25.7 nm, catalyst/polymer=0.5 wt%, 130 °C
35.3 nm, catalyst/polymer=0.5 wt%, 130 °C
Model prediction

(f)

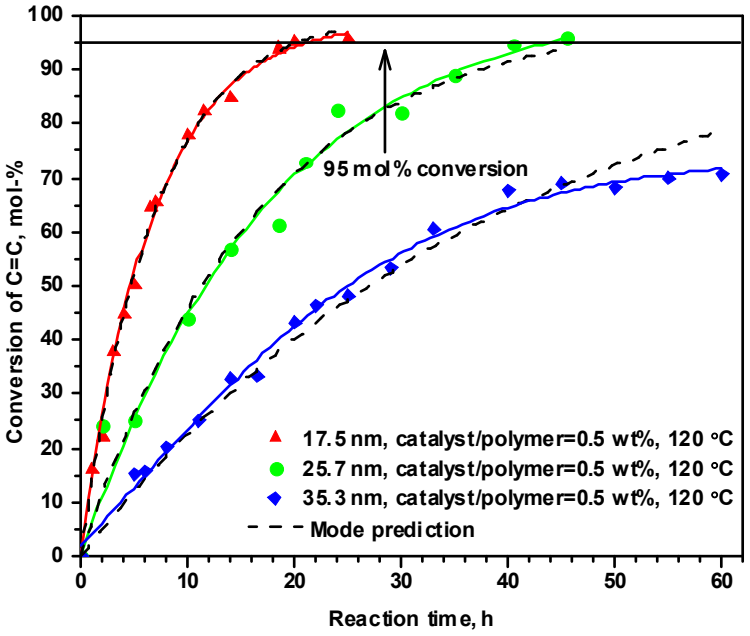
Conversion of C=C, mol-%
Reaction time, h
95 mol% conversion
17.5 nm, catalyst/polymer=0.5 wt%, 120 °C
25.7 nm, catalyst/polymer=0.5 wt%, 120 °C
35.3 nm, catalyst/polymer=0.5 wt%, 120 °C
Mode prediction

(g)

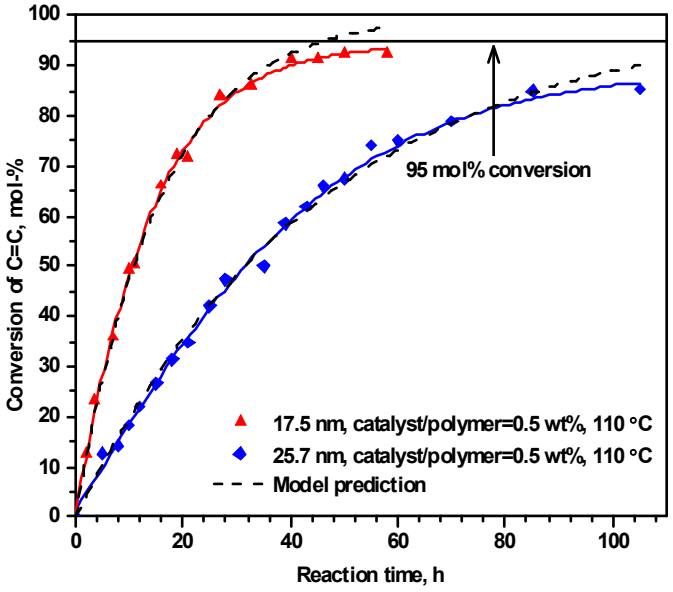
Conversion of C=C, mol-%
Reaction time, h
95 mol% conversion
17.5 nm, catalyst/polymer=0.5 wt%, 110 °C
25.7 nm, catalyst/polymer=0.5 wt%, 110 °C
Model prediction

(h)

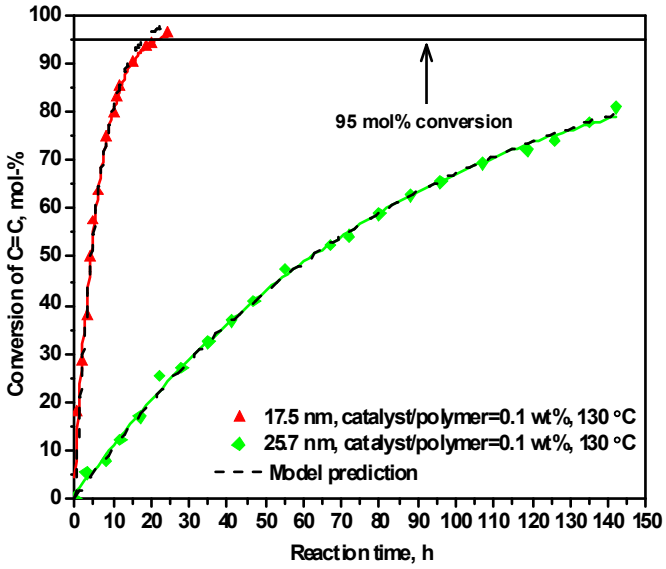


(i)

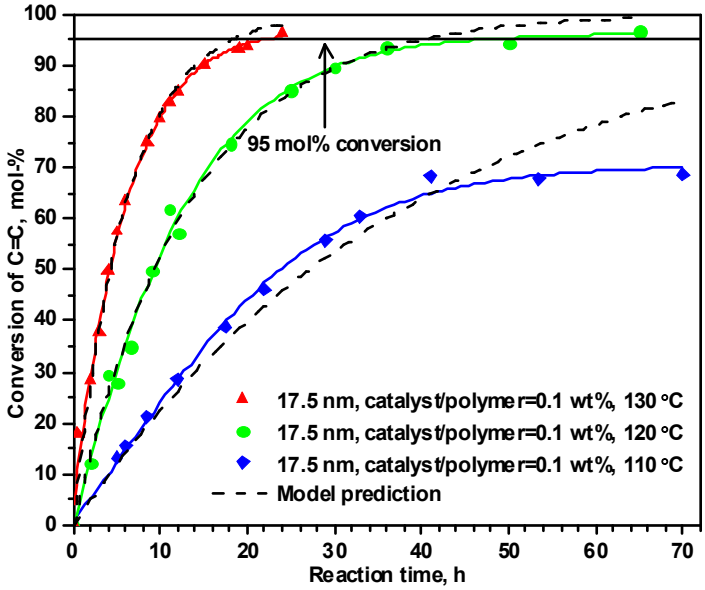


(j)

**Figures 6-4(a-j) Hydrogenation profiles of NBR latex hydrogenation under various experimental conditions. Hydrogenation conditions: $RhCl(PPh_3)_3$/TPP=1:10 (w/w), agitation=600 rpm, $P_{H2}$=1000 psi. In the designed univariate system, the particle size, catalyst**

**loading and temperature are the single variables used to investigate the effect of each factor individually. The solid curve represents the olefin conversion as evolution of time and the dash curve represents the modeled time evolution of olefin conversion using the Eq. (6-8), which was derived based on an apparent first-order dependence on the olefin concentration Eq. (6-8).**

Figures 6-4 shows a completion of the hydrogen uptake data of the olefin units under each experimental condition presented in Table 6-7, which demonstrate that the rate of latex hydrogenation was mainly governed by three factors being the particle size, concentration of catalyst, and reaction temperature.

On the one hand, as shown in Figures 6-4(a-i), the hydrogenation rate displays a pronounced dependence on the particle size. With decreasing particle size, the hydrogenation rate is markedly increased. Upon analyzing the reaction time taken to reach 95 mol% conversion in Figure 6-4a, it can be seen that the 17.5 nm NBR nanoparticles required only around 3 h for near complete hydrogenation; this is in contrast to around 5 h required for the 25.7 nm nanoparticles, 16 h for the 35.5 nm nanoparticles, and 26 h for the 42.2 nm nanoparticles. The latex hydrogenation rate achieved with respect to the 17.5 nm is sufficiently fast to be comparable with the reaction rate of solution hydrogenation.[51] On the other hand, the smaller particle size can produce a high conversion of C=C of more than 95 mol% when the reaction environment becomes milder, such as the experimental runs shown in Figures 6-4(d, i, and j). Specifically, as an example shown in Figure 6-4d, with the same catalyst loading (1 wt%) and low temperature (100 °C), the 17.5 nm particles can reach more than 95 mol% hydrogenation after around 38 h, while the particles of 25.7 nm can only reach about 75 mol% even after a much longer reaction time. The effect of particle size on the catalytic activities of the catalyst can also be reflected by the variation of TOF's. For example, with respect to experiments involving 1 wt% catalyst loading carried out at 130 °C, the catalytic activities decreased dramatically from ~368.86 (17.5 nm in run 5) to 40.50 (42.2 nm in run 13) TOF's (Table 6-7). A point worthy of attention is that due to the small size of 17.5 nm, even a remarkably low level of catalyst can produce high efficiency of hydrogenation. As shown in Figure 6-4i, when the 0.1 wt% catalyst was used, the hydrogen

uptake time to reach 95 mol% conversion at 130 °C is around 20 h. In general, the high catalyst loading and following expensive operation unit of catalyst recovery are the indispensible procedures during the course of catalytic hydrogenation, especially for the bulk and latex hydrogenation processes. Compared to the 1.0 wt% catalyst loading in the previous latex hydrogenation process,[23,52] 0.1 wt% catalyst loading for the 17.5 nm latex particles can reduce the catalyst consumption dramatically by 90 % as well as provide a much faster hydrogenation rate under milder reaction conditions, which thus provides an optimized solution between the production cost and reaction rate. More importantly, this latex hydrogenation eliminates the need for any organic solvent, which can minimize the impact on the environment to the greatest extent. Therefore, this study solves the dilemma encountered between the current lab technology and industrial production, which can facilitate the commercial production of the "green" latex hydrogenation. These exciting results which were obtained lie principally from the much larger SSA of the smaller polymer particles than the larger particles. The larger SSA can not only provide much more exposed area of the C=C substrate at the surface of the particles to interact with the catalyst molecules thereby increasing the reaction rate, but also enhances the capture of the catalyst molecules more efficiently. A more detailed analysis will be presented in the discussion section.

The catalytic activity and catalyst productivity of a catalyst can be evaluated by TOF and TON, respectively. Table 6-7 presents the values of TOF and TON for experimental runs in which 95 mol% hydrogenation was achieved. It can be seen that the obtained TOF varied significantly with different reaction conditions, which was found to be in the range from ~27.54 (run 7) to ~553.29 $h^{-1}$ (run 24), and TON falls between 1101.71 (runs 7-9) and exceptional high 11065.88 (runs 23-24). The highest TOF and TON were both achieved in the same run 24, which only requires 0.1 wt% catalyst loading.

The effect of catalyst loading on the reaction rate can be examined by comparing Figures 6-4(a, f, and i) at 130 °C, (b, g, and j) at 120 °C, and (c, h, and j) at 110 °C, where only the concentration of catalyst is the variable. These three groups of figures suggest that the reaction rate increases with an increase in the catalyst amount. For example, for the three experimental runs using 25.7 nm particles as the substrate at a reaction temperature of 130 °C

[Figures 6-4 (a, f, and i)], the hydrogenation conversion can reach 95 mol% at 1.0 and 0.5 wt% catalyst loading and the required reaction time is around 5 and 30 h respectively, while 0.1 wt% catalyst loading only reaches 80.94 mol% after 142 h.

Figures 6-4 (a-e) with 1.0 wt% catalyst, (f-h) with 0.5 wt% catalyst, and (j) with 0.1 wt% catalyst indicate the favorable effect of temperature on the hydrogenation rate. For example, with respect to the 17.5 nm particles with 1wt% catalyst loading [Figures 6-4 (a-e)], the 95 mol% conversion can be reached at the temperatures ranging from 100 to 130 °C and the required reaction time is around 38, 11, 5.5, and 3 h, respectively. When the temperature was reduced to 90 °C, the achieved hydrogenation degree was about 67.11 mol% after 50 h (run 1 in Table 6-7), and it was very difficult to reach a high conversion like 95 mol% even under high catalyst loading of 1 wt%. In parallel with the positive effect of temperature on the reaction rate, the catalytic activities (TOFs) are found to increase drastically with increasing temperature, for example in runs 2-5 (Table 6-7), the TOFs were increased from ~29.12 (100 °C) to ~368.86 $h^{-1}$ (130 °C).

Decreasing the consumption of catalyst without impairing the hydrogenation rate is one important pursuit of industry. Thus, with the 0.1 wt% catalyst loading, the effects of temperature on the hydrogenation rate of the 17.5 nm latex particles was investigated and is shown in Figures 6-4j. At the relatively high temperature of 130°C, it takes around 20 h for the NBR particles to reach a 95 mol% conversion. When the reaction temperature was decreased to 120 °C, 95 mol% conversion was still reached but it requires a longer time of around 45 h while the catalytic activities decreased from ~553.29 (130 °C) to ~245.91 (120 °C) TOF's. With a further drop in the temperature to 110 °C, the hydrogen degree can only reach 68.65 mol% at 70 h.

In keeping with what have been mentioned above, an optimized experimental condition of latex hydrogenation was found based on a series of univariate experiments as shown in Table 6-7 in the absence of organic solvents: *a 95 mol% conversion was reached within around 20 h for 17.5 nm NBR nanoparticles at 130 °C under 1000 psi hydrogen and only 0.1 wt%*

*catalyst was required. Exceptionally high TON (11065.88) and TOF (~553.29 h-1) were obtained under this optimum latex hydrogenation condition.*

## 6.6 Crosslinking Determination

The crosslinking of hydrogenated product was determined through a solvent extraction technique reported by El-Aasser and coworkers.[29,30] It was observed that the HNBR sample was completely soluble in acetone. The resulting polymer solutions are very clear and no precipitate was found after rigorous centrifugation. In addition, through comparing the weight of HNBR sample ($W_1$) and the weight of HNBR in the sample-acetone solution ($W_2$) after centrifugation, the deviations between $W_1$ and $W_2$ were found to be within the uncertainty of not exceeding 2% based on $W_1$. These phenomena and results suggest that no crosslinking occurs during the course of hydrogenation of NBR nanoparticles, which is consistent with the fact that Wilkinson's catalyst is a highly selective catalyst but without causing a crosslinking problem in the hydrogenation of many types of elastomers, such as NBR, SBR, and BR. Thus, it is expected that processibility of the HNBR resulting from the present latex hydrogenation process will not be adversely affected by this latex hydrogenation technique.

## 6.7 Discussion

### 6.7.1 Model

The uniqueness and success of the present latex hydrogenation process lies in that each latex particle functions as an ideal reactor. In order to gain insight into the kinetic performance of NBR nanoparticles in latex fashion, the modeling of kinetics was very desirable. Of principal interest in a kinetic study is the functional relationship between the reaction rate and the conditions under which the reaction is carried out.

As previously discussed for the mass transfer pathway of hydrogen and catalyst, we have shown that the mass transfer of hydrogen inside the nanoparticles is negligible and Wilkinson's catalyst functions at the molecular-level being homogeneously distributed within the polymer matrix. Now, we need to analyze the effect of diffusion of catalyst

molecules inside the polymer matrix, i.e., catalyst mass transfer resistance on the reaction rate since each catalyst molecule would not just be responsible for one C=C, and after it reduces one C=C it will interact with another C=C, which thus may become a factor to affect the reaction rate. We believe that a high diffusion rate of catalyst molecules can markedly reduce the negative influence generated by the mass transfer resistance of catalyst on the hydrogenation rate. This is consistent with Gilliom's report that sufficient mobility of catalyst molecules within the polymer phase is the premise to successfully achieve a solvent free bulk hydrogenation.[4] In order to reach a high mobility, the three governing factors that are characterized by the particle size, catalyst amount and temperature must be synergically designed, such as the combinations of 42.2 nm-1.0 wt% catalyst-130 °C (run 13), 25.7 nm-0.5 wt% catalyst-120 °C (run 18), and 17.5 nm-0.1 wt% catalyst-130°C (run 24) in Table 6-7. TON and TOF can be used to evaluate the mobility of catalyst molecules inside the polymer particles. As shown in Table 6-7, most of the experiments have a high TON above 1000 and reach a high conversion of above 95 mol% in the absence of any organic solvent, especially in run 24 (17.5 nm-0.1 wt% catalyst-130°C), a very high TON of 11065.88 and TOF of ~553.29 $h^{-1}$ was achieved.

Based on the above analysis, it can be seen that through optimizing the particle size, catalyst loading concentration and temperature, the catalyst mass transfer resistance attributed to the mobility of C=C can be circumvented. In this situation, the hydrogenation of C=C will be controlled by the chemical reaction. Consequently, apparent first order kinetics with respect to C=C should be applicable to describe the reaction rate.[51]

Figures 6-4(a-j) present the plots of conversion of C=C versus reaction time under various experimental conditions, as well as modeled prediction trends (dash line) under each reaction case. The prediction line was modeled according to Eq. (6-8) in terms of conversion of C=C, $x$.

$$\frac{\mathbf{d[C=C]}}{\mathbf{dt}} = -k'\mathbf{[C=C]} \quad (6\text{-}7)$$

$$x = [1 - \exp(-k't)] \times 100\ mol\% \quad (6\text{-}8)$$

where Eq. (6-8) is the integrated form of the differential Eq. (6-7). $x$ is the degree of hydrogenation (i.e., conversion) and $\boldsymbol{k'}$ is the pseudo-first-order rate constant, $h^{-1}$. Through examination of the hydrogen uptake curves shown in Figures 6-4(a-j), it can be seen that for the hydrogenation reactions with a high conversion of above or close to 95 mol%, an apparent overall-first-order dependence in [C=C] was observed. The evolution of the modeled hydrogenation conversion versus reaction time agrees fairly well with the experimental data. The modeling results reverse back to confirm that through adjusting the experimental conditions, the mass transfer resistance of catalyst molecules can be reduced drastically, which thus gives rise to a chemically controlled hydrogenation. The pseudo-first-order rate constant $\boldsymbol{k'}$ is thus readily determined from the modeled trend, which is summarized in Table 6-7.

When the Arrhenius equation was applied to model the data, of which the conversion is low such as less than 80 mol%, a poor agreement was obtained, as shown in Figures 6-4(c, blue curve, run 10), (d, green curve, run 6), (e, run 1), (g, blue curve, run 20), and (j, blue curve, run 22). For instance, in run 6 (the green color trend in Figures 6-4d), the initial hydrogen uptake rate exhibited an approximately first-order before the conversion reached around 60 mol%. After that, the increment of conversion levels off gradually and finally stabilized at around 75 mol%. In these experimental runs of 1, 6, 10, 20, and 22, the failure to reach the required mobility of catalyst molecules is considered to be one important reason resulting in these NBR particles being hard to reach a high conversion such as above 80 mol%. In these cases, the slow diffusion rate of catalyst imparts an important effect on the reaction rate. The slow diffusion rate will result in a longer reaction time that is required to reach a higher conversion. However the long reaction duration will require a longer lifetime of catalytically active species and the probability will be greater for the deactivation of catalyst or being expelled from the catalysis route during the diffusion process. Therefore, the catalyst will become more difficult to contact the remaining C=C within the polymers thereby resulting in the low degree of hydrogenation.

It is known that the polymerization of butadiene can yield three types of C=C, i.e., *trans, cis,* and vinyl. The concentration and distribution of different types of C=C in the latex

particles have a close relationship with the hydrogenation rate and reaction kinetics, due to the fact that the different types of C=C have different reactivities during the hydrogenation. Generally, the order of the reactivity of these three types of C=C is vinyl>*cis*>*trans* in the presence of a Rh catalyst,[53] while the order changes to vinyl>*cis*≈*trans* in the hydrazine/oxidant-induced diimide hydrogenation reaction.[6,55,56] The vinyl-C=C are more often reactive towards chemical modification reactions than 1,4 units due to their lower steric hindrance. In 5.4.1 section (Chapter 5), it was shown that for the synthesized NBR nanoparticles, the *trans*-1,4 units accounts for the majority of the total C=C. Thus, the overall reaction rate was controlled by the hydrogenation of *trans*-C=C.

An interesting phenomenon was found when comparing the experimental trend with the model prediction of the reactions where the 95 mol% conversion was achieved, that is, during the latter stage of those reactions such as Figures 6-4a, the reaction rate deviated gradually from the model predicted reaction rate. Although the observed deviation was occurred only to a small extent, one still can easily observe it. This phenomenon may be caused by the lowered mobility of the polymer or the decreased mobility (i.e. diffusion rate) of the catalyst within the polymer matrix during the later stages of hydrogenation based upon the following two considerations. On the one hand, some physiochemical properties will change during the transition from NBR to HNBR. One major change is the viscosity. The relative viscosity of HNBR with a conversion of higher than 95 mol% is much higher than that of NBR. On the other hand, the nitrile group (C≡N) has a strong coordination function with the catalyst molecules, which forms an independent catalyst cycle to competitively capture the catalytically active species with the C=C. This competitive ability will be strengthened as the reaction proceeding as a result of the decrease in the concentration of C=C.

Note that in the following sections, only the hydrogenation reactions which reach a higher conversion above or close to 95 mol% will be discussed.

### 6.7.2 Influence of Particle Size

Figures 6-4(a-i) clearly show the significant effect of the particle size on the hydrogenation rate. Compared to large particles, smaller particles have a faster reaction rate when other experimental conditions are identical. The first reason lies in that the size of the particles can impose a great influence on the partitioning of catalyst molecules between the particle and water phases. The catalyst transport process shown in Scheme 6-2 is a simplified two-dimensional representation model and in the real conditions, it is not likely to transfer all the catalyst molecules into the latex particles. Therefore, the catalyst molecules involved in latex system will be present at two locations: staying in the water phase (stabilized via surfactant) and entering the polymer phase using TPP as the carriers. Although the role of TPP plays has greatly changed the partitioning percentage of the catalyst between these two locations, there are still certain amounts of catalyst retained in the aqueous phase because of the concentration gradient required for the catalyst diffusion. The smaller particles have two advantages over the particles with a larger size in capturing the catalyst molecules from the aqueous phase. 1) The number of smaller nanoparticles is much larger than that of the larger nanoparticles, because the required surfactant concentration for preparation of smaller particles is greater than that for the larger particles (Table 6-1). For the semibatch polymerization system, the number of particles increases with an increase in the emulsifier concentration according to the below equation proposed by Sajjadi:[57]

$$N_p = k(A[S])\rho_I^{2/3} R_a^{-2/3} \quad \textbf{(6-9)}$$

where $N_p$ is number of polymer particles; $k$ is a numerical constant; $A$ is the adsorption area occupied by a molecule of emulsifier on the surface of polymer particles; $[S]$ is the concentration of surfactant per unit volume of water; $\rho_I$ is the overall rates of radical entry into both micelles and particles, and $R_a$ is the volumetric rate of monomer addition.

2) The smaller particles can give rise to a larger SSA. That is, the smaller latex nanoparticles can capture the catalyst molecules more efficiently from the water phase. Under the same experimental condition, the surface area density of the catalyst molecules absorbed on the

surface of the polymer particles can be assumed to be the same independent of the particle size.[6] Hence, the total number of catalyst molecules absorbed on the small particles will be substantially more than that for the larger particles due to the much larger total surface area ($S_p$) of smaller particles ($S_p$ is inversely proportional to the particle size). Therefore, the catalyst amount retained in the aqueous phase will be reduced accordingly.

The second reason resulted in the superior performance of the smaller particles over the larger particles is the shortened distance for the diffusion of the catalyst molecules from the surface to react with C=C residing in the inner part of the larger particles. The decreased diffusion distance will reduce the changes for the deactivation of catalyst or being expelled from the catalytic cycle as well as the shorter lifetime of catalytically active species before reaching a C=C. In addition, the smaller particles can provide larger exposed area of the olefin substrate at the oil/water interface with a reduction in the diffusion distance.

### 6.7.3 Influence of Catalyst Loading Amount

In the structure of NBR and HNBR, the acrylonitrile unit (C≡N) is a very important component because it is responsible for the oil and fuel resistance and high strength of NBR and HNBR. Unfortunately, the coordination of C≡N to a catalytic intermediate is fairly strong by σ-donation of its lone pair of electrons and thus lessens the hydrogenation activity. Due to this coordination, it will compete strongly with olefin for coordination of C=C, and hence impose a detrimental effect on the hydrogenation activity of $RhH_2Cl(C=C)(P(C_6H_5)_3)_2$ (Figure 6-5). This pronounced inhibitory behavior has been identified by Mohammadi and Rempel in 1987.[51] Besides the rhodium complex catalysts, our previous studies showed that the activities of osmium,[58] ruthenium,[59] and iridium complexes[60] were inhibited as well due to the coordination between C≡N and the metal center of the complexes.

A competition mechanism was proposed based on the previous reports featured by Mohammadi et al.,[51] Guo et al.,[61] and Parent et al.[62] These studies provided a thorough understanding of the catalytic routes, in which the activation of C=C was analyzed to be the rate controlling step based on the kinetic data collected for the solution hydrogenation. These previous studies can be moved further and extrapolated to reveal the

strongly competitive parallels between C≡N and C=C catalytic cycles. With respect to the currently studied the $RhCl(PPh_3)_3$/NBR catalyst system as shown in Figure 6-5, when the hydrogen was charged, $RhCl(PPh_3)_3$ that has been dispersed throughout the polymer matrix will first oxidatively add molecular hydrogen to form the dihydride $RhH_2Cl(PPh_3)_3$. The dissociation of phosphine from $RhH_2Cl(PPh_3)_3$ will produce the catalytically active species $RhH_2Cl(PPh_3)_2$. The complexation of C=C with $RhH_2Cl(PPh_3)_2$ results in the formation of a π-olefin-transition metal complex. Since the coordination of olefin to $RhH_2Cl(PPh_3)_2$ is not a facile process, it is thus proposed to represent the rate determining step for the overall hydrogenation reaction. It is worth noting that this dissociation of TPP from $RhH_2Cl(PPh_3)_3$ is most likely to be encouraged by the elevated temperature and not appreciable at milder conditions. Once $RhH_2Cl(PPh_3)_2$ is formulated, it will be competitively captured between the olefin and nitrile groups and then enter two parallel cycles: olefin cycle and nitrile cycle. Certain conclusions can be drawn from Figure 6-5. First, due to the coordination shown in the C≡N cycle, the effective catalyst used for the reduction of the double bond will be less than the charged amount. Second, with an increase in reaction time, a certain amount of catalyst will be entrapped into the C≡N cycle since of the coordination capability of C≡N is much stronger than C=C. What's more important, with the progression of the reaction, the concentration of C=C decreased gradually, which strengthens the competitive capability of left cycle, thereby more and more $RhH_2Cl(PPh_3)_2$ will be entrapped and retained into the left cycle with the evolution of reaction time. Therefore, the amount of effective catalyst in the left cycle could not maintain constant and this is one important reason that the results in the achieved hydrogenation profile deviate a little from the model predicted reaction during the latter stages of hydrogenation such as shown in Figures 6-4f.

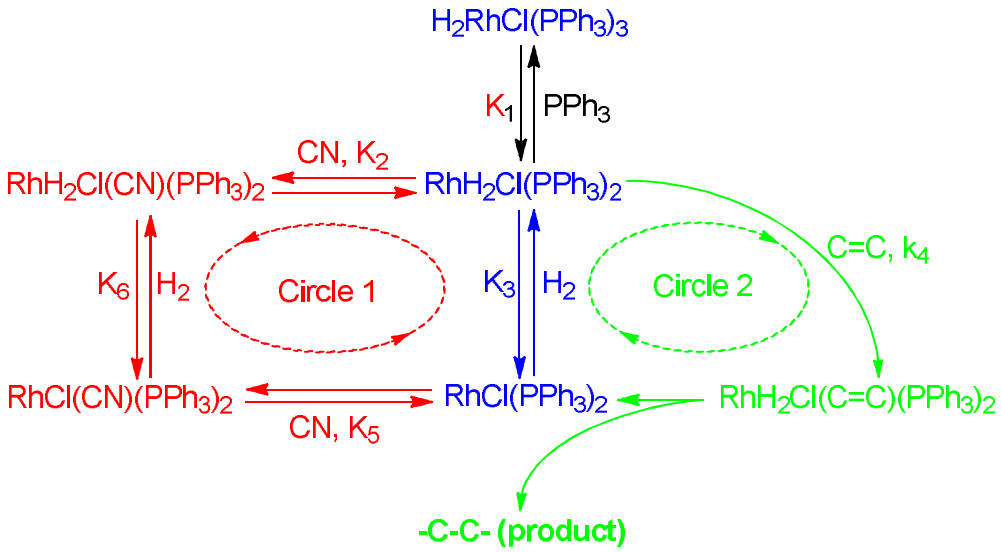


**Figure 6-5 Proposed mechanism for the $RhCl(PPh_3)$/NBR system. Two competitive cycles are existed in the overall hydrogenation routes, characterized by the nitrile cycle (red color) and olefin cycle (green color). The nitrile coordination to the rhodium complex exhibits a inhibitory behavior towards the coordination of C=C to $RhH_2Cl(PPh_3)_2$.**

### 6.7.4 Influence of Temperature

As shown in the modeling part, the reaction rate is apparently first order in the olefinic substrate according to Eqs. 6-7 and 6-8 for more than or close to 95% completion of the reactions. While examining the experiments in which the temperature is the sole variable, the values of the pseudo-first-order rate constant $k'$ (Table 6-7) shows a good linear Arrhenius plot versus the reciprocal of temperature ($1/T$). The activation energy ($E_a'$) was thereafter calculated from a least squares regression analysis of a plot of ln $k'$ versus $1/T$, the data of which is presented in Table 6-7. It can be seen that the obtained $E_a'$ under the studied conditions has values of ranging from 100 to 110 kJ/mol. In addition, with an increase in the temperature, the reaction rate constants involved into the competitive two cycles (i.e., olefin cycle and nitrile cycle) will be increased, which can be reflected by the $k'$ as shown in Table 6-7, which thus can impose a favorable effect on the hydrogenation rate. Furthermore, with

increasing temperature, the viscosities of NBR and HNBR will decrease accordingly; and this will be more likely to increase the mobility of the catalytic active sites within the polymer chains. Meanwhile, the mobility of the soft NBR chains inside of the particles occurs constantly, especially at the elevated temperature. The diffusion of polymer chains would lead to a structure in which the double bonds are uniformly distributed.[6] In addition, the higher temperature may likely to facilitate the dissociation of the catalytically active species $RhH_2Cl(PPh_3)_2$ from the C≡N group attributed to the more intensive vibration of the polymer chains, which therefore can result in more active species entering into the C=C cycle.

## 6.8 Conclusions

The rate of catalytic latex hydrogenation was greatly affected by the particle size, concentration of catalyst, and reaction temperature. An optimized experimental condition of latex hydrogenation was achieved based on a series of univariate experiments where in the absence of organic solvents, a 95 mol% conversion was reached within around 20 h for 17.5 nm NBR nanoparticles at 130 °C under 1000 psi hydrogen and only 0.1 wt% catalyst being required. Exceptionally high TON (11065.88) and TOF (~553.29 $h^{-1}$) were obtained under this optimum latex hydrogenation condition. Particularly no crosslinking was observed in all resultant hydrogenation products, which is independent of the degree of hydrogenation. The diffusion of hydrogen from the gas phase to the polymer phase was not a rate-determining factor. By using liquified TPP as a carrier, oil soluble Wilkinson's catalyst was transported into the latex particles and dispersed homogeneously throughout the nanoparticles. The catalytic latex hydrogenation can be viewed as being equivalent to a "mini-bulk" hydrogenation where numerous nano bulk hydrogenations are carried out inside latex particle at a molecular level of catalysis. With respect to the reaction that has reached or nears 95 mol% conversion, an apparent overall-first-order dependence in olefin was observed. The pseudo-first-order rate constant is thus determined from the first-order rate model. The apparent activation energy was calculated to be in the range of 100 to 110 kJ/mol. The strong coordination of C≡N to the catalytically active species $RhH_2Cl(PPh_3)_2$ imposed a negative effect on the hydrogenation activity and two competitive cycles characterized by nitrile and

olefin catalytic cycles was proposed to explain the inhibitory behavior induced by C≡N. With the progression of the hydrogenation, more and more $RhH_2Cl(PPh_3)_2$ will be entrapped and retained into the nitrile cycle. Thus, the effective catalyst used in the reduction of the double bonds is much less than the charged amount. The present "green" hydrogenation process can be extended to latices made from semibatch microemulsion containing other diene-based polymers. This study may facilitate the commercialization of “green” latex hydrogenation in industry.

# Chapter 7
# Preparation of Poly(methyl methacrylate)-Poly(acrylonitrile-*co*-butadiene) Core-Shell Nanoparticles

## 7.1 Overview

Poly(methyl methacrylate)-poly(acrylonitrile-*co*-butadiene) (PMMA-NBR) core-shell structured nanoparticles were prepared using a two stage semibatch microemulsion polymerization system with PMMA and NBR as the core and shell respectively. The Gemini surfactant 12-3-12 was employed as the emulsifier and found to impose a pronounced influence on the formation of the core-shell nanoparticles. The spherical morphology of core-shell nanoparticles was observed. It was found that there exists an optimal MMA addition amount which can result in minimized size of PMMA-NBR core-shell nanoparticles. The formation mechanism of the core-shell structure and the interaction between the core and shell domains was illustrated. The PMMA-NBR nano-size latex can be used as the substrate for the following direct latex hydrogenation catalyzed by Wilkinson's catalyst to prepare the PMMA-HNBR core-shell nanoparticles. The hydrogenation rate is rapid. In the absence of any organic solvent, the PMMA-HNBR nanoparticles with a size of 30.6 nm were obtained within 3 h using 0.9 wt% Wilkinson's catalyst at 130 °C under 1000 psi of $H_2$. This study provides a new perspective in the chemical modification of NBR and shows promise in the realization of a "green" process for the commercial hydrogenation of unsaturated elastomers.

## 7.2 Introduction

Over the past decade there has been an increasing amount of interest and research in the field of core-shell nano-structured polymers which are composed of at least two distinguished polymer domains in the core and shell phase, respectively.[1-10] The nanoscale core-shell structured polymers have found important uses over a wide range of applications in film fabrication, drug delivery, conducting materials, paper and textile manufacturing, and impact modifiers (enhance the toughness of polymer matrix), by taking advantages of the

synergically enhanced physical, chemical, and biological properties over their single-component counterparts when the core and shell polymers are optimally designed.

The core-shell nano-structured polymers have a remarkable potential to meet a great demand of the market. However, it has been a great challenge to develop robust and economical techniques capable of producing acceptable nanoparticles with a complex architecture. Until now, core-shell polymer nanoparticles are mainly prepared through two known techniques represented by the seeded tandem polymerization[11-15] and self-assembly of block copolymers,[16,17] which however does not exclude the utilization of other techniques such as the heterocoagulation technique.[18] The seeded tandem polymerization technique has a more widespread application scope compared to the self-assembly approach, since it can be realized by miscellaneous polymerization techniques involving graft polymerization,[19] conventional and semibatch emulsion/microemulsion polymerizations,[15] oil-in-oil emulsion polymerization,[11] soap-free emulsion polymerization,[20] seeded suspension polymerization,[21] and ionic polymerization.[22] Particularly, the two stage seeded emulsion or microemulsion polymerization is the most frequently practiced route, which usually involves two monomer addition manners characterized by a continuous addition manner and a batch swelling manner. Depending on the specific circumstance, the two addition manners can be same or different in either stage of polymerization. In this study, a continuous feeding method was employed for both stages of the polymerization. It was reported that the continuous feeding method could endow the polymerization with a kinetically controlled reaction. In fact, in the perspective of thermodynamic control, there is not much difference in Gibbs free energy stemming from interfacial tension variation required to change the pattern of polymer nanoparticles from the core-shell to partially engulfed morphology.

Compared to the great effort spent on studies of core-shell structured polymer nanoparticles, there appears to be no reported research related with the reinforcement of physiochemical properties and expanding the application profiles of nitrile-butadiene rubber (NBR) and its derivatives such as the carboxylated nitrile rubber (XNBR) by means of a core-shell modification. NBR is known to be an extremely important industrial product.

Nevertheless, due to the presence of the olefinic double bonds, NBR suffers from a severe aging problem, and exhibits a poor tensile strength and low resistance to air and ozone.[23] Nowadays, the drawbacks of NBR are usually overcome by two primary techniques characterized by addition of inorganic fillers (physical modification) and hydrogenation (chemical modification). Regarding the physical modification, the reinforcement fillers have their own respective limitations in their composition processes.[24-26] For the chemical modification, the hydrogenation has been commercialized and plays a crucial role in the industry.[27,28] Therefore, in this study, a combination of the core-shell construction and hydrogenation techniques will be used to improve the properties of NBR.

The types and amount of surfactant play an important role in the (micro)emulsion polymerization. It has been known that excess surfactant in the product will have a considerable negative impact on the properties and post-treatment of synthesized bulk polymers or polymeric latices.[29,30] Nevertheless, the separation process is tedious and costly.[30,31] Since the common recipes involved in (micro)emulsion polymerizations still require large amounts of expensive surfactant, there is great interest in the development of new surfactant systems which not only support the interface stabilization of polymerizable (micro)emulsions but enable the synthesis of preserved particles at lower surfactant loads.[32-34] Recent studies showed that two approaches can be used to design and develop new surfactant systems with improved emulsifying properties.[34,35] The first route is to prepare the surfactants with diverse organic counterions by means of the assemblies of conventional cationic surfactants with multivalent counterions.[34] The second one is to replace the conventional single-tail surfactants using the Gemini surfactants.[35] Gemini surfactant (GS) is an amphiphile made up of two conventional surfactant molecules chemically bonded together by a spacer moiety, which has significantly lower critical micelle concentration (CMC) and greatly increased surface activity.[36] For these reasons, the bis(quaternary ammonium) Gemini-type surfactant trimethylene-1,3-bis(dodecyldimethylammonium bromide), denoted as GS 12-3-12 was introduced into this semibatch microemulsion polymerization. GS 12-3-12 is one of the most comprehensively characterized GSs and shows interesting properties in aqueous solution.[37-39] In particular,

GS 12-3-12 has a very low CMC of 1 mM (~0.63 g/L).[36] Up until now, only a few examples have been reported on the use of the assemblies of GS molecules as a platform for the polymerization reactions and the studied monomers were limited to only styrene[35] and aniline.[40]

In line with above, we attempted to prepare the PMMA-NBR core-shell nanoparticles by means of a two stage semibatch microemulsion polymerization technique. GS 12-3-12 was used as the emulsifier. In order to further enhance the properties of PMMA-NBR nanoparticles, the latex hydrogenation was directly carried out on the PMMA-NBR nano-size latex to prepare the PMMA-HNBR nanoparticles.

## 7.3 Experimental

### 7.3.1 Materials for Synthesis of PMMA-NBR Core-Shell Nanoparticles

Methyl methacrylate (MMA, 99%) and acrylonitrile (AN, 99+%) were purchased from Sigma-Aldrich and the inhibitors were removed prior to polymerization by passing the monomers through an alumina column. Initiator ammonium persulfate (APS, 98%, Sigma-Aldrich) was purified by recrystallization from ethanol and dried under vacuum at room temperature. The 2,2′-azobis(2-amidinopropane) dihydrochloride (V50, 99.5%, Sigma-Aldrich) was purified by recrystallization from a water/acetone mixture (1:1 volume).1,3-butadiene (BD) was provided by Lanxess Inc. and used as received. GS 12-3-12 was synthesized by known procedures[41] and used after repeated recrystallization from acetone-ethyl acetate (1:1 volume). The yield was 56~58 wt%. Upon drying in a vacuum oven at room temperature, GS 12-3-12 with a melting point of 195±5 °C, as measured by differential scanning calorimetry (Q2000, TA instruments, US) with scanning rate of 10 °C/min, was obtained.

### 7.3.2 Materials for Direct Hydrogenation in Latex Form

Ultra-high purity hydrogen and nitrogen gas (99.999%, oxygen-free) were used as received from Praxair Inc. Wilkinson's catalyst $RhCl(P(C_6H_5)_3)_3$ was prepared according to the literature.[42,43] Methanol (reagent grade) and methyl ethyl ketone (MEK, reagent grade)

were purchased from Sigma-Aldrich and used as received. Triphenylphosphine (TPP, 99%) was obtained from Strem Chemicals Inc. and further purified by recrystallization using ethanol.

### 7.3.3 Experimental Design

The synthesis of core-shell nanoparticles was performed in a modified 300 mL Parr 316 Stainless Steel reactor under a nitrogen atmosphere. The formulation design employed is presented in Table7-1. Four groups of experiments were implemented differing in the way in which the surfactant ranging from 0.5 to 3 g was fed into the system. With respect to each group, six experiments were carried out differing in the MMA amount used increasing from 1 to 6 ml. For all of the experimental runs, the amount of shell monomers, initiator, and distilled water were identical. Through this design, the PMMA-NBR nanoparticles with different core and shell composition ratios can be synthesized. In addition, the effect of the amount of core monomer and surfactant on the performance of core-shell nanoparticles can be evaluated thoroughly. Triplicate experiments under each experimental condition were carried out.

All the experimental parameters and principal characteristics of the core-shell latex particles are listed in Table7-1 and Table 7-2, respectively.

**Table7-1 Formulation used for the core-shell synthesis**

| Group | Exp. | Core monomer MMA (mL)[a] | Shell monomers AN/BD (mL)[b] | Emulsifier GS (g) | Emulsifier 12-3-12 | Initiator APS (g) | Distilled water (mL) |
|---|---|---|---|---|---|---|---|
| First group | 1 | 1.0 | 2.5/7.5 | 0.50 | | 0.125 | 80.0 |
| | 2 | 2.0 | 2.5/7.5 | 0.50 | | 0.125 | 80.0 |
| | 3 | 3.0 | 2.5/7.5 | 0.50 | | 0.125 | 80.0 |
| | 4 | 4.0 | 2.5/7.5 | 0.50 | | 0.125 | 80.0 |
| | 5 | 5.0 | 2.5/7.5 | 0.50 | | 0.125 | 80.0 |
| | 6 | 6.0 | 2.5/7.5 | 0.50 | | 0.125 | 80.0 |

| | | | | | | |
|---|---|---|---|---|---|---|
| | 7 | 1.0 | 2.5/7.5 | 1.0 | 0.125 | 80.0 |
| | 8 | 2.0 | 2.5/7.5 | 1.0 | 0.125 | 80.0 |
| Second | 9 | 3.0 | 2.5/7.5 | 1.0 | 0.125 | 80.0 |
| group | 10 | 4.0 | 2.5/7.5 | 1.0 | 0.125 | 80.0 |
| | 11 | 5.0 | 2.5/7.5 | 1.0 | 0.125 | 80.0 |
| | 12 | 6.0 | 2.5/7.5 | 1.0 | 0.125 | 80.0 |
| | 13 | 1.0 | 2.5/7.5 | 2.0 | 0.125 | 80.0 |
| | 14 | 2.0 | 2.5/7.5 | 2.0 | 0.125 | 80.0 |
| Third | 15 | 3.0 | 2.5/7.5 | 2.0 | 0.125 | 80.0 |
| group | 16 | 4.0 | 2.5/7.5 | 2.0 | 0.125 | 80.0 |
| | 17 | 5.0 | 2.5/7.5 | 2.0 | 0.125 | 80.0 |
| | 18 | 6.0 | 2.5/7.5 | 2.0 | 0.125 | 80.0 |
| | 19 | 1.0 | 2.5/7.5 | 3.0 | 0.125 | 80.0 |
| | 20 | 2.0 | 2.5/7.5 | 3.0 | 0.125 | 80.0 |
| Fourth | 21 | 3.0 | 2.5/7.5 | 3.0 | 0.125 | 80.0 |
| group | 22 | 4.0 | 2.5/7.5 | 3.0 | 0.125 | 80.0 |
| | 23 | 5.0 | 2.5/7.5 | 3.0 | 0.125 | 80.0 |
| | 24 | 6.0 | 2.5/7.5 | 3.0 | 0.125 | 80.0 |

[a]The reaction temperature of the first stage starving microemulsion polymerization was set as 70 °C. [b]The reaction temperature of the second stage semibatch microemulsion polymerization was set as 45 °C.

**Table 7-2 Principal characteristics of core-shell latex particles**

| Exp.[a] | PMMA size (nm)[b] | PMMA size dispersity[c] | PMMA-NBR size (nm)[d] | PMMMA-NBR size dispersity[c] | PMMA conversion (%) | PMMA-NBR conversion (%) | NBR conversion (%) | PMMA-NBR, $\overline{M}_n$ ($\times10^{-5}$)[e] | PMMA-NBR, $\overline{M}_w$ ($\times10^{-5}$)[e] | PMMA-NBR dispersity= $\overline{M}_w/\overline{M}_n$ |
|---|---|---|---|---|---|---|---|---|---|---|
| 0.50 g[f], appreciable agglomeration was found at the second stage of polymerization | | | | | | | | | | |
| 1 | 42.6 | 1.21 | 90.7 | 1.28 | 75.1 | 56.1 | 53.5 | 7.795 (7%) | 9.914 (8%) | 1.27±0.16 |
| 2 | 62.5 | 1.20 | 110.7 | 1.23 | 73.9 | 56.0 | 51.1 | 5.564 (4%) | 8.978 (5%) | 1.61±0.093 |
| 3 | 63.6 | 1.22 | 114.8 | 1.26 | 72.8 | 58.6 | 52.8 | 9.011 (8%) | 19.25 (10%) | 2.14±0.19 |
| 4 | 64.5 | 1.20 | 116.5 | 1.24 | 73.1 | 60.4 | 53.4 | 9.782 (3%) | 15.10 (4%) | 1.54±0.072 |
| 5 | 65.9 | 1.23 | 118.4 | 1.27 | 74.0 | 59.8 | 50.0 | 9.052 (3%) | 14.628 (5%) | 1.62±0.17 |
| 6 | 90.9 | 1.24 | 144.4 | 1.31 | 74.7 | 63.5 | 54.2 | 6.616 (7%) | 11.20 (8%) | 1.69±0.16 |
| 1.0 g[f] | | | | | | | | | | |
| 7 | 15.8 | 1.17 | 55.1 | 1.20 | 85.2 | 80.9 | 80.3 | 8.075 (4%) | 9.122 (4%) | 1.30±0.083 |
| 8 | 23.1 | 1.20 | 41.5 | 1.22 | 86.1 | 82.8 | 81.9 | 5.580 (5%) | 6.749 (6%) | 1.21±0.12 |
| 9 | 24.8 | 1.21 | 37.1 | 1.25 | 84.2 | 81.3 | 80.1 | 6.879 (5%) | 8.911 (8%) | 1.29±0.14 |
| 10 | 26.0 | 1.14 | 38.6 | 1.24 | 85.7 | 82.0 | 79.9 | 4.961 (6%) | 6.581 (5%) | 1.32±0.12 |
| 11 | 29.4 | 1.16 | 38.9 | 1.20 | 81.6 | 79.2 | 77.5 | 7.272 (6%) | 9.108 (10%) | 1.25±0.17 |
| 12 | 34.9 | 1.18 | 43.0 | 1.23 | 82.0 | 80.1 | 78.6 | 6.003 (3%) | 6.972 (6%) | 1.16±0.092 |

| | | | | | | | | | | |
|---|---|---|---|---|---|---|---|---|---|---|
| 2.0 g[f] | | | | | | | | | | |
| 13 | 6.7 | 1.06 | 45.5 | 1.13 | 85.6 | 87.4 | 87.7 | 4.042 (5%) | 5.315 (6%) | 1.21±0.12 |
| 14 | 13.6 | 1.09 | 34.8 | 1.19 | 87.3 | 91.5 | 92.6 | 5.900 (6%) | 6.753 (6%) | 1.14±0.13 |
| 15 | 20.0 | 1.11 | 30.6 | 1.15 | 88.3 | 91.8 | 93.2 | 5.198 (5%) | 5.751 (8%) | 1.11±0.14 |
| 16 | 22.7 | 1.12 | 31.9 | 1.16 | 86.6 | 90.0 | 91.8 | 4.575 (6%) | 5.586 (5%) | 1.22±0.12 |
| 17 | 27.6 | 1.15 | 35.1 | 1.22 | 83.5 | 87.3 | 89.9 | 6.616 (3%) | 11.20 (5%) | 1.69±0.082 |
| 18 | 30.5 | 1.13 | 37.6 | 1.21 | 90.2 | 92.6 | 94.5 | 6.005 (3%) | 7.853 (4%) | 1.31±0.072 |
| 3.0 g[f] | | | | | | | | | | |
| 19 | 4.1 | 1.08 | 38.5 | 1.12 | 86.7 | 92.0 | 92.7 | 5.480 (6%) | 6.795 (6%) | 1.24±0.12 |
| 20 | 9.4 | 1.07 | 26.6 | 1.18 | 89.6 | 92.9 | 93.8 | 4.548 (4%) | 5.478 (3%) | 1.20±0.073 |
| 21 | 13.6 | 1.10 | 23.8 | 1.14 | 88.5 | 92.4 | 94.0 | 4.757 (3%) | 5.873 (3%) | 1.23±0.060 |
| 22 | 14.5 | 1.16 | 21.5 | 1.18 | 87.7 | 91.4 | 93.5 | 4.311 (4%) | 4.915 (3%) | 1.14±0.073 |
| 23 | 15.7 | 1.12 | 23.1 | 1.17 | 87.6 | 90.8 | 93.0 | 3.245 (3%) | 4.413 (5%) | 1.35±0.082 |
| 24 | 21.4 | 1.11 | 28.1 | 1.16 | 85.0 | 89.4 | 93.1 | 3.742 (1.6%) | 4.856 (1.6%) | 1.29±0.032 |

[a]The experimental trials provided in Table 1 and Table 2 are consistent. [b]Mean diameter of triplicate experiments under each experimental condition is based on the number average size measured by DLS technique at the end of the first stage of polymerization. [c]The dispersity of particle size defined by weight-average diameter ($D_w$) over number-average diameter ($D_n$) was estimated by DLS technique.[33b] [d]Mean diameter of triplicate experiments under each experimental condition is based on the number average size measured by the DLS technique at the end of the second stage of polymerization. [e]Determined by SEC. [f]Amount of GS 12-3-12 in 80 mL distilled water.

### 7.3.4 Experimental Procedures

#### 7.3.4.1 Synthesis of PMMA-NBR Core-Shell Nanoparticles

In the first stage of the preparation of PMMA seeded latex, different amounts of surfactant, 0.125 g APS, and 80 mL distilled water were charged into the stainless steel reactor equipped with an impeller stirrer, an addition tube, and a thermal couple. Oxygen was removed by purging a slow stream of nitrogen gas for 20 min while stirring was maintained at 200 rpm. The reactor was then heated up to the reaction temperature for the first stage of the reaction at 70 °C. The core monomer MMA was fed continuously into the reactor using a designed addition tube at a constant rate of 0.06~0.07 mL/min. After the MMA feeding was completed, the reaction system was allowed to proceed for an additional 1 h. 4~5 mL PMMA latex was withdrawn by an outlet tube, which was used for the next conversion calculations and particle size measurements. The temperature was decreased from 70 to 45 °C as the copolymerization of AN and BD for the shell formation was carried out at 45 °C. It is important to increase the pressure inside the reactor to at least 22 psi using nitrogen gas (80 psi used in our studies), since the saturated vapor pressure of BD in the adding tube is around 22 psi at room temperature. The addition tube filled with 10 mL AN and BD (~22 psi) was then connected with the reactor (80 psi) and the pressure between the reactor and addition tube was thereafter balanced. Under the same stirring speed of 200 rpm, the mixture of 2.5 mL AN and 7.5 mL BD were added continuously with a slow and constant rate of 0.06~0.07 mL/min via the addition tube. After completion of the addition, the polymerization was aged for a given time in order to reach a reasonable conversion.

### 7.3.4.2 Direct Hydrogenation of PMMA-NBR Core-Shell Nano-size Latex

The latex hydrogenation of core-shell nanoparticles was carried out in the same 300 mL Parr 316 Stainless Steel reactor. A measured volume of latex (25 mL) with added distilled water (75 mL) was first mixed with the required additive TPP with a weight ratio of 10:1 to the mass of Wilkinson's catalyst. The mixture was then degassed with three nitrogen gas cycles and subjected to bubbling nitrogen under 200 psi for 20 min at room temperature. The resulting mixture was heated up to 130 °C and stabilized for 30 min before the hydrogen gas at a pressure of 1000 psi was charged into the reactor. The hydrogenation reaction commenced upon after Wilkinson's catalyst with 0.9 wt% of the NBR shell mass was charged into the reactor using a catalyst addition device installed in the head of the reactor. The hydrogen pressure and reaction temperature were maintained constant throughout the reaction period. After a given reaction time, the system was cooled to room temperature and depressurized to obtain the final product.

## 7.4 Results and Discussion

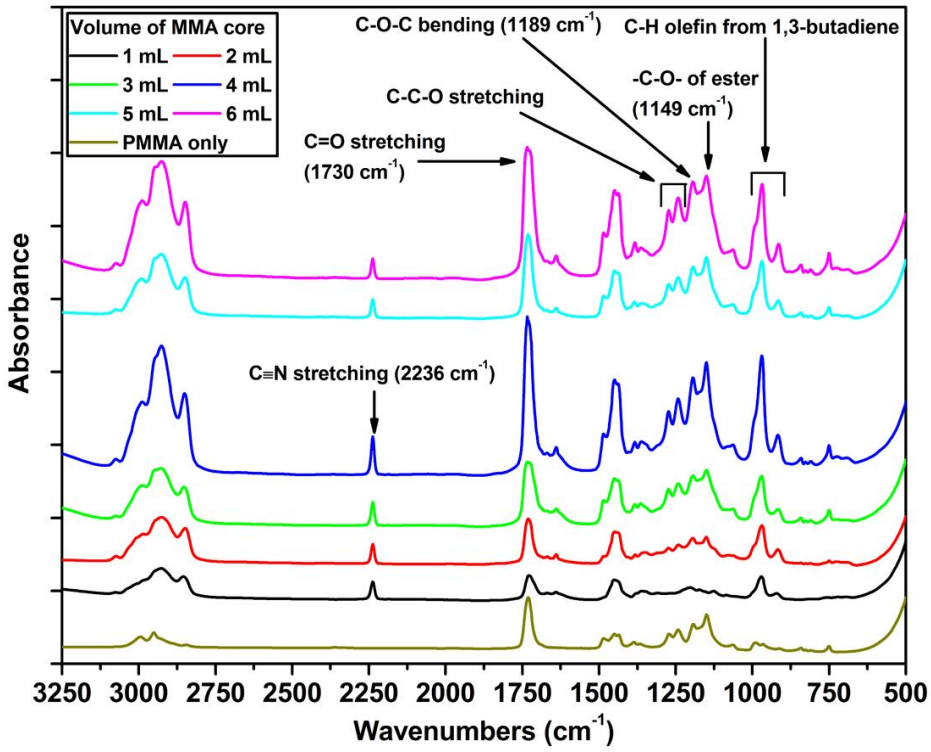

**Figure 7-1 FTIR spectra of a group of PMMA-NBR core-shell nanoparticles prepared in Exp.13-18 and a PMMA sample prepared at the first stage of Exp. 18. Polymerization conditions: MMA volumes varying from 1 to 6 mL; GS 12-3-12 =2.0 g in 80 mL distilled water, APS=0.125 g, T=70 °C at the first stage; AN=2.5 mL, BD=7.5 mL, T=45 °C at the second stage.**

All of the PMMA-NBR core-shell structured nanoparticles produced were first characterized via Fourier transform infrared spectroscopy (FTIR). Figure 7-1 shows a set of representative FTIR spectra of PMMA-NBR core-shell nanoparticles prepared in the third group of experiments (Exp.13-18) as well as a PMMA spectrum (sampled in Exp. 18). The IR spectra of the core-shell nanoparticles show a strong C=O stretching vibration at 1730 $cm^{-1}$, C-O-C bending at 1189 $cm^{-1}$, and -C-O- of an ester functional group at 1149 $cm^{-1}$ as well as C-C-O stretching vibration, which indicates the incorporation of the polyacrylate ester into chains. On the other hand, the 2236 $cm^{-1}$ peak is assigned to the cyano group (C≡N) and the 970 $cm^{-1}$ peak is the characteristic of the level of unsaturated olefin present, i.e. the proton vibration of the C=C-H group. The peaks at 2236 $cm^{-1}$ and 970 $cm^{-1}$ provide solid evidence for the formation of NBR. Furthermore, the acrylonitrile content characterized by 39.31 wt% of NBR shell was calculated from the peak intensity of 2236 $cm^{-1}$ and 970 $cm^{-1}$ according to thr ASTM D5670-95 (2009) test method.

It can be seen from Figure 7-1 that with an increase in MMA volume from 1 to 6 mL stepwise, the relative peak area ratios of 1730 $cm^{-1}$ assigned to the C=O group of PMMA over 2237 $cm^{-1}$ attributed to C≡N group of NBR increase correspondingly. As shown in Table 7-2, the polymerization conversions between the six experimental runs in the third group of experiments are comparable either at the first or second stage, which indicates that the area ratios of $A_{1730}/A_{2237}$ can be reflected upon the ratios of PMMA compositional fractions in the PMMA-NBR nanoparticles. These area ratios are expected to approximately comply with the ratios of the initial MMA injection amounts as the amount of NBR is designed to be identical in all runs. According to the characteristic peak areas given by the Bio-Rad Merlin software of the IR instrument used, the peak area ratios represented by

$A_{1730}/A_{2237}$ are calculated to be 1: 1.8: 2.8: 3.9: 4.8: 5.9, which show a good agreement with the ratios of MMA addition volume of 1: 2: 3: 4: 5: 6, respectively.

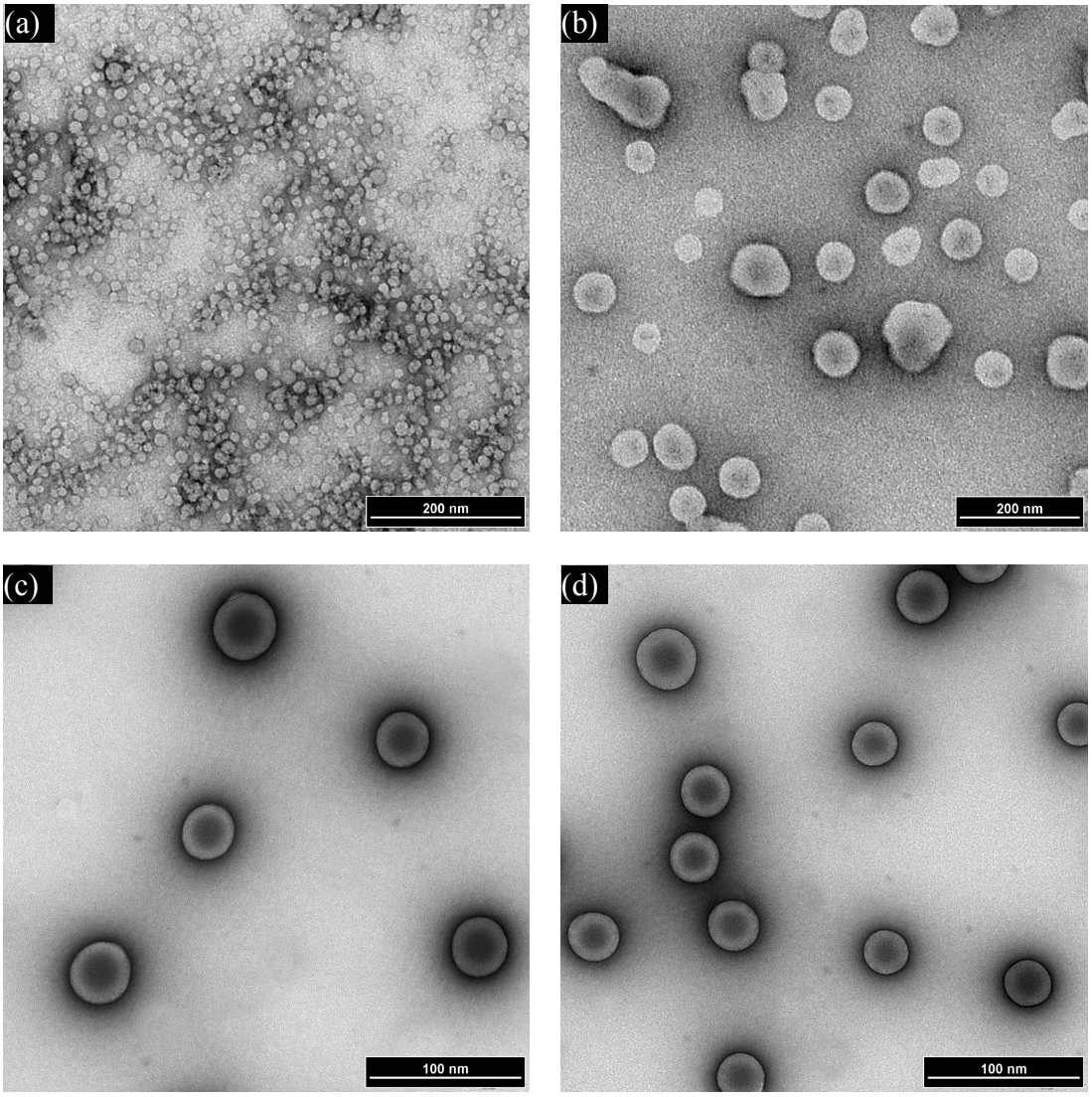

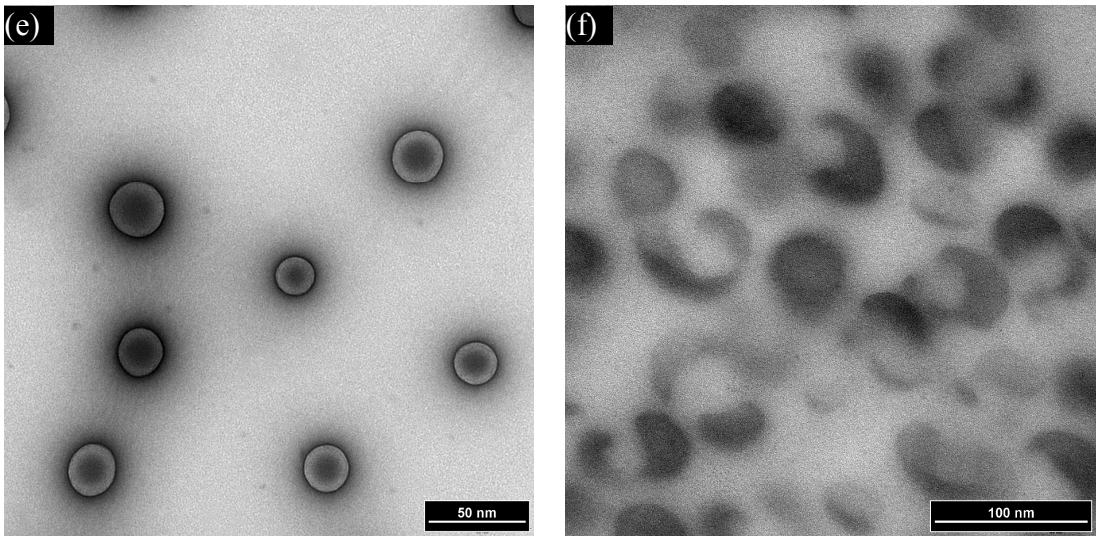


**Figure 7-2 TEM imaging of PMMA core nanoparticles and PMMA-NBR core-shell nanoparticles. Figs. (a)-(e) are the normal TEM photographs and Fig. (f) is the cross section TEM photograph. (a) is PMMA specimen obtained at the first stage of Exp. 22. (b)-(e) are PMMA-NBR nanoparticles prepared from Exp. 1 (b), Exp. 10 (c), Exp. 16 (d), and Exp. 22 (e), respectively. (f) is the image of PMMA-NBR nanoparticles prepared from Exp. 12 and the sample was carefully ground before sending for the cross section TEM.** Polymerization conditions**: Figs. (a) MMA=4 mL, GS 12-3-12=3 g, sampled at the end of first stage; (b) MMA=1 mL, GS 12-3-12=0.5 g; (c) MMA=4 mL, GS 12-3-12=1 g; (d) MMA=4 mL, GS 12-3-12=2 g; (e) MMA=4 mL, GS 12-3-12=3 g; (f) MMA=6 mL, GS 12-3-12=1 g. The other experimental conditions include APS=0.125 g, T=70 °C at the first stage; AN=2.5 mL, BD=7.5 mL, T=45 °C at the second stage; the distilled water=80 mL.**

The size of PMMA-NBR nanoparticles was observed to increase after the second stage of polymerization compared to the size of PMMA nanoparticles obtained at the end of the first stage of polymerization (Table 7-2, Figure 7-2). This growth suggests that the monomers added during the second stage were polymerized over the core seeded nanoparticles. The most commonly used apparatus for observing the morphology, structure and the particle size of nanoparticles is the electron microscopy. Figure 7-2a shows the size and morphology of PMMA nanoparticles prepared in Exp. 22 and Figure 7-2b-e show a set of representative

TEM images of PMMA-NBR core-shell nanoparticles obtained in four groups of experiments, represented by Exp. 1, Exp. 10, Exp. 16, and Exp. 22, respectively. As shown in Figure 7-2b-e, the light domains correspond to the NBR shell whereas the PMMA core exhibits dark regions. Figure 7-2b-e suggest that the distinct core-shell morphology has been obtained in the synthesized PMMA-NBR nanoparticles, even when the agglomeration occurred in Exp. 1 (Figure 7-2b). Furthermore, the produced core (Figure 7-2a) and core-shell (Figure 7-2c-e) nanoparticles using higher surfactant concentrations give rise to a spherical morphology (Figure 7-2c-e). The particle size distribution can be evauated by the ratio of $D_w/D_n$, where $D_w$ is the weight-average diameter and $D_n$ is the number-average diameter. It is commonly accepted that $D_w/D_n$ values ranging from 1.0-1.1 can be regarded as monodisperse while those ranging from 1.1-1.2 are near-monodisperse.[33b] The dipsersity values of particle size presented in Table 7-2 show that with increasing in surfactant concentration, the distributions of both core and core-shell particles go through a transition from the polydisperse to near-monodisperse. While $D_w/D_n$ values of PMMA nanoparticles produced in Exps. 13, 14, 19-21 (<1.1) suggest that a markedly narrow distribution can be obtained under the high surfactant to polymer weight ratio. This trend in the particle size distribution with variation in surfactant concentration is consistent with the results reported by Sajjadi,[30] and a detailed discussion can also be found in his report. In order to compare the results obtained from the normal TEM images, the cross-section TEM was carried out to further show the core-shell structure (Figure 7-2f). It can be seen in Figure 7-2f that the phase separation between the core and shell was observed due to the grinding operation before sending the samples for the analysis by TEM. The NBR shell was cracked and bent. The spheres are believed to be the PMMA cores. On the other hand, Figure 7-2a-e demonstrate that the sizes of PMMA and PMMA-NBR nanoparticles determined by the TEM approach are consistent with those obtained from the DLS technique (Table 7-2). It is worth noting that the latices prepared in the second, third, and fourth group of experiments can maintain stability for at least half a year.

The mechanism involved in the formation of the core-shell structured nanoparticles using PMMA as seeds is different from that of when the shell particles are formed without

seeds.[44-48] In the core-shell situation, the core monomers are first initiated and then polymerized to form numerous nanoparticles, which are considered to provide the nuclei for shell monomers to polymerize. Therefore, the nucleation energy barrier for the shell polymer needs to be overcome when no seeds are used, is eliminated, so that the core-shell nanoparticles are formed under kinetic control. Meanwhile, the formation of secondary particles nucleation is prevented during the second stage of polymerization. Furthermore, because a large number of loci are created by the core seeds, the amount of shell monomers in the region of each seed is decreased, which will be beneficial for preparing many types of smaller polymer nanoparticles. One of our previous reports has shown that using PMMA seeds is an effective route to prepare smaller polystyrene nanoparticles.[47]

Although the sequential preparation of core and shell in two stages has been shown to be an effective approach to obtain the core-shell structured nanoparticles, there are still many factors which can influence the morphology of the resulting nanoparticles, such as the type and amount of surfactant and initiators, the manner of monomer feeding, the relatively hydrophilicity of the core and shell monomers, and other thermodynamic and kinetic parameters.[15,20,49] The core-shell structure of PMMA-NBR nanoparticles which can be realized is primarily attributed to the following aspects. In the first and second stage reaction systems, the monomers are both charged in a continuous manner. One advantage of the semibatch process over the batch method is featured in that the addition rate is less than the chain growing rate, which induces a narrow particle size distribution as well as a smaller particle size.[30,50] Furthermore, the starving induced addition method plays an important role in the formation of well defined core-shell structure.[14,15] In this process, the shell monomers have always been at a starving status, resulting in that the shell monomers have no time to diffuse into the inner space of core polymer and hence are driven to polymerize onto the surface of core nanoparticles to a greatest extent. In addition, due to the tight packing capability of the long hydrophobic $C_{12}$ alkyl chains,[51] the relatively high internal viscosity of the seeded polymerizing particles limits the diffusivity of the shell polymer chains, which will prevent the shell polymer chains from undergoing Ostwald ripening to form the separate spherical microdomains in the core region.[20] Meanwhile, the constricted packing property

of GS 12-3-12 results in a cohesive and stable interfacial film around the oil phase during the first stage of polymerization, which enhances the absorption energy between the core particles with surfactant molecules and resists the desorption and repartitioning of the surfactant to stabilize the newly created NBR primary particles.[14,51] Therefore, the formation of secondary NBR nanoparticles is further prevented.

It can be deduced from the nucleation and growth processes of core-shell nanoparticles that the amount of surfactant plays an important role in the polymerization. In the case of the low surfactant concentration (the first group of experiments), a small amount of PMMA precipitate was found at the first stage of polymerization while the substantial agglomeration of PMMA-NBR was observed at the second stage of polymerization. In contrast, the agglomeration phenomenon was not observed in the second, third, and fourth group of experiments. These phenomena show a good agreement with the measured ζ-potentials of both core and core-shell latex particles presented in Table 7-3. It is generally accepted that particles with ζ-potentials more positive than +30 mV or more negative than -30 mV are normally considered stable. It can be seen in Table 3 that in the experimental runs using 0.5 g surfactant, the ζ-potentials of PMMA latex particles are almost below 30 mV. For the PMMA-NBR latex particles, the ζ-potentials are quite low in the range 5-10 mV, which represents the instability of an emulsion. In contrast, the ζ-potentials of core and core-shell particles are all above 30 mV using 1 g surfactant and more than 40 mV at high surfactant concentrations of 2 and 3 g in 80 mL water. A discussion of this phenomenon will be presented in the following section. Meanwhile, Table 7-3 suggests that the core-shell latex particles have smaller ζ-potentials than the core seeds. This is considered to be caused by the decrease in the surface charge density of particles due to increasing of particle size during the second stage of polymerization.

**Table 7-3 Zeta potentials of core and core-shell latex particles**

| Surfactant amount in 80 mL distilled water (g) | MMA volume (mL) | Zeta potential of PMMA (mV)[a] | Zeta potential of PMMA-NBR (mV)[a] |
|---|---|---|---|
| 0.50[b] | 1 | 31.4 | 6.70 |
| | 2 | 26.6 | 5.10 |
| | 3 | 24.8 | 5.34 |
| | 4 | 29.7 | 5.32 |
| | 5 | 25.1 | 5.05 |
| | 6 | 20.7 | 5.26 |
| 1.0 | 1 | 52.9 | 34.6 |
| | 2 | 48.4 | 36.7 |
| | 3 | 44.9 | 41.0 |
| | 4 | 41.4 | 38.7 |
| | 5 | 42.6 | 39.4 |
| | 6 | 43.6 | 35.9 |
| 2.0 | 1 | 70.3 | 43.3 |
| | 2 | 67.7 | 46.8 |
| | 3 | 65.4 | 56.3 |
| | 4 | 63.0 | 50.2 |
| | 5 | 60.2 | 49.8 |
| | 6 | 58.6 | 44.3 |
| 3.0 | 1 | 71.4 | 46.4 |
| | 2 | 66.8 | 50.8 |
| | 3 | 64.2 | 53.2 |
| | 4 | 63.9 | 59.8 |
| | 5 | 61.3 | 55.3 |
| | 6 | 60.3 | 55.5 |

[a]Mean value of triplicate measurements for each sample is determined using a Zetasizer Nano ZS.

On the other hand, the TEM image shown in Figure 7-2b indicates that the core-shell nanoparticles prepared under the low surfactant amount (0.5 g) have a broader size distribution and the morphologies of a few nanoparticles in Figure 7-2b exhibit alternative structures including a raspberry-like rather than spherical pattern. This deviation in the morphology as well as the observed agglomeration were considered due to the counteract effect of the negative charges (e.g. $SO_4^{\bullet -}$) originating from the decomposition of APS on the electrostatic stabilization built up by the cationic GS 12-3-12. In the absence of the surfactant, the generated sulfate free radicals and subsequent addition of a few MMA molecules are able to afford a role of a kind of "anionic surfactant" and this role can stabilize particles thus leading to the latex featuring a negative ζ-potential. While in the present study employing the cationic GS 12-3-12, the surfactant will impose a counterbalance effect on the negative ζ-potentials, which leads to the positive ζ-potentials of particles as shown in Table 7-3. However, at the lower surfactant amount (0.5 g), this counterbalance effect was relatively small and thus the stabilizing effect derived from surfactant was in a large part neutralized by the anions derived from the initiator. Therefore, the low colloidal stability of latex and substantial deviation in the morphology were produced in these samples. In order to verify this explanation, a cationic initiator 2,2′-azobis (2-amidinopropane) dihydrochloride (V50, using the same mole number as APS) was used to initiate the polymerization in the presence of GS 12-3-12. Except for the initiator, the other experimental conditions are the same with those of Exp. 1. The TEM imaging of the prepared samples using GS 12-3-12 and V50 is shown in Figure 7-3. On comparing Figure 7-2b and Figure 7-3, it can be seen that the particles shown in Figure 7-3 have a core-shell spherical morphology and no agglomeration was observed during the course of polymerization, which provides strong evidence for the neutralization effect stemming from APS on the positive charges at the surface of the particles. This may explain the observed phenomenon that increasing the surfactant amount

(0.5-2 g) resulted in an increase in the ζ-potentials for both the core and core-shell particles. With addition of more surfactant, more numerous particles were generated and thus the effect of negative charges on the ζ-potential for each particle was reduced accordingly as the amount of APS is identical in all experimental runs. Therefore, a higher ζ-potential was measured. When the surfactant amount reached 2 g, the ζ-potential attained a maximum and showed only a slight difference with a further increase in the surfactant amount, which indicated that the neutralization effect originating from APS was very weak and could be considered as being negligible.

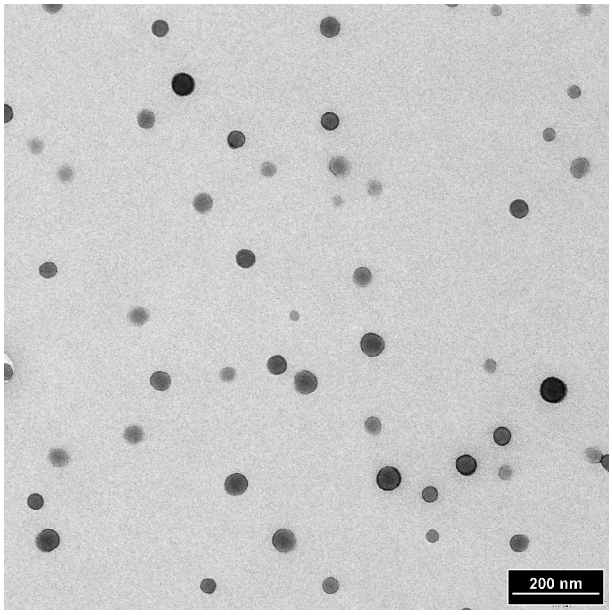


**Figure 7-3 TEM imaging of PMMA-NBR core-shell nanoparticles. Polymerization conditions: MMA=1 mL, GS 12-3-12=0.5 g, V50=0.146 g, T=70 °C at the first stage; AN=2.5 mL, BD=7.5 mL, T=45 °C at the second stage; the distilled water=80 mL.**

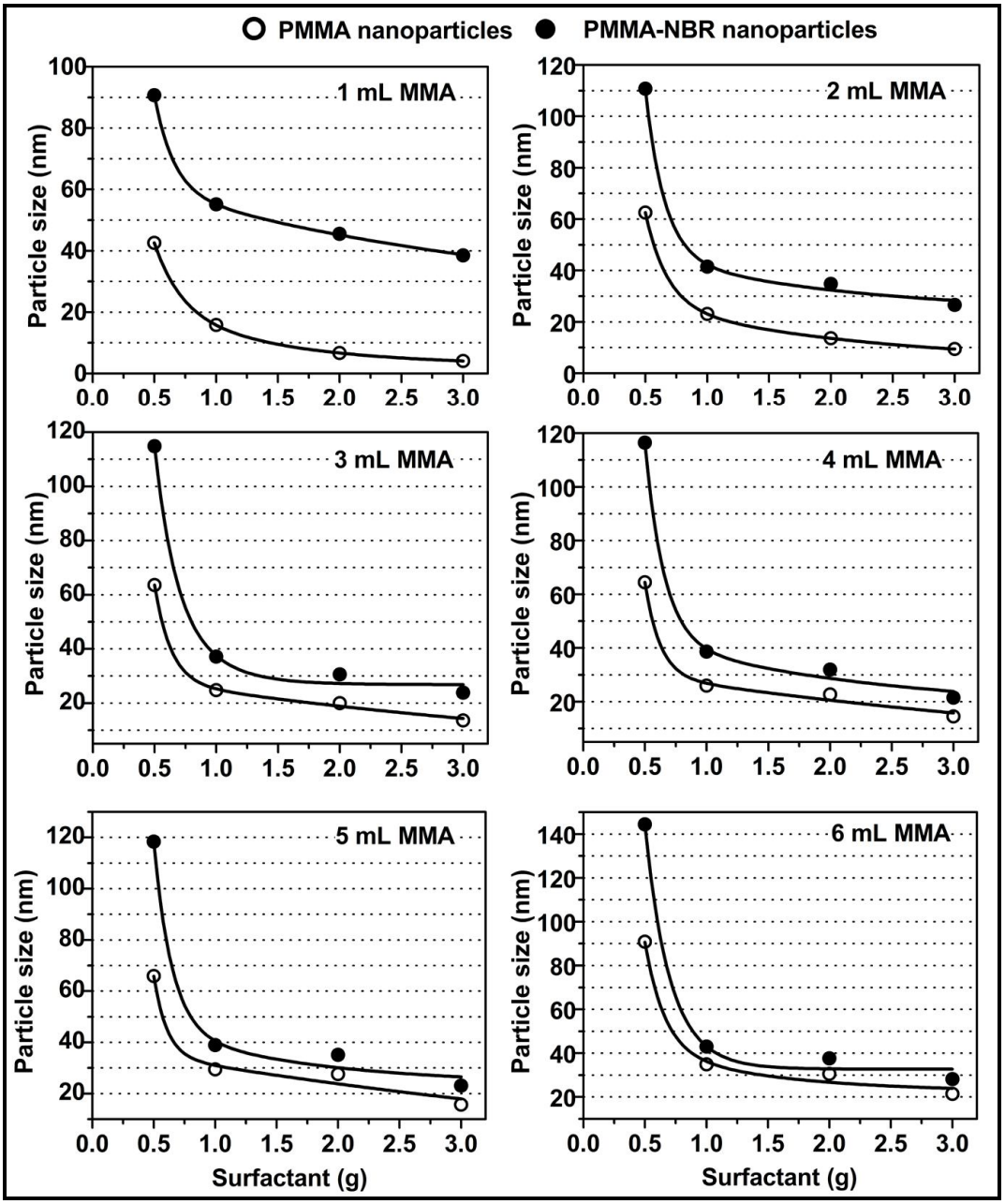


**Figure 7-4 Effect of GS 12-3-12 amount on the size of core and core-shell nanoparticles under different amount of core monomer. The partial agglomeration was found at the second stage of polymerization when 0.5 g surfactant was employed. Polymerization conditions: GS 12-3-12 and MMA amounts are variables; distilled water=80 mL, APS=0.125 g, T=70 °C at the first stage; AN=2.5 mL, BD=7.5 mL, T=45 °C at the second stage.**

Figure 7-4 presents the considerable influence of surfactant amount on the particle size of core and core-shell polymer nanoparticles under each core monomer addition volume ranging from 1 to 6 mL. With respect to each reaction system, the sizes of PMMA and PMMA-NBR nanoparticles decrease in the two distinct phases with the stepwise increase of surfactant amount from 0.5 to 3 g. Initially, a rapid decrease of the particle sizes of PMMA and PMMA-NBR is caused by a minor increase of surfactant amount from 0.5 to 1 g. Then, the particle sizes drop slowly and smoothly with the surfactant amounts increasing from 1 to 3 g. This phenomenon suggests that when the surfactant amount reaches 1g in 80 mL water, the surfactant concentration is high enough to provide a sufficient number of micelles to encapsulate all the generated and newly formed polymer nanoparticles. Meanwhile, on comparing the experimental runs using the same MMA addition amount, for example the comparison among Exp. 2, Exp. 8, Exp. 14, and Exp. 20, the polymerization conversions of both PMMA and PMMA-NBR nanoparticles are found to increase due to the increase of the surfactant concentration (Table 7-2). This is due to that the high surfactant levels lead to both a decreased particle size and more numerous particles in the reactor thereby creating more reaction domains.

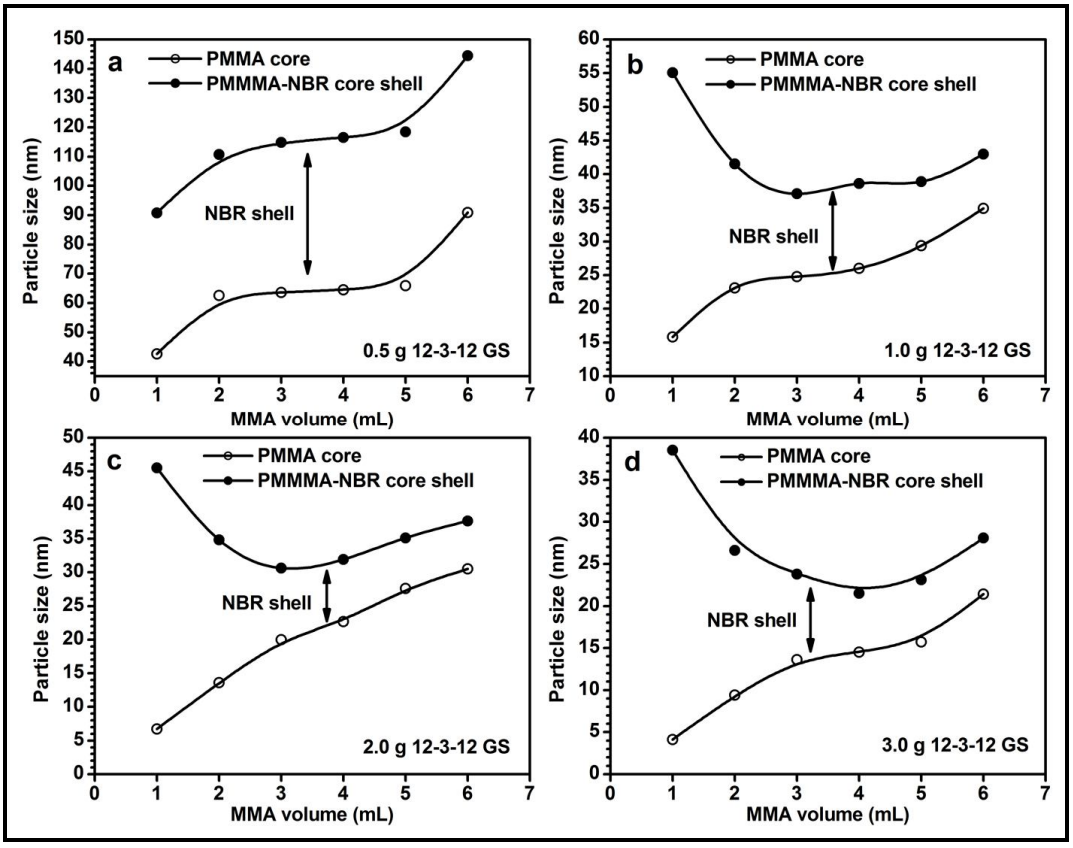


**Figure 7-5 Effect of core monomer addition volume on the size of core and core-shell nanoparticles under different surfactant amount. The partial agglomeration was found at the second stage of polymerization when 0.5 g surfactant was employed. Polymerization conditions: GS 12-3-12 and MMA amounts are variables; distilled water=80 mL, APS=0.125 g, T=70 °C at the first stage; AN=2.5 mL, BD=7.5 mL, T=45 °C at the second stage.**

Figure 7-5 shows the effect of the MMA addition amount on the size of PMMA and PMMA-NBR nanoparticles. As shown in Figure 7-5a-d, the particle size of PMMA increases with the stepwise increase of MMA amount from 1 to 6 mL. Interestingly, Figure 7-5b-d show that the particle size of PMMA-NBR however does not follow the same trend with that of PMMA nanoparticles. The particle size of PMMA-NBR initially decreases gradually with an increase in MMA volume. Then the plot reaches a minimum value, and after that the core-shell particle size increases progressively with an increase in MMA amount.

The occurrence of a minimized size of core-shell nanoparticles is due to an interplay consequence of the size change of the PMMA nanoparticle and the opposite change of thickness of NBR shell during the formation of core-shell nanoparticles. As shown in Figure 7-5b-d, with an increase of MMA amount, under each surfactant condition, the particle size of PMMA nanoparticles will increase continuously. Nevertheless, the NBR shell layer will become thinner simultaneously because the diameter of seeds gets larger. Therefore, the particle size of PMMA-NBR is a compromised result from the core particle size and thickness of the shell layer.

The relation between the size of the core and core-shell nanoparticles can be correlated using the following equation:[48]

$$V_s=\pi/6\ (d_{cs}^3 N_{cs}-d_{core}^3 N_{core}) \tag{7-1}$$

where $V_s$ is the volume of the shell polymer; $d_{core}$ and $N_{core}$ are the particle size and number of core nanoparticles respectively; $d_{cs}$ and $N_{cs}$ are the particle size and number of core-shell nanoparticles respectively. If the number of the particles during the shell monomer polymerizing process remained constant ($N_{core}=N_{cs}$), then:

$$V_s/N_{cs}=\pi/6\ (d_{cs}^3-d_{core}^3) \tag{7-2}$$

Above two equations provide a way to examine whether a secondary nucleation or particle coagulation occurred or not. In the absence of a secondary nucleation or coagulation, it is expected to observe the convergence between the sizes of PMMA and PMMA-NBR nanoparticles with an increase in the MMA volume. Nevertheless, this convergence result was not observed in the first group of experiments (Figure 7-5a), which is in a large part due to the low conversions as a result of coagulation. Figure 7-5b-d suggest a good agreement with the anticipation from Eq. 7-2. It can be seen in Figure 7-5b-d that with increasing in MMA volume, the size difference of the core-shell and core nanoparticles decreases gradually. For example, in Figure 7-5c, the difference of PMMA-NBR and PMMA nanoparticles are 38.8, 21.2, 10.6, 9.2, 7.5, and 7.1 (Table 7-2) as the MMA volume increased from 1 to 6 mL.

As shown in Table 7-2, the molecular weights represented by number-average molecular weight $\overline{M}_n$ and weight-average molecular weight $\overline{M}_w$ of PMMA-NBR nanoparticles are found to decrease with an increase in the surfactant concentration. For instance, the $\overline{M}_w$ of nanoparticles obtained in the second group of experiments involving 1 g of surfactant is found to be over the range of 6.6 to $9.1\times10^5$ g/mol, which is obviously higher than that of 4.4 to $6.8\times10^5$ g/mol in the fourth group of experiments using 3 g of surfactant. Meanwhile, the polydispersity index (PDI) characterized by $\overline{M}_w/\overline{M}_n$ is found to be over a narrow range of 1.1 to 1.3 in most experimental runs except for the first group of experiments, which indicates that the average number of polymer chains within each particle should be very small.

## 7.5 An Extended Study of Direct Catalytic Latex Hydrogenation of PMMA-NBR Core-Shell Nanoparticles

There has been a progressively heightened demand for the evolvement of process focusing on the catalytic hydrogenation of unsaturated polymers in an environmentally friendly manner.[28] It has been a widely used technique to hydrogenate the unsaturated polymers in a large amount of organic solvent, i.e. solution hydrogenation.[23] However, this solution hydrogenation suffers from drawbacks stemming from the high viscosity of the reaction medium and the usage of a large amount of organic solvent, which not only increases the cost of the process but raises the environmental concerns. Due to the fact that the diene-based polymers are mostly produced commercially as an emulsion, the direct latex hydrogenation is of great increasing interest as an alternative to the solution hydrogenation.

A preliminary study of the latex hydrogenation was carried out based on the prepared PMMA-NBR nanoparticles with a size of 30.6 nm. The main purpose of this section is to show that the hydrogenation of PMMA-NBR nanoparticles in the latex form has the technical feasibility for the large-scale production and potentials for further exploration and applications.

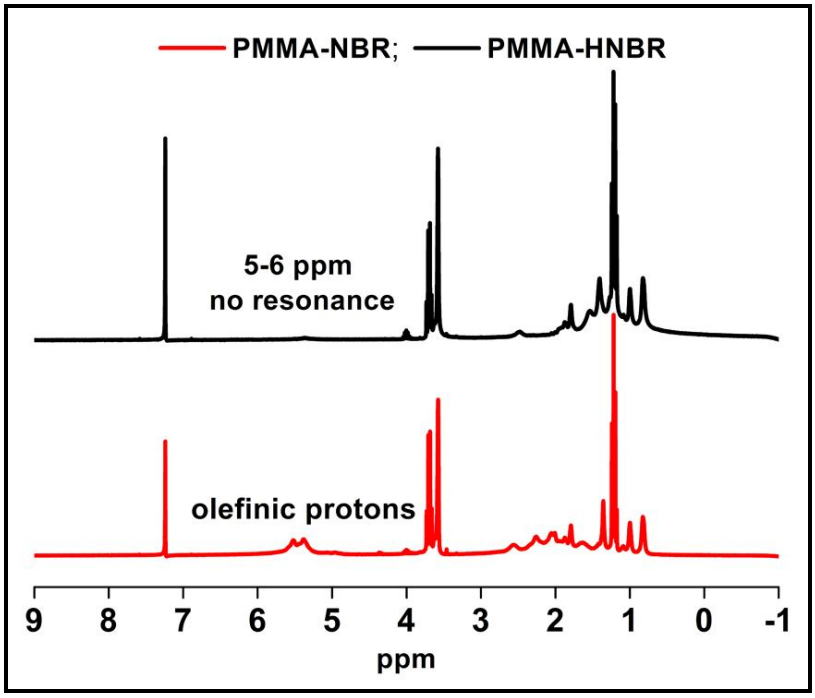


**Figure 7-6 $^{1}$H NMR spectra of non-hydrogenation and post-hydrogenation of PMMA-NBR nanoparticles prepared in Exp. 15. Experimental conditions of synthesis of PMMA-NBR nano-size latex: GS 12-3-12 =2.0 g in 80 mL distilled water, APS=0.125 g, MMA=3.0 mL, T=70 °C at the first stage; AN=2.5 mL, BD=7.5 mL, T=45 °C at the second stage. Hydrogenation conditions: $RhCl(P(C_6H_5)_3)_3$/NBR shell is 0.9 wt%, $RhCl(P(C_6H_5)_3)_3$/TPP is 10 wt%, 600 rpm of agitation, 130 °C, 1000 psi of $H_2$, reaction time=3 h.**

Wilkinson's catalyst, $RhCl(P(C_6H_5)_3)_3$, is the most well-known catalyst for the hydrogenation of unsaturated elastomers.[52,53] A typical application of Wilkinson's catalyst commercially is the hydrogenation of NBR in the solution form which is principally attributed to the fact that it is a highly active catalyst capable of achieving complete hydrogenation of the olefin content without any reduction of the nitrile group present in NBR, as well as effectively suppressing any crosslinking problem which generally occurs using the non-catalytic routes such as the diimide reduction hydrogenation technique.[54,55] Figure 7-6 shows the $^{1}$H NMR spectra of PMMA-NBR latex pre- and post-hydrogenation reaction catalyzed by $RhCl(P(C_6H_5)_3)_3$. The double peaks in the region of 5.0-5.8 ppm are

assigned to the olefinic protons due to the existence of the butadiene unsaturated units. The intensity of the double peaks in the olefinic region decreased gradually during the hydrogenation and no resonance was observed in this range of 5.0-5.8 ppm after 3 h with a $RhCl(P(C_6H_5)_3)_3$/NBR shell weight ratio of 0.9 wt% at 130 °C under 1000 psi of $H_2$, which indicated that essentially complete hydrogenation of the PMMA-NBR core-shell nanoparticles was obtained. Wei et al.[56] reported the direct hydrogenation of 70 nm NBR latex and 97 mol% conversion was reached after 55 h at a temperature of 145 °C under 1000 psi of $H_2$ pressure with a $RhCl(P(C_6H_5)_3)_3$/NBR weight ratio of 1 wt%. With less catalyst loading and a lower temperature, the PMMA-NBR core-shell nano-size latex shows a much faster reaction rate compared with that reported by Wei et al.[56] The significant improvement in hydrogenation rate is first due to the fact that the PMMA-NBR nanoparticles prepared in Exp. 15 have a small particle size of 30.6 nm, which gives rise to more than double the specific surface area (SSA) than that of the commercial NBR nanoparticles which have a size of around 70 nm. Furthermore, the NBR layer in the core-shell nanoparticles is very thin with a thickness of around 5 nm (calculated from the radius difference of PMMA-NBR and PMMA particles), which provides a considerable benefit for the diffusion of the catalyst into the NBR polymer chains. In contrast, the commercial NBR nanoparticles with larger particle size will impose a considerable limitation effect on the diffusion of catalyst into the latex particles.

During the hydrogenation operations, no coagulation of the latex was observed, which indicates that this catalytic hydrogenation has no adverse effect on the latex stability. In addition, the number-average particle size before and after hydrogenation remained almost unchanged. In order to detect whether any cross-linking occurred in the resultant HNBR shell, the hydrogenated latex product was dried and then re-dissolved in acetone. It was found that final hydrogenated polymer was completely soluble in acetone and no visible gel was observed. Therefore, the processibility of the hydrogenated shell will not be adversely affected by this hydrogenation operation. The present direct catalytic latex hydrogenation demonstrates that a fast reaction rate can be achieved in the absence of any organic solvent,

which may offer exciting avenues in the future for the realization of a "green" hydrogenation process.

## 7.6 Conclusions

PMMA-NBR core-shell structured nanoparticles were successfully synthesized by a two stage semibatch microemulsion polymerization method using GS 12-3-12 as the emulsifier. The TEM imaging suggests that two distinct phases are formed. The structure and composition of produced core-shell nanoparticles were examined by FTIR and $^{1}$H NMR, which confirmed the incorporation of the functional groups of PMMA and NBR. The formation mechanism of core-shell nanoparticles was illustrated. Two factors are considered to impose favorable effects on the formation of core-shell structure, which are represented by the employment of a continuous addition mode and well-behaved interfacial activity of GS 12-3-12. The particle size and morphology of PMMA-NBR were greatly influenced by GS 12-3-12 concentration. When the surfactant concentration was in a low level, appreciable agglomeration and irregularity of morphology of core-shell latex particles were observed because the stabilizing effect of the cationic surfactant was in a large part neutralized by the negative charges derived from initiator. In contrast, stable latex and spherical morphology were achieved under the higher surfactant concentration. It was found that there exists an optimal feeding amount of core monomer MMA, which can result in a minimized size of PMMA-NBR nanoparticles. Finally, the latex hydrogenation of PMMA-NBR nanoparticles was carried out in the presence of Wilkinson's catalyst. The $^{1}$H NMR spectra suggest that for the 30.6 nm PMMA-NBR nanoparticles, an almost complete hydrogenation was obtained within 3 h when using 0.9 wt% Wilkinson's catalyst at 130 °C under 1000 psi of $H_2$. The present synthesis and following "green" hydrogenation process can be extended to latices made from semibatch microemulsion containing other diene-based polymers. This study provides a new perspective on the chemical modification of NBR by means of the combination of a core-shell technique with subsequent latex hydrogenation.

# Chapter 8
# Conclusions

## 8.1 Milestones and Contributions

As a result of this research project, a new polymerization technique the so-called micellar nucleation semibatch microemulsion polymerization was developed, by which polymer nanoparticles below 20 nm with a narrow distribution of PDI close to 1 was produced in free radical polymerization. Meanwhile, a high solid content was reached with using a low level of surfactant. This technique will pioneer a significant new way to use a simple but practical method to synthesize narrow PDI polymers, which is a very meaningful new development.

The central challenge that has been limiting the commercialization of green latex hydrogenation processes, i.e., optimal interplay of accelerating the hydrogenation rate, decreasing the required quantity of catalyst, and eliminating the need for an organic solvent was overcome through applying novel nanoscale functional diene-based polymer nanoparticles as the substrates for the catalytic hydrogenation in latex form. These new latex hydrogenation processes meet all the major requirements for developing a green catalytic commercial process, and solve the dilemma encountered between the current lab technology and industrial production, which thus constitutes a significant milestone for the improvements of polymer modification technologies.

Chapter 6 provides a comprehensive study that covers almost every aspect of the catalytic latex hydrogenation, which presents a significant breakthrough in the research field related to the hydrogenation of unsaturated polymer in solution, bulk, and latex forms.

The present synthesis and following “green” hydrogenation process shows the significance in designing nanoscale materials and can be further extended to latices made from semibatch microemulsion containing other diene-based polymers.

## 8.2 Detailed Conclusions

(1) We systematically studied the semibatch microemulsion system and further extended the benefits of the system to a considerable extent by introducing the BPO initiator which resulted in a micellar nucleation mechanism. With BPO as the initiator, the PMMA nanoparticles below 20 nm with narrow size distribution and molecular weight distribution ($\overline{M}_w / \overline{M}_n \sim 1.1$) were prepared and stabilized with a very low SDS/MMA and SDS/$H_2O$ weight ratio of 1:16 and 1:100 respectively as well as with a high solid content of more than 13 wt%. The size of PMMA nanoparticles initiated by BPO is much smaller than that by AIBN and APS under the same SDS concentration in the semibatch microemulsion polymerization systems. In addition, the monomer addition experiments indicate that there exists a minimum required addition time to obtain the minimized particle size. As the addition time was decreased, the polymerization changed gradually from microemulsion polymerization to emulsion polymerization.

(2) NBR nanoparticles were successfully synthesized in a semibatch microemulsion polymerization system using GS 12-3-12 as the emulsifier. An enhanced decomposition rate of initiator APS was achieved even under the low temperature of 50 °C which is attributed to the acidic initiation environment that exists when using GS 12-3-12 as the emulsifier. The FT-IR and $^1$H NMR characterizations demonstrate that the monomers have been incorporated into the produced nanoparticles and the 1,4-*trans* double bonds account for a major percentage of the olefin units in the synthesized polymers. The produced latices show a comparable stability to a conventional microemulsion while the required surfactant/monomer and surfactant/water weight ratios are much lower than those of the microemulsion system. The latex nanoparticles exhibit a spherical morphology and a particle size of below 20 nm can be realized. The obtained NBR nanoparticles are spherical in shape and exhibit near-monodisperse PSDs with $D_w/D_n$ ranging from 1.13 to 1.20. The obtained NBR nanoparticles have high molecular weights and narrow PDIs within the range of 1.42-1.78. The kinetic data suggests that the initial monomer feed fraction ($f_{AN}$ = 30 mol%) is in an azeotropic composition region and the level of bound AN was found to be in the range of 31-35 wt% depending on the surfactant concentrations used. These results agree with the theoretical

azeotropic composition simulated by use of the Mayo-Lewis equation. The $T_g$ values were found to increase from -25.01 to -16.55 °C with an increase in $\overline{M}_n$ from around 329 900 to 707 000 g/mol. The linearity of $T_g$ versus $1/\overline{M}_n$ shows a good agreement with the Fox-Flory equation. The GS 12-3-12 system has notable advantages in reaching much higher polymerization conversion and solid content than for the SDS system. The present synthesis process can be extended to latices made from semibatch microemulsions containing other diene-based polymers. The obtained fine NBR nanoparticles may find many useful applications in various fields, particularly in the improvement of the hydrogenation rate of the diene-based polymers in latex form.

(3) The rate of catalytic latex hydrogenation was greatly affected by the particle size, concentration of catalyst, and reaction temperature. An optimized experimental condition for latex hydrogenation was achieved based on a series of univariate experiments where in the absence of organic solvents, a 95 mol% conversion was reached within around 20 h for 17.5 nm NBR nanoparticles at 130 °C under 1000 psi hydrogen and only 0.1 wt% catalyst was required. Exceptionally high TON (11065.88) and TOF (~553.29 $h^{-1}$) were obtained under this optimum latex hydrogenation condition. In particular, no crosslinking was observed in all of the resultant hydrogenation products, which is independent of the degree of hydrogenation. The diffusion of hydrogen from the gas phase to the polymer phase was not a rate-determining factor. By using TPP as the catalyst carrier, oil soluble Wilkinson's catalyst was transported into the latex particles and dispersed homogeneously throughout the nanoparticles. The catalytic latex hydrogenation can be viewed as being equivalent to a "mini-bulk" hydrogenation where numerous nano bulk hydrogenation was carried out inside the latex particles at the molecular level of catalysis. With respect to the reaction that has reached or nears 95 mol% conversion, an apparent overall-first-order dependence in olefin was observed. The pseudo-first-order rate constant is thus determined from a first-order rate model. The apparent activation energy was calculated to be in the range of 100 to 110 kJ/mol. The strong coordination of C≡N to the catalytically active species $RhH_2Cl(PPh_3)_2$ imposed a inhibition effect on the hydrogenation activity and two competitive cycles characterized by nitrile and olefin catalytic cycles was proposed to explain the inhibitory

behavior induced by C≡N. With the progression of the hydrogenation, more and more $RhH_2Cl(PPh_3)_2$ will be entrapped and retained into the nitrile cycle. Thus, the effective catalyst used in the reduction of double bond is much less than the charged amount. The present "green" hydrogenation process can be extended to latices made from semibatch microemulsion polymerizations containing other diene-based polymers. This study may facilitate the commercialization of "green" latex hydrogenation in industry.

(4) PMMA-NBR core-shell structured nanoparticles were successfully synthesized by a two stage semibatch microemulsion polymerization method using GS 12-3-12 as the emulsifier. The TEM imaging suggests that two distinct phases are formed. The structure and composition of the produced core-shell nanoparticles were examined by FTIR and $^1$H NMR, which confirmed the incorporation of the functional groups of PMMA and NBR. The formation mechanism of core-shell nanoparticles was illustrated. Two factors are considered to impose favorable effects on the formation of the core-shell structure, which are represented by the employment of a continuous addition mode and a well-behaved interfacial activity of GS 12-3-12. The particle size and morphology of PMMA-NBR was greatly influenced by GS 12-3-12 concentration. When the surfactant concentration was at a low level, appreciable agglomeration and irregularity in the morphology of the core-shell latex particles was observed because the stabilizing effect of the cationic surfactant was in a large part neutralized by the negative charges derived from initiator. In contrast, stable latex and spherical morphology were achieved under higher surfactant concentration. It was found that there exists an optimal feeding amount of core monomer MMA, which can result in a minimum size of PMMA-NBR nanoparticles. Finally, the latex hydrogenation of PMMA-NBR nanoparticles was carried out in the presence of Wilkinson's catalyst. The $^1$H NMR spectra suggest that for the 30.6 nm PMMA-NBR nanoparticles, an almost complete hydrogenation was obtained within 3 h catalyzed by 0.9 wt% Wilkinson's catalyst at 130 °C under 1000 psi of $H_2$. The present synthesis and following "green" hydrogenation process can be extended to latices made from semibatch microemulsion containing other diene-based polymers. This study provides a new perspective for the chemical modification of NBR by means of the combination of a core-shell technique and the subsequent latex hydrogenation.

# Chapter 9
# Recommendations for Future Research

1. Synthesis of new functional polymer nanoparticles. With the increasing requirements of polymer nanoparticles in practical applications, it is of great interest to find novel pathways to prepare polymeric materials with enhanced property profiles. One recommended research goal is to reach a better processibility for good control of the desired molecular weight and PDI of the targeted polymer nanoparticles. For example, the synthesis of the block NBR latex nanoparticles through applying controlled/living radical copolymerization of acrylonitrile and 1,3-butadiene in the emulsion media is worthy of pursuit.

2. Exploration of different types of surfactants in the semibatch microemulsion polymerization system. The development of new surfactant systems with improved emulsifying properties is an important aspect for technical applications, since the structure of the surfactant has a decisive influence on the amount of an emulsifier used in polymerization.

3. Modeling of the synthesis and hydrogenation reactions. The process of semibatch microemulsion polymerization is important in industry for making a great variety of polymer nanoparticles. It is very desirable to develop a sophisticated model that can be used for the large-scale production of synthesis of polymer nanoparticles. It is likewise important for the modeling of the scale up of green latex hydrogenation production, especially given that the present latex hydrogenation system has fulfilled the requirements of a green catalytic process.

4. Catalyst separation study. In the present latex hydrogenation, although the consumed catalyst has been reduced drastically, there is still a small amount of catalyst left in the final product. Therefore, how to separate and recycle the metal residues in the resulting hydrogenated polymer is an important concern. Two research directions are recommend: (1) to develop water-soluble catalyst systems which can transfer the metal back to the water phase after the reaction, for example the water soluble analog of Wilkinson's catalyst; (2) to develop new techniques to separate the catalyst from the latex particles, for example $CO_2$-

expanded liquids (CXLs) which have been launched for chemical processing based on the principles of green chemistry and engineering.

# Appendix A
# Nomenclature

| | |
|---|---|
| $j_{cr}$ | critical chain length |
| $f_{H_2}$ | fugacity of hydrogen gas, which is estimated as 70.703 atm under 1000 psi |
| $K$ | corrected Henry's coefficient, atm |
| $K_H$ | Henry's constant of $H_2$ in water, MPa |
| $N_{H_2}$ | mole fraction of hydrogen in water |
| $\bar{v}$ | partial molar volume of hydrogen in water, L/mol |
| $P_l^{sat}$ | vapor pressure of water at saturation, MPa |
| $T^* = T/T_c^l$ | $T$ is the absolute temperature and $T_c^l$ is the critical temperature of water which is equal to 647.14 K |
| $D$ | diffusion coefficients, $cm^2/sec$ |
| $C_g$ | concentration of hydrogen in gas phase ($mol/m^3$) |
| $E_d$ | activation energy of diffusion, kJ/mol |
| $C_0$ | concentration of hydrogen at the out surface of NBR nanoparticles, mol/L |
| $n_c$ | the number of carbon atoms in the single alkyl chain |
| b | concentration of reactive double bonds, mol/L |
| $A$ | interface area per surfactant molecule at the latex particles, $Å^2$ |
| δ | thickness of surfactant layer, Å |
| $\rho_m$ | density of monomer, $g/cm^3$ |
| $k'$ | pseudo-first-order rate constant, $h^{-1}$ |

| | |
|---|---|
| $[S]$ | concentration of surfactant per unit volume of water, mol/L |
| $\rho_I$ | overall rate of radical entry into both micelles and particles, mol/(L•h) |
| $E_a'$ | activation energy, kJ/mol |
| $d_c$ | particle size of core nanoparticles, nm |
| $N_{core}$ | number of core nanoparticles |
| $d_{cs}$ | particle size of core-shell nanoparticles, nm |
| $N_{cs}$ | number of core-shell nanoparticles |
| $V_s$ | volume of the shell polymer, $nm^3$ |
| $r_{AN}$ | reactivity ratios of acrylonitrile |
| $r_{BD}$ | reactivity ratios of 1,3-butadiene |
| $f_{AN}$ | instantaneous compositions of monomer |
| $F_{AN}$ | instantaneous compositions of copolymer |
| $\overline{F}_{AN}$ | cumulative copolymer composition |
| $D_w$ | weight-average diameter, nm |
| $D_n$ | number-average diameter, nm |
| PSD=$D_w/D_n$ | particle size distribution |
| $R_a$ | monomer feed rate, L/(s•L(aq)) |
| $R_p$ | rate of polymerization, = $k_p[M]_p$ in particles, $s^{-1}$ |
| $k_p$ | propagation rate constant, L/(mol•s) |
| $k_d$ | rate coefficient for the decomposition of the initiator, $s^{-1}$ |
| $N_p$ | number of latex particles per unit volume of water |
| $\tilde{n}$ | average number of free radicals per particle |

| | |
|---|---|
| $N_c$ | number of polymer chains per particle |
| $[M]_p$ | monomer concentration in the particle, mol/L |
| $N_A$ | Avogadro's constant |
| $\overline{M}_n$ | number-average molecular weight |
| $\overline{M}_w$ | weight-average molecular weight |
| PDI= $\overline{M}_w / \overline{M}_n$ | molecular weight polydispersity index |
| $T_g$ | glass transition temperature, K |
| $T_g^\infty$ | glass transition temperature for a polymer of infinite chain length, K |
| AIBN | 2,2'-azobisisobutyronitrile |
| AN | acrylonitrile |
| AOT | Aerosol OT (AOT, sodium bis(2-ethylhexyl) sulfosuccinate) |
| APS | ammonium persulfate |
| BA | butyl acrylate |
| BD | 1,3-butadiene |
| BPO | benzoyl peroxide |
| $CDCl_3$ | deuterated chloroform |
| CMC | critical micelle concentration |
| C/LRP | controlled/living radical polymerization |
| CSC | critical stability concentration |
| CTAB | cetyltrimethylammonium bromide |
| DAC | dodecylammonium chloride |
| DLS | dynamic light scattering |
| DSC | differential scanning calorimetry |
| DTAB | dodecyltrimethylammonium bromide |
| EDL | electrical double layer |
| EFTEM | Energy Filtered Transmission Electron Microscopy |

| | |
|---|---|
| FESEM | Field Emission Scanning Electron Microscopy |
| GS 12-3-12 | Gemini surfactant trimethylene-1,3-bis (dodecyldimethylammonium bromide) |
| HLB | hydrophile-lipophile balance |
| HNBR | hydrogenatd NBR |
| HPMA | N-(2-hydroxypropyl)-methacrylamide |
| KPS | potassium persulfate |
| KK equation | Krichevsky-Kasarnovsky |
| MCB | monochlorobenzene |
| MEK | methyl ethyl ketone |
| MMA | methyl methacrylate |
| NBR | poly(butadiene-co-acrylonitrile) |
| NR | natural rubber |
| PA | polyacetylene |
| PANI | polyaniline |
| PB | polybutadiene |
| PBA | poly(butyl arylate ) |
| PCL | polycarprolactone |
| PEDOT | poly(3,4-ethyelenedioxythiophene) |
| PEG | Polyethylene glycol |
| PEO | poly(ethylene oxide) |
| PFB | poly(9,9-dioctylfluorene-2,7-diyl-co-bis-N,N' -(4-butylphenyl)-bis-N,N'-phenyl-1,4-phenylenediamine) |
| PFBT | poly(9,9-dioctylfluorene-2,7-diyl-co-benzothiadiazole) |
| PGA | polyglutamic acid |
| PLA | polylactic acid |
| PLGA | poly-d,l-lactide-co-glycolide |
| PMA | poly(methyl acrylate) |
| PMMA | Poly(methyl methacrylate) |

| | |
|---|---|
| PPV | poly(para-phenylene vinylene) |
| PPy | polypyrrole |
| PS | polystyrene |
| PT | polythiophene |
| PVA | poly(vinyl acetate) |
| RESOLV | rapid expansion of supercritical solution into liquid solvent |
| RESS | rapid expansion of supercritical solution |
| SBR | styrene butadiene rubber |
| SDS | sodium dodecyl sulfate |
| SEC or GPC | size exclusion chromatography or gel-permeation chromatography |
| St | styrene |
| THF | tetrahydrofuran |
| TMS | tetramethylsilane |
| TOF | turn over frequency, $h^{-1}$ |
| TON | number of turnovers |
| TPP | Triphenylphosphine |
| V50 | 2,2′-azobis(2-amidinopropane) dihydrochloride |
| VA | vinyl acetate |
| Wilkinson's catalyst | $RhCl(PPh_3)_3$, $RhCl(P(C_6H_5)_3)_3$, or $RhCl(TPP)_3$ |

# Appendix B

## Diagram of Modified Parr 316 Stainless Steel Reactor

The synthesis of nanoparticles and hydrogenation was performed in a modified Parr 316 Stainless Steel reactor under a nitrogen atmosphere.

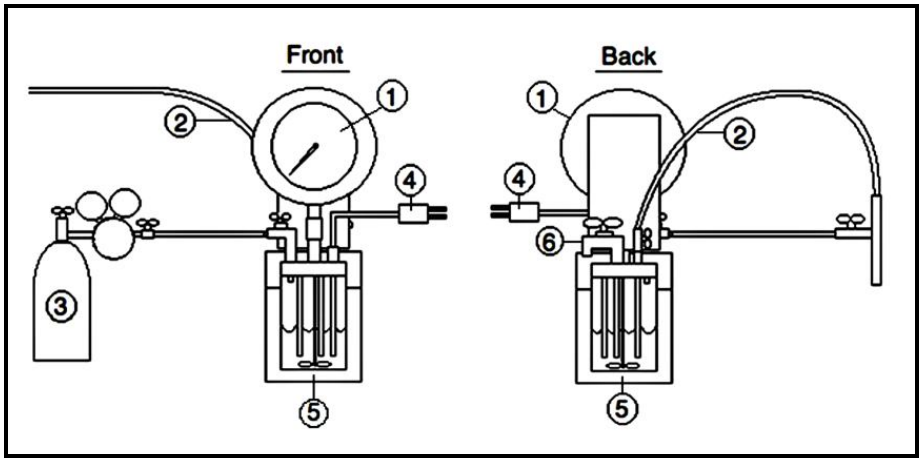


Modified Parr 316 Stainless Steel Reactor. ① pressure gauge; ② monomer adding tube; ③ nitrogen cylinder; ④ thermocouple; ⑤ reactor autoclave; ⑥ sample taken outlet tube. The two ends of adding tube (②) are connected to the reactor separately in order to maintain the pressure inside the reactor (⑤) equal to the pressure above the monomer interface inside the tube (②). Therefore, the monomer could be added into the reactor with a constant rate by the force of gravity.

# Bibliography


1 Whitesides GM. Small 2005, 1, 172.

2 Mirkin CA. Small 2005, 1, 14.

3 Rao JP, Geckeler KE. Prog Polym Sci 2011, 36, 887.

4 Paul DR, Robeson LM. Polymer 2008, 49, 3187.

5 Couvreur P, Dubernet C, Puisieux F. Eur J Pharm Biopharm 1995, 41, 2.

6 Yallapu MM, Jaggi M, Chauhan SC. Drug Discov Today, 2011, 16, 457.

7 Chemistry of Nanomaterials: Synthesis, Properties and Applications. Edited by C. N. R. Rao, A. Mu¨ller, A. K. Cheetham. 2004 WILEY-VCH Verlag GmbH & Co. KGaA, Weinheim. pp 3-4.

8 Rempel GL, Pan Q, Wu J. in "Handbook of Homogeneous Hydrogenation" (G. de V. Johannes., and J. E. Cornelis. Ed.) Vol. 2 p. 547-579. Wiley-VCH, Germany, 2006.

9 Singha NK, Bhattacharjee S, Sivaram S. Rubber Chem Technol 1997, 70, 309.

10 McManus NT, Rempel GL. J Macromole Sci Part C-Polym Rev 1995, 35, 239.

11 Gilliom LR. Macromolecules 1989, 22, 662.

12 Gilliom LR, Honnell KG. Macromolecules 1992, 25, 6066.

13 Wideman LG. US 4 452 950 (1984), The Goodyear Tire & Rubber Company. Wideman LG. Chem Abstr 1984, 101, 56322.

14 Lin X, Pan Q, Rempel GL. Appl Catal A 2004, 276 (1-2), 123.

15 Singha NK, Sivaram S, Talwar SS. Rubber Chem Technol 1995, 68, 281.

16 Mahittikul A, Prasassarakich P, Rempel GL. J Appl Polym Sci 2006, 100, 640.

17 Mahittikul A, Prasassarakich P, Rempel GL. J Mol Catal A Chem 2009, 297, 135.

18 Chemtob A, Heroguez V, Gnanou Y. Macromol Rapid Commun 2005, 26, 1711.

19 Kotzabasakis V, Hadjichristidis N, Papadogianakis G. J Mol Catal A Chem 2009, 304, 95.

20 Kotzabasakis V, Georgopoulou E, Pitsikalis M, Hadjichristidis N, Papadogianakis G. J Mol Catal A Chem 2005, 231, 93.

21 Wei Z, Wu J, Pan Q, Rempel GL. Macromol Rapid Commun 2005, 26, 1768.

22 Dhar S, Gu F, Langer R, Farokhzad O, Lippard, S. PNAS 2008, 105, 7356.

23 Karnik R, Gu F, Basto P, Cannizzaro C, Dean L, Kyei-Manu W, Farokhzad O, Langer R. Nano Lett 2008, 8, 2906.

24 Gu F, Zhang L, Teply B, Mann N, Wang A, Radovic-Moreno A, Langer R, Farokhzad O. PNAS 2008, 105, 2586.

25 Gu F, Karnik R, Wang A, Alexis F, Levy-Nissenbaum E, Hong SP, Langer R, Farokhzad OC. Nano Today 2007, 2, 14.

26 Karp JM, Langer R. Curr Opin Biotechnol 2007, 18, 454.

27 Farokhzad OC, Karp JM, Langer R. Expert Opin Drug Deliv 2006, 3, 311.

28 Yang H, Fung S, Pritzker M, Chen P. J Am Chem Soc 2007, 129, 12200.

29 Keyes-Baig C, Duhamel J, Fung S, Bezaire J, Chen P, J Am Chem Soc 2004, 126, 7522.

30 Fung S, Yang H, Bhola PT, Sadatmousavi P, Muzar E, Liu M, Chen P. Adv Funct Mater 2008, 18, 1-10.

31 Barreto JA, O'Malley W, Kubeil M, Graham B, Stephan H, Spiccia L. Adv Mater 2011, 23, H18.

32 Cho K, Wang X, Nie S, Chen Z, Shin DM. Clin Cancer Res 2008, 14, 1310.

33 Kumari A, Yadav SK, Yadav SC. Colloids Surf B 2010, 75, 1.

34 Wang X, Wang Y, Chen Z, Shin DM. Cancer Res Treat 2009, 41, 1.

35 Cegnar M, Kristl J, Kos J. Expert Opin Biol Ther 2005, 5, 1557.

36 Vauthier C, Bouchemal K. Pharm Res 2009, 26, 1025.

37 Mora-Huertas CE, Fessi H, Elaissari A. Int J Pharm 2010, 385, 113.

38 Qiao W, Wang B, Wang Y, Yang L, Zhang Y, Shao P. J Nanomater 2010, 2010, 1.

39 Vinogradov SV, Bronich TK, Kabanov AV. Adv Drug Deliv Rev 2002, 54, 135.

40 Goldberg M, Langer R, Jia XQ. J Biomater Sci Polym Ed 2007, 18, 241.

41 Peppas NA, Bures P, Leobandung W, Ichikawa H. Eur J Pharm Biopharm 2000, 50, 27.

42 Cegnar M, Kristl J, Kos J. Expert Opin Biol Ther 2005, 5, 1557.

43 Barreto JA, O'Malley W, Kubeil M, Graham B, Stephan H, Spiccia L. Adv Mater 2011, 23, H18.

44 Nasongkla N, Bey E, Ren J, Ai H, Khemtong C, Guthi JS, Chin SF, Sherry AD, Boothman DA, Gao J. Nano Lett 2006, 6, 2427.

45 Langer R, Vacanti JP. Science 1993, 260, 920.

46 Cima LG, Langer R. Chem Eng Prog 1993, 6, 46.

47 Freed LE, Vunjak-Novakovic G. Adv Drug Deliv Rev 1998, 33, 15.

48 Freyman TM, Yannas I, Yokoo VR, Gibson LJ. Biomaterials 2001, 22, 2883.

49 Wang YZ, Kim UJ, Blasioli DJ, Kim HJ, Kaplan DL. Biomaterials 2005, 26, 7082.

50 Nahmias Y, Schwartz RE, Verfaillie CM, Odde D. J Biotechnol Bioeng 2005, 92, 129.

51 Badylak SF, Record R, Lindberg K, Hodde J, Park K. J Biomater Sci Polymer Ed 1998, 9, 863.

52 Mauck RL, Yuan X, Tuan RS. Osteoarthritis Cartil 2006, 14, 179.

53 Marijnissen W, van Osch G, Aigner J, van der Veen SW, Hollander AP, Verwoerd-Verhoef HL, Verhaar JAN. Biomaterials 2002, 23, 1511.

54 Ciardelli G, Chiono V. Macromol Biosci 2006, 6, 13.

55 Wang Y, Ameer GA, Sheppard BJ, Langer R. Nature Biotechnol 2002, 20, 602.

56 Barrera DA, Zylstra E, Lansbury PT, Langer R. J Am Chem Soc 1993, 115, 11010.

57 Shirakawa H, Louis EJ, MacDiarmid AG, Chiang CK, Heeger AJ. Chem Commun 1977, 578, 20.

58 Chiang CK, Fincher CR, Park YW, Heeger AJ, Shirakawa H, Louis EJ. Phys Rev Lett 1977, 39, 1098.

59 Wan M. Adv Mater 2008, 20, 2926.

60 Jang J. Adv Polym Sci 2006, 199, 189.

61 Kietzke T, Nehrer D, Kumke M, Montenegro R, Landfester K, Scherf U. Macromolecules 2004, 37, 4882.

62 Kietzke T, Nehrer D, Landfester K, Montenegro R, Guntner R, Scherf U. Nat Mater 2003, 2, 408.

63 Pron A, Rannou P. Prog Polym Sci 2002, 27, 135.

64 Vanderhoff JW, El Aasser MS, Ugelstad J. Polymer emulsification process. US Patent 4,177,177 (1979).

65 Bindschaedler C, Gurny R, Doelker E. Process for preparing a powder of water-insoluble polymer which can be redispersed in a liquid phase, the resulting powder and utilization thereof. US Patent 4,968,350 (1990).

66 Fessi H, Puisieux F, Devissaguet JP, Ammoury N, Benita S. Int J Pharm 1989, 55, R1–4.

67 Jeon HJ, Jeong YI, Jang MK, Park YH, Nah JW. Int J Pharm 2000, 207, 99.

68 York P. Pharm Sci Technol Today 1999, 2, 430.

69 Weber M, Thies MC. Understanding the RESS process. In: Sun YP, editor. Supercritical fluid technology in materials science and engineering: synthesis, properties, and applications. New York: Marcel Dekker; 2002. p. 387–437.

70 Sun YP, Rolling HW, Bandara J, Meziani JM, Bunker CE. Preparation and processing of nanoscale materials by supercritical fluid technology. In: Sun YP, editor. Supercritical fluid technology in materials science and engineering: synthesis, properties, and applications. New York: Marcel Dekker; 2002. p. 491–576.

71 Hearn J, Wilkinson MC, Goodall AR, Chainey M. J Polym Sci Polym Chem Ed 1985, 23, 1869.

72 Landfester K, Musyanovych A, Mailander V. J Polym Sci Part A Polym Chem 2010, 48, 493.

73 Min K, Gao H, Matyjaszewski K. J Am Chem Soc 2005, 127, 3825.

74 Min K, Matyjaszewski K. Macromolecules 2005, 38, 8131.

75 Yan F, Texter J. Soft Matt 2006, 2, 109.

76 Odian G. Principles Of Polymerization, 4th Ed., John Wiley & Sons, Inc., New Jersey, USA, 2004, pp. 363-364.

77 Deinega YF, Ul'berg ZR, Marochko LG, Rudi VP, Denisenko VP. Kolloidn Zh 1974, 36, 649.

78 Menger FM, Keiper JS Angew Chem Int Ed Engl 2000, 39, 1906.

79 Bakshi MS, Sharma P, Banipal TS. Mater Lett 2007, 61, 5004.

80 Dreja M, Tieke B. Langmuir 1998, 14, 800.

81 Chern CS. Prog Polym Sci 2006, 31, 443.

82 Chow PY, Gan LM. Adv Polym Sci 2005, 175, 257.

83 Sajjadi S. AIChE J 2009, 55, 3191.

84 Sajjadi S, Yianneskis M. Polym React Eng 2003, 11, 715.

85 Antonietti M, Hentze HP. Adv Mater 1996, 8, 840.

86 Dreja M, Pyckhout-Hintzen W, Mays H, Tieke B. Langmuir 1999, 15, 391.

87 Yang J, Ding Y, Chen G, Li C. Eur Polym J 2007, 43, 3337.

88 In M, Zana R. J Disp Sci Technol 2007, 28, 143.

89 Zana R. Adv Colloid Interface Sci 2002, 97, 205.

90 Odian G. Principles Of Polymerization, 4th Ed., John Wiley & Sons, Inc., New Jersey, USA, 2004, pp. 352-354.

91 Meyer T, Keurentjes J. Handbook of Polymer Reaction Engineering. WILEY-VCH Verlag GmbH & Co. KGaA, Weinheim, Germany, 2005, pp. 252.

92 Chern CS, Tang HJ. J Appl Polym Sci 2005, 97, 2005.

93 Larpent C, Tadros TF. Colloid Polym Sci 1991, 269, 1171.

94 Gan LM, Chew CH, Lee KC, Ng SC. Polymer 1993, 34, 3064.

95 Guo JS, Sudol ED, Vanderhoff JW, El-Aasser MS. J Polym Sci Pol Chem 1992, 30, 691.

96 Hentze HP, Kaler EW. Curr Opin Coll Interface Sci 2003, 8,164.

97 Mendizabal E, Flores J, Puig JE, Katime I, Lopez-Serrano F, Alvarez J. Macromol Chem Phys 2000, 201, 1259.

98 Landfester K. Angew Chem Int Ed 2009, 48, 2.

99 Chern CS. Principles and Applications of Emulsion Polymerization; John Wiley & Sons, Inc.: Hoboken, New Jersey, 2008; pp 132-133.

100 Tsavalas J, Gooch J, Schork F. J Appl Polym Sci 2000, 75, 916.

101 Gooch J, Dong H, Schork F. J Appl Polym Sci 2000, 76, 105.

102 Li M, Daniels E, Dimonie V, Sudol E, El-Aasser M. Macromolecules 2005, 38, 4183.

103 Wang C, Chu F, Graillat C, Guyot A, Gauthier C, Chapel JP. Polymer 2005, 46, 1113.

104 Guo J, Schork FJ. Macromol React Eng 2008, 2, 265.

105 Antonietti M, Hentze HP. Adv Mater 1996, 8, 840.

106 Sajjadi S. Langmuir 2007, 23, 1018.

107 Xu XJ, Chew CH, Siow KS, Wong MK, Gan LM. Langmuir 1999, 15, 8067.

108 Ming W, Jones FN, Fu S. Macromol Chem Phys 1998, 199, 1075.

109 Jiang W, Yang W, Zeng X, Fu S. J Polym Sci Polym Chem Ed 2004, 42, 733.

110 Hermanson KD, Kaler EW. Macromolecules 2003, 36, 1836.

111 Wang H, Pan Q, Rempel GL. Eur Polym J 2011, 47, 973.

112 Gan LM, Lian N, Chew CH, Li GZ. Langmuir 1994, 10, 2197.

113 Loh SE, Gan LM, Chew CH, Ng SC. J Macromol Sci Pure Appl Chem 1996, A33, 371.

114 Chudej J, Capek I. Polymer 2002, 43, 1681.

115 Xu XJ, Siow MK, Wong MK, Gan LM. Langmuir 2001, 17, 4519.

116 Ramirez AG, Lopez RG, Tauer K. Macromolecules 2004, 37, 2738.

117 Sosa N, Peralta RD, Lopez RG, Ramos LF, Katime I, Cesteros C, Mendizabal E, Puig JE. Polymer 2001, 42, 6923.

118 Xu X, Chow PY, Quek CH, Hng HH, Gan LM. J Nanosci Nanotechnol 2003, 3, 235.

119 Roy S, Devi S. Polymer 1997, 38, 3325.

120 Rabelero M, Zacarias M, Mendizabal E, Puig JE, Dominguez JM, Katime I. Polym Bull 1997, 8, 695.

121 Wessling RA. J Appl Poly Sci 1968, 12, 309.

122 Chern CS, Hsu H, Lin FY. J Appl Polym Sci 1996, 60, 1301.

123 Roy S, Devi S. Polymer 1997, 38, 3325.

124 Ming W, Jones FN, Fu S. Polym Bull 1998, 40, 749.

125 He G, Pan Q, Rempel GL. Macromol Rapid Commun 2003, 24, 585.

126 He G, Pan, Q. Macromol Rapid Commun 2004, 25, 1545.

127 Sajjadi S, Brooks BW. J Appl Polym Sci. 1999, 74, 3094.

128 Zeaiter J, Romagnoli JA, Barton GW, Gomes VG, Hawkett BS, Gilbert RG. Chem Eng Sci 2002, 57, 2955.